

EXPERIMENTAL STUDY AND NUMERICAL SIMULATION OF FLOW AND
SEDIMENT TRANSPORT AROUND A SERIES OF SPUR DIKES

by

ANU ACHARYA

Copyright © Anu Acharya 2011

A Dissertation Submitted to the Faculty of the
DEPARTMENT OF CIVIL ENGINEERING AND ENGINEERING MECHANICS

In Partial Fulfillment of the Requirements

For the Degree of

DOCTOR OF PHILOSOPHY
WITH A MAJOR IN CIVIL ENGINEERING

In the Graduate College

THE UNIVERSITY OF ARIZONA

2011

UMI Number: 3454308

All rights reserved

INFORMATION TO ALL USERS

The quality of this reproduction is dependent upon the quality of the copy submitted.

In the unlikely event that the author did not send a complete manuscript and there are missing pages, these will be noted. Also, if material had to be removed, a note will indicate the deletion.



UMI 3454308

Copyright 2011 by ProQuest LLC.

All rights reserved. This edition of the work is protected against unauthorized copying under Title 17, United States Code.



ProQuest LLC
789 East Eisenhower Parkway
P.O. Box 1346
Ann Arbor, MI 48106-1346

THE UNIVERSITY OF ARIZONA
GRADUATE COLLEGE

As members of the Dissertation Committee, we certify that we have read the dissertation prepared by Anu Acharya

entitled Experimental Study and Numerical Simulation of Flow and Sediment Transport around a Series of Spur Dikes

and recommend that it be accepted as fulfilling the dissertation requirement for the Degree of Doctor of Philosophy

_____ Date: January20, 2011
Jennifer Duan

_____ Date: January20, 2011
Kevin Lansey

_____ Date: January20, 2011
Muniram Budhu

_____ Date: January20, 2011
Juan Valdes

Final approval and acceptance of this dissertation is contingent upon the candidate's submission of the final copies of the dissertation to the Graduate College.

I hereby certify that I have read this dissertation prepared under my direction and recommend that it be accepted as fulfilling the dissertation requirement.

_____ Date: January20, 2011
Dissertation Director: Jennifer Duan

STATEMENT BY AUTHOR

This dissertation has been submitted in partial fulfillment of requirements for an advanced degree at the University of Arizona and is deposited in the University Library to be made available to borrowers under rules of the Library.

Brief quotations from this dissertation are allowable without special permission, provided that accurate acknowledgment of source is made. Requests for permission for extended quotation from or reproduction of this manuscript in whole or in part may be granted by the copyright holder.

SIGNED: Anu Acharya

ACKNOWLEDGEMENTS

I would like to express my heartfelt gratitude to Dr. Jennifer Duan, my advisor and mentor, for her consistent support, guidance, encouragement and suggestions throughout this study. Her continual efforts have motivated me not only to complete this dissertation but also to trust myself on my capability.

I am equally grateful to my dissertation committee: Dr. Kevin Lansey, Dr. Juan B. Valdes and Dr. Muniram Budhu for their instructions, valuable suggestions and support throughout the entire process of this study.

I also extend my special thanks to my colleagues Mary Yaeger, Shiyang Zhang and Vincent Steiner for helping me on the flume experiments and providing me the necessary data and support throughout the course of the study. I would like to thank my colleague Doo Sun Kang and all my friends whom I met in the University of Arizona, for their continuous friendship, warm support and encouragement.

I would like to express my love and thanks to my parents, brother and sister. Without their unconditional love, support and guidance, I would not have been able to come this long. My sincere appreciation goes to my parents-in-law and sister-in-law for their continuous support and help.

My eternal dedication and devotion goes to my husband and best friend Amit Karki. This dissertation could not be completed without his encouragement, patience, continuous support and love. Thank you for being there for me.

TABLE OF CONTENTS

ABSTRACT	6
1. INTRODUCTION	9
1.1 Background	9
1.2 Literature Review.....	12
1.2.1 Development of a Unified Total Sediment Load Formula	13
1.2.2 Experimental Study of Mean Flow and Turbulence Distribution around a Series of Angled Dikes	16
1.2.3 Numerical Modeling of Three Dimensional Flow Field around a Series of Spur Dikes	19
1.3 Summary of Literature.....	25
1.4 Format of Dissertation	26
2. PRESENT STUDY.....	28
2.1 Objective of Study	28
2.2 Dissertation Outline	29
2.2.1 Summary: A Unified Total Sediment Load Formula	30
2.2.2. Summary: Near-Bed Turbulence and Local Scour around Series of Three Dikes	34
2.2.3. Summary: Three Dimensional Simulation of Flow Field around Series of Spur Dikes	39
2.3. Uniqueness of Study	43
2.4. Conclusions and Future Work	44
REFERENCES	47
APPENDIX A: A UNIFIED TOTAL SEDIMENT LOAD FORMULA	57
APPENDIX B: NEAR-BED TURBULENCE AND LOCAL SCOUR AROUND SERIES OF THREE DIKES.....	92
APPENDIX C: THREE DIMENSIONAL SIMULATION OF FLOW FIELD AROUND SERIES OF SPUR DIKES	139

ABSTRACT

The intensive research on sediment transport indicates a need of an appropriate equation for predicting the total sediment load in rivers to manage reservoirs, operate dam and design in-stream hydraulic structures. None of the available equations in sediment transport has gained universal acceptance for predicting the total sediment transport rate. These facts indicate the need of a general formula to represent all these formula for predicting the sediment transport rate. The first goal of this dissertation is to find a unified total sediment transport equation for all rivers. On the other hand, scour around hydraulic structures such as spur dikes and bridge piers can be a serious problem that weakens structural stability. An investigation on the turbulent flow field and turbulence distribution around such hydraulic structures is essential to understand the mechanism of local scour and to determine which turbulence properties affect the local sediment transport. In addition, a universal turbulent model that is valid for all cases of turbulent flow in open channels does not exist. This dissertation thoroughly examined the turbulent flow field and turbulence distribution around a series of three dikes. The goal is to determine the significant turbulent properties for predicting the local sediment transport rate and to identify the appropriate turbulence model for simulating turbulent flow field around the dikes.

To develop a general unified total load equation, this study evaluates 31 commonly used formulae for predicting the total sediment load. This study attributes the deviations of calculated results from different formulae to the stochastic properties of bed

shear stresses and assumes that the bed shear stress satisfies the log-normal distribution. At any given bed shear stress, Monte Carlo simulation is applied to each equation, and a set of bed shear stresses are randomly generated. Total sediment load generated from each Monte Carlo realization of all the equations are assembled to represent the samples of total sediment load predicted from all the equations. The statistical properties of the resultant total sediment loads (e.g. standard deviation, mean) at each given bed shear stress are calculated. Then, a unified total sediment load equation is obtained based on the mean value from all the equations. The results showed the mean of all the equations is a power function of dimensionless bed shear stress. Reasonable agreements with measurements demonstrate that the unified equation is more accurate than any individual equation for predicting the total sediment load.

An experimental study and numerical simulation of the flow field and local scour around a series of spur dikes is performed in a fixed flat bed and scoured bed condition. A micro-Acoustic Doppler Velocimeter (ADV) is used to measure the instantaneous velocity field in all the three spatial directions and the measured velocity profiles are used to calculate the turbulence properties. Results show that the local scour develops around the first dike. Turbulence intensity together with the mean velocity in the vertical direction measured at the flat bed closely correlates to the scour depth. In addition, the maximum bed shear stress, occurring at the tip of the second dike in the three-dike series, does not correspond to the maximum scour. Large bed load transport due to bed shear stress may not initiate bed scouring, but turbulence bursts (e.g. sweeps and ejections) will entrain sediment from bed surface and develop the local scour.

A three-dimensional numerical model FLOW-3D is used to simulate the turbulent flow field around a series of spur dikes in flat and scoured bed. This study examines Prandtl's mixing length model, one equation model, standard two-equation $k - \varepsilon$ model, Renormalization-Group (RNG) $k - \varepsilon$ model, and Large Eddy Simulations (LES) turbulence model. The Prandtl's mixing length model and one equation model are not applicable to flow field around dikes. Results of mean flow field by using the standard two-equation $k - \varepsilon$ model, and RNG $k - \varepsilon$ turbulence model are close to the experimental data, however the simulated turbulence properties from different turbulent model deviate considerably. The calculated results from different turbulence models show that the RNG $k - \varepsilon$ model best predicts the mean flow field for this series of spur dikes. None of the turbulence closure models can predict accurate results of turbulence properties, such as turbulence kinetic energy. Based on those results, this study recommends the use of RNG $k - \varepsilon$ model for simulating mean flow field around dikes. Further improvements of FLOW-3D model is needed for predicting turbulence properties near this series of spur dikes under various flow conditions.

1. INTRODUCTION

1.1 Background

The accurate prediction of sediment load in rivers is essential to manage reservoirs, operate dams, and design instream hydraulic structures. Sediment transport rate is a function of flow intensity and sediment properties, such as size, gradation, and density. Gilbert proposed the first sediment transport equation in 1914 (Gilbert 1914). Since then, many sediment transport equations have been derived for either single or multi-grain sized sediment in steady uniform open channel flow.

Some of these equations are for total sediment load that does not differentiate bed load and suspended load, and some are only for bed load or suspended load. Among them, the total load equations are the most frequently used by engineering practitioners. For example, the newly developed sediment model in HEC-RAS 4.1 included five total load equations and two bed load equations (HEC 2010).

Although all of the equations were verified and tested by using series of laboratory and field data, predictions from these equations can be order-of-magnitude different for the same hydraulic condition. The inconsistent results from these sediment transport formulae indicate that the understanding of sediment transport is still incomplete, especially how instantaneous flow turbulence entrain and transport sediment, and how instantaneous bed shear stresses affect sediment motion. None of the available equations in sediment transport has gained universal acceptance for the calculation of

total sediment transport rate. Therefore, predicting the total sediment load in rivers is still a challenge to river engineers, which requires a universal equation that unifies the existing equations and gives accurate predictions of existing measurements.

On the other hand, bank and bed erosion, and sediment transport in natural and manmade channels is a common problem in water resources management (Duan 2005). Spur dikes have been widely used to redirect flow in channels and to protect eroding stream banks. These structures extend outward perpendicularly or at some angle from the bank of a stream or river into the stream flow. They have been used to enhance the aquatic habitats in unstable streams (Klingeman et al. 1984; Shields et al.1995a), because their presence create and maintain a stable pool for habitat.

Scour around hydraulic structures such as spur dikes and bridge piers can be a serious problem that weakens structural stability. Predicting volume of local scour in the vicinity of these structures in open channel flow has challenged river engineers for decades. Flow turbulence and high bed shear stress around the structures initiates erosion and facilitates the formation of scour hole. However, the influence of the turbulence flow field, bed shear stress, and sediment transport on the scour depth has not been widely researched. In addition, the parameters affecting the scour depth has not been fully understood. There is no consensus in the literature on which of the mean or turbulence flow property estimates the equilibrium scour depth. Additionally, there is still discussion on whether or not the scour depth is proportional to bed shear stress.

An investigation on the turbulent flow field and turbulence distribution around such hydraulic structures is essential to understand the mechanism of local scour. Further,

it is important to determine the significant turbulence property in predicting the local sediment transport rate. The turbulence property and the locally increased bed shear stress define the initiation of scour hole and correlate the scour depth with these properties. A better understanding of these processes will aid river engineers for designing the embankments for the prevention of bank erosion and scour around the bridge piers as well as providing the maximum benefits to aquatic habitats.

Information regarding different types of river structures and their flow pattern has been studied in laboratory experiments, physical models, and computational models. Prior to the emergence of computer technology, physical models are often used for designing large hydraulic structures, such as dams, canals. With the technology advances in computers, especially personal computers, computational models have become reliable and cost-effective tools for engineering designs. A validated and verified computational model can be used repetitively for analyzing different design alternatives. Nowadays computational modeling analysis is essential for hydraulic engineering design, watershed assessment, and river analysis. Computational Fluid Dynamics (CFD) models originally developed for mechanical engineering are modified for hydraulic engineering. CFD models can simulate a variety of flow field, such as flow through bridge piers and structures, around dikes, at river confluences, in river meandering bends.

Although CFD models are in general cost-effective tools for engineering design, not all CFD models are valid for turbulent flow field around dike due to the limitation of turbulence closures, or numerical techniques, or boundary conditions. There is a necessity to check the accuracy of the CFD model's hydrodynamic computations by comparing the

numerically modeled results with the experimental data. Three-dimensional models are often used in engineering design to determine mean and turbulence flow field around the dikes. However, a universal turbulent model that is valid for all cases of turbulent flow in open channels currently does not exist. Some turbulent closures offer advantages over others in specific turbulent flow field depending on the nature of turbulence. Simple turbulent closures, such as eddy viscosity and mixing-length models, are more applicable to engineering field practice where less detailed information of turbulent fluctuations and Reynolds stresses is required. Solutions with more detailed turbulent flow field are necessary to examine local scour development under the effect of turbulence. Two-equation turbulent models began with the standard $k - \varepsilon$ model that solves two transport equations for turbulent kinetic energy and its dissipation rate to obtain the eddy viscosity. Besides the standard $k - \varepsilon$ model, several improved $k - \varepsilon$ models, such as renormalized and realizable $k - \varepsilon$ models are also available for complex flow field around dikes. However, the applicability of those turbulence closures to turbulent flow field near dikes remains unknown. This shows the necessity of identifying the appropriate turbulence model for simulating turbulence flow field around dikes.

1.2 Literature Review

The dissertation consists of three parts: (1) development of a unified total sediment load formula; (2) experimental study of mean flow and turbulence distribution

around a series of angled dikes; and (3) numerical modeling of three-dimensional flow field around a series of spur dikes.

1.2.1 Development of a Unified Total Sediment Load Formula

Sediment load carried by rivers and canals has been the subject of intensive research for centuries due to its importance in river regulations and canal systems. Sediment transport study is necessary in order to make proper provisions for sediment storage in reservoirs, design of channels, and solve other problems due to sediment (Bishop et al. 1965).

Sediment is eroded from one place and deposited to another. Sediment transport is driven by gravity, and drag forces between the sediment and surrounding air or water. Sediment transport depends on sediment properties, characteristics of bed material, and properties of the flow. While designing a hydraulic structure, it is important to predict sediment load carried by the flow or river under the given hydraulic conditions.

The sediment transportation process has been described in literature by a variety of empirical and semi-empirical relations, which are based on flow and sediment properties (Tywoniuk 1972). Considerable research on sediment transport started after Einstein (1950) presented the bed-material discharge function. Many sediment transport equations (e.g. DuBoys 1879; Meyer-Peter and Muller 1948; Lane and Kalinske 1941; Einstein and Chien 1954; Brooks 1963) are developed and calibrated for bed load only or suspended load only, or for the computation of total load only.

The total sediment load formulae are classified into three categories according to their theoretical basis: formulae based on the advection-diffusion equations; empirical

equations based on the regression analysis and graphical methods; formulae based on the energy concept (Julien 1995). The unit stream power theory by Yang (1973), the stream power theory by Bagnold (1966), and the gravitational theory by Velikanov (1954) are the three schools of thought on sediment transport, which are based on the relationship between the energy dissipation rate and the sediment transport rate (Yang and Kong 1991). Bagnold (1966) introduced the concept of stream power to the study of sediment transport and defined stream power as the product of shear stress along the bed and average flow velocity. Not all of the existing sediment transport equations can be used for computing the total sediment load because some of them are developed for computing bed load only while others are developed for suspended load only.

Engelund and Hansen (1967) described the total sediment load as the wash load and the bed material load. According to the type of movement, the total sediment load can also be defined as the sum of bed load and the suspended load (Yang 1996) when wash load is negligible. Wash load is poorly related to the hydraulic conditions and it does not play a significant role in total load prediction except in a few cases. Bed material load is closely related to hydraulic characteristics of river and transported entirely as bed load; or a part as suspended load (Ranga Raju et al. 1981). This study excluded wash load from the total load prediction. The total load can be predicted in two ways by computing bed-load and suspended load separately and adding them together or by determining the total load directly without dividing into suspended and bed load (Garde 1977; Yang 1996). Garde (1977) reviewed the existing methods of both categories and suggested the

need of additional work for the improved computational technique. Both categories of existing methods are used in this study for calculating the total load.

Many theories and equations have been developed for predicting total sediment load, which are based on the assumption of different mechanism dominating sediment transport. An investigator, who studies the effects of these factors on the total load discharge, is likely to obtain graphs or equations that differ from those developed by another investigator. Some of the defined or suggested relationships are fundamentally different; some are superficial that may need considerable study to decide the significant difference (Colby 1964). Most of the equations are supported by the data collected under carefully designed experimental conditions. These equations show poor results when applied to different flow conditions. It requires engineers to take a critical view of the validity of the assumptions made in the sediment transport equations.

Various methods exist for determining the total sediment discharge rate of alluvial streams. Graf (1971), Willis (1979), Yang (1973, 1979), Maddock (1976), Ackers and White (1973), and Shen and Hung (1972) summarized the important equations both theoretically and empirically, for calculating the total sediment load. Similarly, Yang and Molinas (1982) compared the accuracy of seven existing sediment transport equations with the measured data. None of the available total load equations has gained universal acceptance in predicting the sediment transport rate confidently (Vanoni 1971; Yang and Molinas 1982). The calculated results from different equations often differ drastically from each other, and from the observed data. These facts indicate the possibility that the

assumptions made in the derivation of these equations may be true only under limited circumstances and it should not be accepted as a general equation (Yang 1973).

The present study aims to develop a universal sediment discharge relation that is applicable to all open channel flows. The available laboratory and field data from canals and natural rivers, which covers a large range of sediment and stream flow characteristics, have been used to verify the developed function.

1.2.2 Experimental Study of Mean Flow and Turbulence Distribution around a Series of Angled Dikes

Different numerical investigations, such as Large Eddy Simulation (LES) models have been widely used to predict the location and amount of scour occurring in the vicinity of different hydraulic structures such as, abutments, dikes, piers and embankments (Zhang et al. 2005; Haltigin et al. 2007; Koken and Constantiescu 2008; McCoy et al. 2008). Several theoretical analysis have formulated equations for the bed shear stress in turbulent flows (Dey and Lambert 2005; Coleman and Nikora 2008; Tanaka and Eaton 2008). In addition, different experiments have been carried out in laboratory flumes using laser visualization techniques, particle image velocimetry (PIV), and Acoustic Doppler Velocimeters (ADV), to determine flow field around different hydraulic structures such as spur dikes and abutments (Uijttewaal 2005; Zhang et al. 2005). The theoretical and numerical studies are often validated with experimental results.

After the introduction of ADVs in 1993, they have been widely used for measuring the three dimensional flow field in turbulent flows (Nikora and Goring 2000; Wahl 2000; Song and Chiew 2001; Ferro 2003; Garcia et al. 2005; Zhang et al. 2005; Cea et al. 2007; Duan 2009; Duan et al. 2009). Kraus et al. (1994) and Sontek (2001) give a complete technical description of ADV. ADV measures instantaneous flow velocities in three dimensions at a given spatial point that can be used to compute the mean velocity, Reynolds stresses, shear stresses, turbulent kinetic energy and other statistical parameters. The quality of the measurements depends on the behavior of seeding particles within the flow as the ADV measures the velocity of those particles (Cea et al. 2007). Doppler noise and the aliasing of the Doppler signal are the most common errors in turbulence measurement (Nikora and Goring 1998; Wahl 2000; Goring and Nikora 2002; Garcia et al. 2005; Cea et al. 2007). This results in the spike in the sample due to the lack of correlation among the dataset. Filtering can be applied to remove samples with low correlation scores or signal-to-noise ratios(Wahl 2000).

Three-dimensional measurements of velocity can then be used to determine turbulence intensities, Reynolds stresses, and bed shear stress. Using ADV, Dey and Barbhuiya (2005) studied the turbulent flow field around a short rectangular abutment oriented at 90° on a fixed plane bed and an equilibrium scour hole. In his experiments, the maximum bed shear stresses were about 3.2 times that of the incoming flow and turbulent kinetic energy inside the scour hole was greater than that of the plane bed condition. In a similar study, using a submerged dike oriented at 90° , Kuhnle et al. (2008) found the maximum bed shear stress to be 3 times that of the incoming flow around the

dike. Using similar techniques, Duan (2009) and Duan et al. (2009) performed a flume experiment on a single dike oriented 90° to the wall of a flume on a fixed and flat bed. In this case, the bed shear stress calculated from the Reynolds stresses was 2 – 3 time that of the incoming flow. All the results were comparable to earlier studies of emergent, straight-sided dikes, which had amplification factors of about 3 to 5 times that of the incoming flow. In spite of the differences in dike shape and flow Reynolds number, all three studies showed similar amplification factors of bed shear stress. Since the bed shear stress was greater than that of the critical shear stress of the sand on the bed, there would have been a scour if the bed had been mobile.

The orientation angle plays an important role on the amount of scour around a spur dike (Zhang and Nakagawa 2008). Dikes angled against the direction of flow repel the flow whereas the dikes angled in the direction of flow attract the flow towards the banks. Kuhnle et al. (2002) examined the effects of three different orientation angles on scour around spur dikes for the purpose of creating scour holes for aquatic habitats and minimizing bank erosion. Results showed the maximum amount of scour occurrence near the 135° dikes (upstream skew) and bank erosion little bit more than the erosion for 90° dikes. In the experiment with alternating series of three dikes on both sides of the flume, Tominaga and Matsumoto (2006) found a maximum scour occurring in the upstream skew dikes in a sand bed flume. For submerged dikes in series, the maximum scour was located around the tip of the first dike. Biron et al. (2005) also examined the effects of orientation angle on turbulent flow with both emerged and submerged flow, and plane

bed and mobile bed. Results showed the spatial location of maximum shear stress in the plane bed to be different from the location of the maximum scour in the mobile bed runs.

Scour hole forms due to the combined effects of high bed shear stress and turbulence near the hydraulic structures (Chrisohoides et al. 2002). A practical interest in the turbulent flow field around a series of spur dike is the need to predict location and geometry (e.g. size, depth) of the scour zone accurately in a dike series. However, the influence of the turbulence flow field, bed shear stress, and sediment transport on the scour depth has not been widely researched. Therefore, an experimental study around a series of dikes is necessary to determine the three dimensional flow fields, turbulent fluctuations and the bed shear stress. The results, which include flow turbulence and locally increased bed-shear stress, can then be used to explain the initiation of scour holes and correlate the scour depth with these properties.

1.2.3 Numerical Modeling of Three Dimensional Flow Field around a Series of Spur Dikes

Spur dikes are generally used to protect river banks from erosion or to maintain instream hydraulic structures, such as bridges. A single spur dike can only change flow field locally. Spur dikes in series are more effective to stabilize the eroded banks and to relocate the channel. Pools formed due to the local scour around spur dikes can enhance aquatic habitat in unstable streams (Shields et al. 1995; Kuhnle et al. 2008). Despite the important role of spur dikes in stabilizing river banks, realigning channel, restoring fish habitats; there is no solid guideline for their design. The designs of spur dikes based on

previous experience are only applicable to streams or rivers of similar nature (Copeland 1983). Better understanding of the interaction between the three-dimensional flow field around the spur dikes with the entrainment and transport of sediment will advance engineering design.

Over the last few decades, most studies have focused on local scour around river hydraulic structures by physical modeling of bridge piers, spur dikes and abutments. Since spur dikes and abutments are similar in many aspects, the studies on these hydraulic structures are comparable. The investigations on this type of obstruction have been studied extensively (Garde et al. 1961; Laursen 1963; Gill 1972; Kwan and Melville 1994; Lim 1997; Rahman et al. 1998; Kuhnle et al. 2008). Based on the experimental results, several formulas for estimating local scour depth based on flow characteristics have been derived by means of dimensional analysis (e.g., Garde et al. 1961; Melville 1992) or the analytical approaches (e.g., Laursen 1963; Lim 1997; Rahman et al. 1998). Extensive investigations regarding local scour were conducted for bridge piers (Melville and Raudkivi 1977, 1996; Dey et al. 1995; Raudkivi and Ettema 1977, 1985; Raudkivi 1986; Elliott and Baker 1985; Ettema et al. 1998; Laursen 1963; Breusers et al. 1977; Jain 1981). All the above studies reveal that the local scour pattern depends on the complex flow field around bridge piers, channel bed materials, and pier characteristics. For cylindrical bridge piers, maximum scour is a result of the strong downflow and horseshoe vortex surrounding the upstream and lateral sides of the pier weakening the bridges (e.g., Melville and Raudkivi 1977; Graf and Yulistiyanto 1998; Istiyato and Graf 2001; Kwan and Melville 1994). Though a substantial amount of experimental research

(Uijttewaal 2005, Weitbrecht et al. 2003) has been completed, the flow hydrodynamics around the groyne is yet to be fully comprehended.

The existence of spur dikes creates a three-dimensional flow (Chrisohoides et al. 2003; Nagata et al. 2005; Haltigin et al. 2007). The three-dimensional flow field around a spur dike is extremely complex due to separation and generation of multiple vortices. The complexity of the flow field is further magnified due to the interaction between the flow and the scouring mechanism around a spur dike during scouring. The flow field initiates and controls the progress of local scour around a dike, which in turn modifies the flow field by continuous interaction (Raudkivi 1986). Accurate prediction of scour pattern around dikes strongly depends on resolving the flow structure and the mechanism of sediment movement during the development of scour hole (Mendoza and Cabrales 1993). The local scours initiated with the increase in shear stress caused by the acceleration of flow around the dike (Kuhnle et al. 2008). Knowledge of near bed turbulence and the bed shear stress can provide useful information on the local-scale morphological changes that will develop around the dike (Uijttewaal 2005).

Most studies have examined the impact of the groyne on the flow field as the structures orient at 90^0 , 45^0 , 135^0 and 150^0 to the flow (Chrisohoides et al. 2003; Biron et al. 2005; Nagata et al. 2005; Haltigin et al. 2007). Similar to the flow field around a vertical circular pier, the flow field around dikes is characterized by several vortex systems of different sizes, which are developed due to the presence of the dike and are considered as the basic mechanism for scour initiation and development (Posey 1949; Shen et al. 1969; Dargahi 1987; Raudkivi 1990; Ahmed 1995). A substantial amount of

research on flow field around bridge piers (Uijtewaal 2005, Weitbrecht et al. 2003; Melville 1975; Stevens et al. 1991; Dey et al. 1995; Ahmed and Rajarantnam 1998; Graf and Istiarto 2002) has been completed. The flow hydrodynamics around the groyne can be very different from the flow field around piers, which requires further investigations.

There are few previous studies about the flow in the vicinity of non-submerged spur dikes. Kwan and Melville (1994) have experimentally detected the three-dimensional flow field for local scour at a wing wall abutment by using hydrogen bubble technique. On the other hand, the flow field at the groyne and abutment placed on a plain bed were investigated by Rajaratnam and Nwachukwu (1983), and Ahmed and Rajaratnam (2000) respectively. Yu et al. (2002) also studied the flow field in the main channel in the presence of abutments. The flow and scour processes around a vertical spur dike have many similarities to the ones around a bridge abutment.

Better predictive methodologies for the estimation of local scour may be developed through the application of three-dimensional hydrodynamic models (Richardson and Panchang 1998). Olsen and Melaan (1993) used a steady state Navier-Stokes solver coupled with a sediment transport algorithm to simulate the growth of a scour hole at the base of a circular pier and concluded that "three-dimensional numerical models may be able to calculate the scour around an obstacle in a general complex geometry. "Since the early work of Olsen and Melaan (1993), several three dimensional numerical models have been successfully applied to model the flow field around the hydraulic structures. The recent developments in computer software have advanced the use of Computational Fluid Dynamics (CFD) to analyze flow field around the spur dikes.

In order to predict both scour depth and scour geometry, a numerical model is considered as a cost-effective tool. Laboratory and field investigations are time consuming and expensive because a large number of measurements are needed. With the recent advances, numerical solutions are increasingly considered a more reliable approach (Dargahi 1987). Recently, several numerical models have been developed and used to calculate the three-dimensional flow field around different river hydraulic structures (Jia and Wang 1993, 1996; Mayerle et al. 1995; Ouillon and Dartus 1997; Michiue and Hinokidani 1992; Richardson and Panchang 1998; Olsen and Melaaen 1993; Olsen and Kjellesvig 1998; Roulund et al. 1998; Haltigin et al. 2007; Smith and Foster 2005; Salaheldin et al. 2004; Ferguson and Parsons 2003; Bradbrook et al. 2001; Zhang et al. 2005; Nagata et al. 2005). Different computational fluid dynamics software are available commercially for the numerical modeling of three dimensional flow field around the hydraulic structures (e.g. FLUENT; FLOW-3D, PHOENICS). Since flow around spur dikes are highly three dimensional, a three-dimensional model where all three velocity components are solved simultaneously is needed for simulating flow field.

The commercially available computational fluid dynamics software, FLOW-3D (Sicilian et al. 1987) solves the transient Navier-Stokes equations by the volume-of-fluid method (Hirt and Nichols 1981). In addition to the basic abilities, the model supports several turbulent closure using a number of advanced and widely accepted numerical schemes (Launder and Spalding 1972; Rodi 1980; Abbot and Basco 1989; Shaw 1992) for simulating turbulent flows. These include Prandtl's mixing length theory, one equation turbulent energy (k), the two-equation ($k - \varepsilon$), Renormalization-Group (RNG), and Large

Eddy Simulation (LES) closure schemes. The RNG $k - \varepsilon$ model of Yakhot and Orszag (1986) is an extension of the $k - \varepsilon$ model (Rodi 1980). However, it requires less reliance on empirical constants and provides a better solution in areas affected by high shear (Sicilian et al. 1987). Standard values of turbulence parameters (Rodi 1980; Yakhot and Orszag 1986) have been used to develop FLOW-3D (Flow Science 2009). The model also has a number of other features, such as the ability to construct non-uniform grids, automatic time-step selection, graphical post-processing, etc., which are extremely advantageous for this study.

Several turbulence models have been used in simulating three-dimensional flow field around spur dikes and bridge piers. Mendoza-Cabrales (1993) used the $k - \varepsilon$ turbulence closure model to solve three-dimensional flow around circular piers and computed the associated bed shear stress. Melville (1975) found a large discrepancy between the experimental data and his numerical model results showing inadequacy of the $k - \varepsilon$ turbulence model for vertical three-dimensional flow. Smith and Foster (2005) compared the result of LES and the standard $k - \varepsilon$ turbulence model to solve three-dimensional flow around a cylinder over a scoured bed and predicted the accuracy of the $k - \varepsilon$ model. Haltigin et al. (2007) and Bradbook et al. (2001) showed that the RNG $k - \varepsilon$ model gives a good estimation of the velocity field.

The present study will examine various turbulence models using the FLOW-3D software. The appropriate turbulence model will be used for simulating flow field and sediment transport around the spur dikes.

1.3 Summary of Literature

Considerable research has been done to determine the total sediment load transport rate. The total sediment load equations are derived using different approaches i.e. theoretical basis, regression analysis and graphical methods, energy concept. Some sediment transport equations are for computing the total load, some for computing bed load, while others for suspended load. Up to date, many researchers have conducted a thorough comparison of different total load equations for a given flow and sediment condition and showed results of different orders of magnitude. Although all the equations are supported by some laboratory or field data, these equations showed poor results when applied to different flow conditions. No universal transport equation exists to date for determining the total sediment load on all rivers although numerous equations exist in the literature.

Different theoretical approaches, numerical investigations, and experimental studies have been widely used to determine the mechanism of turbulent flow and local scour in the vicinity of hydraulic structures. Experiments have been carried out extensively in laboratory flumes using Laser visualization techniques, particle image velocimetry (PIV), and Acoustic Doppler Velocimeter (ADV) to determine flow field around hydraulic structures such as spur dikes, abutments, and bridge piers. Three-dimensional measurements of instantaneous velocity can then be used to determine the turbulence properties and therefore bed shear stresses. Previous studies showed that the orientation of the dikes to the flow plays an important role on the amount of scour seen around the dike tip as well as on flow patterns around the dike. Some studies show that

the scour hole is resulted from high bed shear stresses whereas others argue that it is a combined effect of bed shear stress and turbulence around the hydraulic structures. An intensive research is needed to quantify the influence of the turbulence flow field, bed shear stress, and sediment transport on the scour depth.

Several CFD models available commercially for simulating three-dimensional flow field around hydraulic structures are increasingly considered as reliable and cost effective tools for studying turbulence flow field around structures. Accurate prediction of scour pattern around dikes strongly depends on resolving the flow structure and the mechanism of sediment transport as the scour hole develops. Since there is no universal turbulent model that is applicable to all turbulence flow field in open channels, several turbulence models have been used in simulating three-dimensional flow field around spur dikes and bridge piers. However, no study has attempted to evaluate all the turbulence closure models and select the most appropriate one for flow around a series of spur dikes in flat and scoured bed condition.

1.4 Format of Dissertation

The format of this dissertation is defined by The University of Arizona Graduate College's Manual for Theses and Dissertations and is, therefore, subject to repetition of information. It includes a first chapter 'INTRODUCTION' describing the relevance of this research, in the context of previous research, and a second chapter 'PRESENT STUDY' that briefly summarizes the objectives, methods and results of the three manuscripts included in Appendices A, B, and C, and discusses the conclusions, and

potential future work of the current study. Appendix A is a scientific manuscript regarding a unified total sediment load formula developed in this study, and has been submitted to the Journal of Hydraulic Engineering. Appendix B is a scientific manuscript regarding the distributions of mean flow and turbulence around a series of three spur dikes, and has been submitted to the Journal of Hydraulic Engineering. Appendix C is a scientific manuscript on the numerical modeling of three dimensional flow field around a series of spur dikes, and is planned for submission to Computers and Geosciences Journal.

2. PRESENT STUDY

2.1 Objective of Study

The 1st objective of this study is to unify the existing total sediment transport formula. To accomplish this goal, three tasks were completed, which are (1) deriving a unified total sediment load equation based on the mean value from evaluating thirty one commonly used equations; (2) verifying the statistically derived equation with 6,999 sets of laboratory and field data; and (3) assessing the accuracy of the unified equation by comparing it with individual equation for predicting the total sediment load.

The 2nd set of objectives of this study are (1) to understand the mechanism of scour around a series of spur dikes (2) to analyze the turbulence distributions around these structures and (3) to determine the correlation of the turbulence properties to the scour depth.

The 3rd set of objectives of this study are (1) to simulate the flow field over a series of spur dikes by using a three-dimensional numerical model; (2) to check the accuracy of the modeling results by comparing the simulated results with the experimental data on a flat bed and scoured bed around a series of spur dikes; (3) to examine the performance of several turbulence models in simulating three dimensional flow field around a series of spur dikes; (4) to determine the best turbulence model for simulating flow field around a series of spur dikes in flat bed and scoured bed.

2.2 Dissertation Outline

This dissertation is comprised of three journal articles in Appendices A to C. The goal is to achieve the three main objectives shown in Figure 1.

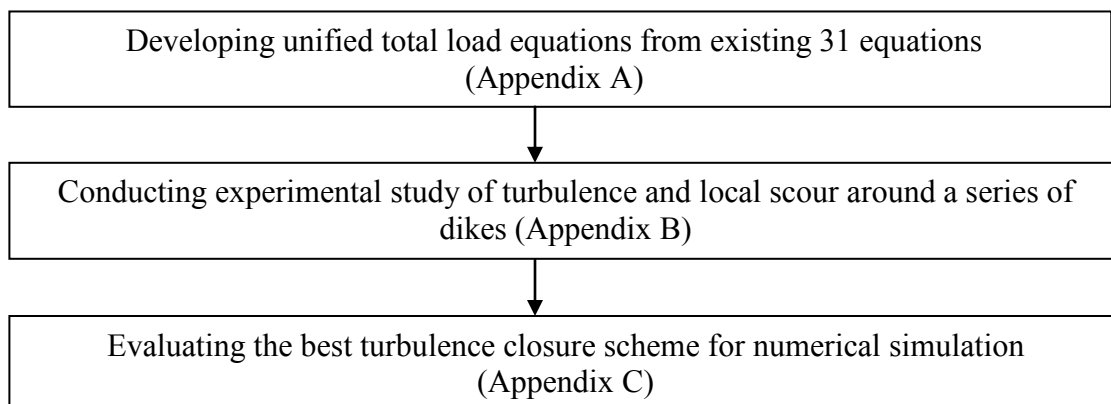


Figure 1. Sequence of study

In the first paper, a unified total load equation is derived from the existing thirty-one total load equations. The derived equation is compared and verified with the existing 6,999 data collected between 1914 and 1980 from various sources.

In the second paper, an experimental study around a series of spur dikes is performed to understand the mechanism of scour around the dikes. The turbulence distribution around the structures is analyzed for fixed flat bed and scoured bed. Finally, the correlation of the turbulence properties to the scour depth is determined.

In the third paper, a CFD model, FLOW-3D, is used to determine the best turbulence model for a series of spur dikes in a fixed flat bed and the scoured bed. Five different turbulence models are analyzed. The computed results are compared with the measured data on a fixed flat bed and scoured bed case from the second paper. Statistical

analysis is performed to determine the best performing turbulence model. Detailed summaries of the methods and conclusions are given below:

2.2.1 Summary: A Unified Total Sediment Load Formula

Many equations for predicting total sediment load in rivers and canals exist in literature. Results from Different total load equations for the same hydraulic parameters give results that vary by orders of magnitude, which show that there is significant uncertainty in those equations.

This study aims to develop a universal sediment discharge relation that is more universal than existing equations. The resulting sediment transport function needs to be a general equation that can predict sediment discharge under a wide range of flow conditions. Available laboratory and field data from canals and natural rivers, which involve a wide variety of sediment and stream characteristics, are used to verify the developed function.

The study is based on an assumption that the different results from individual total load equation are outcomes of stochastically distributed bed shear stresses. In addition, this study adopted the assumption that the bed shear stress satisfies a standard log-normal distribution as in Cheng and Law (2003) and Duan and Barkdoll (2008) so that the calculated total sediment load from those equations is a random variable.

Among the existing total load equations, thirty-one commonly used formulae from various approaches are selected for single grain-sized sediment in steady uniform or gradually varied flows. The equations include the original work of Einstein (1950; 1954)

to the work of Yang and Lim (2003). Some of the equations determine the total load directly whereas other equations predict the total load by computing bed load and suspended load separately and adding them together. The sediment transport rate is calculated as a function of flow parameters, such as the mean flow velocity, bed shear stress, and sediment properties. All the equations are converted into a function between a dimensionless sediment transport rate and the dimensionless shear stress as: $q_s^* = f(\Phi, d)$ where, q_s^* is the Einstein parameter adopted to quantify the dimensionless total sediment transport rate, d is the sediment size and Φ is the dimensionless shear stress. All the thirty-one formulae are used to predict the total load for sediment sizes ranging from 0.125 mm to 28 mm and dimensionless bed shear stresses, also known as the Shields parameter, ranging from 0.01 to 25.0.

Since this study assumes that the bed shear stress is a random variable of a log-normal distribution, the calculated total sediment load from those equations is a random variable. Monte Carlo simulation of each sediment transport equation is then performed at given sediment size and bed shear stress. The standard deviation is taken as 5% of the mean values because most of the available experimental and field data measurements are obtained at fully turbulent flows with Reynolds number greater than 100,000. At a given sediment size and shear stress, a set of bed shear stresses are randomly generated based on the log-normal distribution. The total sediment loads are calculated by applying all the equations based on these series of bed shear stresses. Therefore, at each bed shear stress and sediment size, each sediment formula yields 1,000 total sediment load predictions. Not all the 31 equations are valid for the defined sediment size range. Each sediment

equation is calculated only for their limited size range. A maximum of 31,000 predicted total load transport rates are completed if all the 31 equations calculate for the sediment sizes from 0.125mm to 28mm. The realizations are sufficient because additional realizations did not change the statistical properties of the output.

The total sediment load data generated from each Monte Carlo realization using all approached equations are assembled to represent the samples of total sediment load predicted from all the equations. Then, at a given flow, statistical analysis is performed to obtain the mean sediment transport rate of all the samples at each defined bed shear stress. A unified total load transport formula is then obtained by fitting equation to mean values of the total sediment loads.

This unified equation is tested and verified using 6,999 sets of measurements consisting all of the original data points in the 31 noted equations. The 6,999 data sets from various sources cover sediment sizes ranging from 0.011 mm to 76.113 mm, flow depths from 0.0091m to 17.28 m, velocities from 0.086 m/s to 6.180 m/s, and channel slopes from 0.000003 to 0.0367. To compare the data set with the derived equation, the unified equation is used to calculate the total sediment load using measured flow velocity and sediment size. First, the shear velocity is calculated from the depth-averaged velocity using the logarithmic law, then the dimensionless shear stress is computed, and finally the total load sediment transport rate is estimated using the derived unified equation. The root mean square error (RMSE), mean absolute error (MAE), bias (%) and Nash-Sutcliffe efficiency (E) are calculated as follows to determine the accuracy of the unified equation, i.e.,

$$RMSE = \sqrt{\frac{1}{n} \sum_{i=1}^n (O_i - P_i)^2}, MAE = \frac{1}{n} \sum_{i=1}^n |O_i - P_i|, E = 1 - \frac{\sum_{i=1}^n (O_i - P_i)^2}{\sum_{i=1}^n (O_i - \bar{O})^2}$$

where O_i and P_i are the observed and predicted values, respectively; \bar{O} is the mean of the observed data; and n is the number of observations. The statistical comparison of different equations is done with the intensive data set (Table 1).

Table 1. Statistical comparison of the measured and calculated results for different equations in ppm

Equations	MAE	RMSE	Nash-Sutcliffe Efficiency	Standard. Deviation
Unified Equation	710.00	1490.00	0.82	1300.00
Velikanov (1954)	1125.58	2825.53	0.38	2591.84
Maddock (1976)	2356.20	5768.49	0.25	5265.72
Graf and Acaroglu (1968)	2755.04	2999.10	0.34	2755.04
Graf and Suszka (1987)	2180.50	2384.29	0.56	2180.50
Yang and Lim (2003)	1208.47	3068.20	0.27	2820.39

The following results are observed in this study:

- (1) The derived unified total load equation $q_s^* = 10.69(\Phi)^{3.08}$ is based on the statistical mean of predicted total sediment load from the 31 equations that unifies the predictions from each individual equation. The comparison of statistically derived equation with several original total sediment load equations and observed data show that none of the existing 31 noted equations perform well for the collected dataset from different sources. The statistical analysis of the computed results and the measured data determines the accuracy of the unified equation. This equation is much

- accurate than the noted 31 individual equation for the specified range of sediment size and the bed shear stress if sediment load measurements are not available.
- (2) The correlation coefficient between the dimensionless shear stress and the dimensionless transport rate of the unified total load equation is 0.99. It indicates the mean total load transport rate is highly dependent on the mean dimensionless shear stress.
- (3) The computed results from the unified equation agree very well with 6,999 measurements from flume and natural rivers compared to the other individual equations as shown in Table 1. The statistical comparison shows that the derived equation is more accurate than any noted 31 individual equation for this data set. Over 75% of measured data fall within the 95% confidence interval of the unified total load equation. The equations of Yang and Lim (2003), Maddock (1976), Graf et al. (1968, 1987), and Velikanov (1954) are the closest ones to the unified equation.

2.2.2. Summary: Near-Bed Turbulence and Local Scour around Series of Three Dikes

Local scour in the vicinity of hydraulic structures such as bridge piers and spur dikes has been a challenging task to water resource engineers for decades. To predict the cause and the amount of local scour around these hydraulic structures, numerical investigation, theoretical analysis and experimental study of the bed shear stress and turbulence properties are necessary.

This study presents a methodology for an experimental study of turbulence and local scour around a series of spur dikes in a mobile bed. Experiment was conducted in a

12.2 m long and 60cm wide flume located in the courtyard of the Civil Engineering and Engineering Mechanics Department at the University of Arizona. Three spur dikes of 30 cm length, 4-mm thickness and 40 cm height, spaced 30 cm apart were protruded from the left-wall of the channel facing upstream at an angle of 150° . The first angled dike was located at 1.8 m downstream of the flume inlet. A broad-crested weir of 10 cm height was placed 10.6 m downstream of the inlet. A valve was used to control the mean water depth to a desired 20 cm height at the weir resulting in 10 cm of water above the weir. The total discharge at the weir was $0.035\text{m}^3/\text{s}$. The study reach was divided into forty-one cross sections and the 10 cm of bed surface was covered with a well-sorted sand and gravel mixture having a median grain diameter of 0.85 mm. The duration of the experimental run was 24 hours to allow the local scour to reach a steady state. A 16MHz SonTek micro-ADV was used to measure the full velocity profile consisting of 10 verticals starting at 5 mm from the bed and extending at 1 cm intervals for all the nodal points. The ADV was moved manually in all three directions to measure flow velocities at any location in the cross sections. The sampling frequency of this ADV application was 25 Hz, with a sampling duration of 4 to 5 minutes for 5000 instantaneous velocities at three respective directions at each measuring node.

The origin of the Cartesian coordinate was set at the intersection of the bed surface before scouring occurs at the right wall of the flume and 0.63 m upstream of the tip of the first spur dike. The x-axis was defined as being along the main flow longitudinally, the y-axis was pointing to the left bank in the transverse direction, and the z-axis was towards the water surface in the vertical. The velocity components were

denoted as u , v , and w respectively. WinADV software was used to filter the raw data. All the measurements showing signal-to-noise ratio (SNR) less than 20 were removed from the dataset. The shear velocity, $u_* = 1.30$ cm/s, and zero velocity level, z_0 , were determined by fitting logarithmic velocity profile and assuming the von Karman constant as 0.41 for the erodible bed run. The measured velocity profiles were used to calculate the different turbulence characteristics as: (a) mean velocities in the longitudinal, transverse, and vertical directions denoted as \bar{u} , \bar{v} and \bar{w} respectively; (b) Reynolds stresses, $-\rho\overline{u'v'}$, $-\rho\overline{v'w'}$, $-\rho\overline{u'w'}$, $-\rho\overline{u'u'}$, $-\rho\overline{v'v'}$, $-\rho\overline{w'w'}$ in which ρ is flow density, and u' , v' and w' are turbulence fluctuations in the longitudinal, transverse, and vertical directions, respectively; (c) bed shear stress using four different methods: (i) turbulent kinetic energy method from Biron et al. (2004); $\tau = C_1 [0.5\rho(u'^2 + v'^2 + w'^2)]$, where ρ is mass density and $C_1 = 0.19$ is a proportionality constant (Kim et al. 2000; Pope 2006), (ii) Reynold's stress method from Dey and Barbhuiya (2005); $\tau = \sqrt{[(-\rho\overline{u'v'}) + (-\rho\overline{u'w'})]^2 + [(-\rho\overline{v'w'}) + (-\rho\overline{v'v'})]^2}$ (iii) Reynold's stress using w' only; $\tau = (-\rho\overline{u'w'}) + (-\rho\overline{v'w'})$ (iv) turbulent kinetic energy method (Biron et al. 2005); $\tau = 0.9\rho\overline{w'^2}$; and (d) turbulent kinetic energy (TKE), calculated as $\frac{1}{2}(u'^2 + v'^2 + w'^2)$. In addition, the parameters are non-dimensionalized for the further analysis purpose. The dimensionless mean velocity, \bar{u}/u_0 , shear stress, $\tau/\rho u_{*0}^2$, turbulence intensities, u'/u_{*0} , and Reynolds stress, $-\rho\overline{u'v'}/\rho u_{*0}^2$ are calculated.

The experimental study of flat bed for a series of spur dikes was conducted by Yaeger (2009). The results from the flat bed case were compared with the mobile bed case for a detailed analysis of local scour, velocity, turbulent kinetic energy, Reynolds stresses and bed shear stress.

The following results are observed for the scoured bed in this study:

- (1) The maximum scour depth is at the tip of the first dike. The mean velocities in the transverse and vertical directions are much more negative than in the longitudinal direction. Both \bar{u} and \bar{v} components have the maximum values around the second dike. In contrast, the maximum value of the \bar{w} component is upstream of the first dike.
- (2) The dimensionless values of u' , v' and w' are obtained by dividing the individual velocity fluctuations by the shear velocity of the incoming flow, u_{*0} . The maximum values of u' and v' components are around the second dike whereas w' component occurs at the tip of the second dike. The w' component reduced significantly at the first dike where the maximum scour depth occurs. The amplification factors around the dikes in longitudinal and transverse directions are about 4 to 8 times the incoming flow turbulence intensities. However, the maximum w' component occurred at the first dike regardless of the dike alignment in the flat bed case.
- (3) The largest magnitude of the Reynolds stress $-\overline{\rho u'v'}$ appears at the tip of the second dike. For $-\overline{\rho u'w'}$, the highest magnitude is positive, and the series shows a zone of positive $-\overline{\rho u'w'}$ circulating near the tip of the first and second dikes.

- (4) Comparison of different methods for calculating bed shear stresses shows that the TKE method is the most reliable method and the methods using w' are inappropriate for the complex flow field around the dikes. The maximum bed shear stress occurs at the upstream of the tip of the second dike, which is similar to the result for both the straight and angled dikes with different flow cases for the fixed flat bed condition. The bed shear stress near the tip of the second dike is 14 times that of the incoming flow. A patch of high bed shear stress is seen just downstream of the first dike in this experimental run. Since the experimental results from the mobile bed and plane bed study shows that the maximum shear stress is at the tip of the second dike in a three dike series, the maximum shear stress does not correlate with the scour depth.
- (5) Since the location of maximum scour is noticed around the first dike similar to the distribution of velocity fluctuation, w' , and mean velocity, \bar{w} , in fixed flat bed condition, the initiation and development of local scour is determined by the turbulence intensity in the vertical direction rather than the bed shear stress. Higher shear stresses will transport more bed load, but not necessarily result in local scour.
- (6) The maximum scour depth depends on the maximum mean vertical velocity or the maximum velocity fluctuation in the vertical direction. After the local scour has reached equilibrium, the maximum correlation coefficient is very low, which shows that none of the measured flow properties has a strong correlation with the scour depth. This may confirm the perception in Haltigin et al. (2007) that the scour depth should be predicted using the measured flow properties on a flat bed.

2.2.3. Summary: Three Dimensional Simulation of Flow Field around Series of Spur Dikes

With the advancements in computing technology since the 1980s, Computational Fluid Dynamics (CFD) analysis has emerged as a powerful hydraulics design tool (Griffith et al. 2007). A CFD model is selected for this study as it has been shown that a robust three-dimensional hydrodynamic model can effectively complement experimental studies in understanding complex flow field, and the scour initiation process around bridge piers of various sizes, shapes, and dimensions.

In this study, the simulations were conducted using the commercially available CFD software 'FLOW-3D' (Flow Science 2009), which simultaneously solves the three-dimensional, transient Navier-Stokes equations on a structured grid. FLOW-3D software was used for this study due to its ability to accurately model problems involving free surface flows, to construct non-uniform grids, for automatic time-step selection, and for graphical post processing, etc. The software uses the volume of fluid (VOF) method for tracking fluid-air or fluid-fluid interfaces. The fractional area-volume obstacle representation (FAVOR) method is utilized for modeling of solid obstacles, which is a trademark of FLOW-3D. In addition, it accounts for cells that are not wholly wet or dry, by determining their fractional influence on the flow.

In the present investigation, a comparative study of five different turbulence models, Prandtl's mixing length, one equation turbulent energy (k), the two-equation $k - \varepsilon$, Renormalization-Group (RNG), and Large Eddy Simulation (LES) closure schemes, is made to analyze flow field around a series of spur dikes in fixed flat bed and scoured bed condition. From the preliminary analysis, it is determined that an advanced

turbulence closure model is required for complex flow field around a series of dikes. As such, detailed analysis is completed only for the RNG $k - \varepsilon$, the standard $k - \varepsilon$, and the LES models.

A non-uniform computational mesh was constructed within a rectangular coordinate system with the dimensions of the experimental flume. The smallest horizontal grid size was 3 mm, which provided adequate discretization of the spur dike geometry. A modeling grid with 197,000 nodes was found to be sufficient to reproduce the three-dimensional flow field accurately. The spur dikes were created as solid objects, and inserted into the domain at the appropriate locations as in the experimental setup. The spur dikes were resolved nicely into the model. To initialize the model, volume flow rate, mean approach velocity of 0.29 m/s, and flow depth of 0.25 m in z-direction were defined at the inlet of the channel. The appropriate boundaries were provided and the boundaries bordering the dikes were assumed to have a non-slip rough surface. The roughness values for the flume and the bed for these simulations was 0.00085 m. The bathymetry of the scoured bed surface was directly imported into the model as the model input. The model was run for the flat bed case and scoured bed case until it reached the steady flow state for various turbulence closure schemes. In all simulations, the default values of the various turbulence model coefficients were used.

Results obtained after the steady state flow condition of each simulation were compared to the experimental results. In order to match modeled velocities with those measured using the ADV, the model output was sampled at grid cells equivalent to the measurement locations. The computed velocity field and the total kinetic energy for the

flat bed case and scoured bed case were compared with the experimental data.

The following results are observed in this study:

- (1) The FLOW-3D model is able to resolve the spur dikes correctly and reproduces the three-dimensional flow field around the spur dikes for the fixed flat bed and scoured bed conditions.
- (2) From the comparison of the modeled velocities and turbulent kinetic energy with the measurement, the best turbulence closure scheme is investigated. It appears that the RNG $k - \varepsilon$ model, standard $k - \varepsilon$ model, and LES model perform better than the Prandtl's mixing length model and one equation model for the complex flow field around the dikes for flat and scoured bed conditions.
- (3) Although the simulated mean flow field is close to the experimental data, the simulated turbulence properties from different turbulent model deviate considerably. Comparison of the results from the RNG $k - \varepsilon$ model with the standard $k - \varepsilon$ model and LES model shows the importance of selecting an appropriate turbulence models even for simple geometries. The predictions of RNG $k - \varepsilon$ agree better than other turbulence models when compared with the existing experimental results for the plane bed and scoured bed.
- (4) For RNG $k - \varepsilon$ model, the correlation coefficients show an overall good agreement for the longitudinal and transverse velocity, with average squared correlation (R^2) values (for the flat and scoured bed cases) of 0.793 and 0.889, respectively. However, much lower agreements are found for the vertical component (w) and turbulent

kinetic energy (TKE), with R^2 ranging between 0.187-0.464 and 0.384-0.434 for w and TKE, respectively. Lower velocity correlations may be due to the smaller range of velocities in the vertical component, or the differences in the position of the center of the simulation cells compared to the ADV sampling volume. The calculated results from different turbulence models show that the RNG $k - \varepsilon$ model best predicts the mean flow field for this series of spur dikes. However, none of the turbulence closure models can predict accurate results of turbulence kinetic energy.

(5) Since the model was able to predict the interaction between the dikes correctly, FLOW-3D can be used as a hydraulic design tool. However, further improvements of the model are needed for predicting turbulence properties near this series of spur dikes under various conditions.

2.3. Uniqueness of Study

The first part of this dissertation aims to formulate a general relation between the dimensionless sediment transport parameter and the dimensionless bed shear stress. The unified formula is derived from the existing 31 total load equations. It will be an excellent choice to river engineers, if no sediment measurement is available. It has advantages over existing formulae because it is not only the average of results from many existing formulae but also the most accurate one for this intensive data set. The second part of this dissertation aims to determine the turbulence flow field, bed shear stress, and sediment transport around spur dikes. From the experiments on flat bed surface and scoured bed surface for a series of spur dikes, the maximum bed shear stress occurring at the tip of the second dike in the three-dike series does not correspond to the maximum scour. Rather, the local scour develops around the first dike where the mean vertical flow (\bar{w}) and turbulence intensity (w') are the largest in the series. The low correlation coefficient between scour depth and turbulence property after the local scour reached equilibrium indicates that the scour depth should be predicted using the measured flow properties at the flat bed. Higher shear stresses will transport more bed load, but not necessarily result in local scour. This study investigates the impact of turbulence intensity and the mean velocity in the vertical direction on scour depth.

The third part of this dissertation aims to analyze numerically the three-dimensional flow field; examine the performance of several turbulence models in simulating three-dimensional flow field around a series of spur dikes; and determine the

best turbulence closure scheme for a series of spur dikes in flat bed and scoured bed surface. This study provides information on how accurately a commercially available CFD model, FLOW-3D can predict the flow field around a series of spur dikes. Since a universal turbulent model does not exist for turbulent flow in open channels, this study found out the best turbulence closure scheme for a series of spur dikes in flat bed and scoured bed surface.

2.4. Conclusions and Future Work

The proposed unified total load equation is obtained by using the statistical mean of total load predictions from 31 of the commonly used formulae. This study is an attempt to unify the existing total sediment transport formulae by the Monte Carlo simulations. Although several existing total load transport formulae are very close to the derived equation at a given range of shear stress, none of the formulae matches the unified equation for the entire range of shear stresses. Therefore, the unified total sediment load formula can be considered as a general representation of all the existing equations. Unless flow and sediment compositions are unique in a given river reach, this study believes that the unified equation will give better predictions than any individual formula.

The limitation of this study is that the derived formula is limited to sediment sizes from 0.0125 mm to 28 mm, and dimensionless shear stress from 0.01 to 25. The equation is tested and verified with only 6,999 sets of available data. Further studies can be conducted to test the derived equation for broader range of sediment sizes and bed shear

stresses. In addition, the unified equation can be generated for suspended load or bed load only, and can be verified with the available measurements on bed load or suspended load. It is also possible to find an appropriate probability distribution function to represent the distribution of each sediment load prediction.

The experimental study on a scoured bed shows that the maximum scour depth occurs at the tip of the first dike in a three dike series. Of the three turbulence intensities, u' and v' are the most significant, with w' being much smaller than the other two. In the case of the Reynolds stresses, the horizontal component $-\rho\overline{u'v'}$ is the largest, with the other two components being roughly equal to each other. The highest magnitude of bed shear stress calculated by turbulent kinetic energy is consistently around the second dike in the series. However, the location of maximum scour is observed around the first dike in coincidence with the distribution of velocity fluctuation w' and mean velocity \bar{w} in plane bed condition. This indicates that the initiation and development of local scour is determined by the turbulence intensity in the vertical direction rather than the bed shear stress. Higher shear stresses will transport more bed load, but not necessarily result in local scour. However, the quantitative relation between local scour and turbulence intensity in the vertical requires a numerical modeling for this purpose.

The commercially available CFD model, FLOW-3D, is used to simulate the turbulent flow field around a series of three spur dikes in flat and scoured bed. This study examines Prandtl's mixing length model, one equation model, standard two-equation $k-\varepsilon$ model, RNG $k-\varepsilon$ model and LES turbulence model. Experimental data from a laboratory study of flow in a flat bed and scoured bed around a series of three dikes are

used to verify the results from the numerical model. Although the simulated mean flow field is close to the experimental data, the simulated turbulence properties from different turbulent model deviate considerably. None of the turbulence closure models can predict accurate results of turbulence kinetic energy. Modeling results using the LES and standard $k - \varepsilon$ model showed over 50% discrepancy from the measured vertical velocity and turbulent kinetic energy. Since the simulated results of mean flow field qualitatively agree with the experimental data, this study recommends the use of RNG $k - \varepsilon$ model for simulating the mean flow field around the dikes for fixed flat and scoured bed. Since FLOW-3D model was able to reproduce the three-dimensional flow field around the dikes correctly and solve the problem of free surface flows, the model can be used for the numerical simulation of mean flow field for a series of spur dikes under various flow conditions. Since none of the turbulence closure model was able to predict accurately the turbulence properties (e.g. TKE) near the dikes, improvements in FLOW-3D is needed for better predicting turbulence flow properties by using direct numerical simulation technique.

Since only two experimental cases for a series of spur dikes are considered in this study for the verification of the RNG $k - \varepsilon$ turbulence closure scheme and CFD model FLOW-3D, further studies are recommended for other types of hydraulic structures i.e. bridge piers, abutments and embankments for the universal acceptance of the model.

REFERENCES

- Abbot, M., and Basco, D. (1989). *Computational fluid dynamics: An introduction for Engineers*.
- Ackers, P., and White, W. R. (1973). "Sediment transport: New approach and analysis." *J. Hydraul. Div.*, ASCE, 99(11), 2041-2060.
- Ahmed, F. (1995). "Flow and erosion around bridge piers." *PhD Dissertation*, Dept. of Civil Engineering, Univ. of Alberta, Edmonton, Alta., Canada.
- Ahmed, F., and Rajaratnam, N. (1998). "Flow around bridge piers." *J. Hydraul. Eng.*, 124(3), 288 – 300.
- Ahmed, F., and Rajaratnam, N. (2000). "Observations of flow around bridge abutment." *J. Eng. Mech.*, 126(1), 51 – 59.
- Bagnold, R. A. (1966). "An approach to the sediment transport problem from General Physics." *U. S. Geological Survey Professional Paper 4221*, U. S. Government Printing Office, Washington, D.C.
- Biron, P. M., Robson, C., LaPointe, M. F., and Gaskin, S. J. (2005). "Three-dimensional flow dynamics around deflectors." *River Research and Applications*, 21, 961–975.
- Biron, P. M., Robson, C., Lapointe, M. F., and Gaskin, S. J. (2004). "Comparing different methods of bed shear stress estimates in simple and complex flow fields." *Earth Surf. Process. Landforms*, 29, 1403-1415.
- Bradbrook, K. F., Lane, S. N., Richards, K. S., Biron, P. M., and Roy, A. G. (2001). "Role of bed discordance at asymmetrical river confluences." *J. Hydraul. Eng.*, 127(5), 351-368.
- Breusers, H. N. C., Nicollet, G., and Shen, H. W. (1977). "Local scour around cylindrical piers." *J. Hydraul. Res.*, 15(3), 211-252.
- Brooks, N. H. (1963). "Calculation of suspended load discharge from velocity concentration parameters." *Proceedings of Federal Interagency Sedimentation Conference*, U.S. department of Agriculture, Miscellaneous Publication no. 970.
- Cea, L., Puertas, J., and Pena, L. (2007). "Velocity measurements on highly turbulent free surface flow using ADV." *Exp Fluids*, 42, 333–348.

- Cheng, N. S., and Law, A. W. K. (2003). "Fluctuations of turbulent bed shear stress." *J. Eng. Mech.*, ASCE, 129(1), 126-130.
- Chrisohoides, A., Sotiropoulos, F., and Sturm, T.W. (2003). "Coherent Structures in Flat-Bed Abutment Flow: Computational Fluid Dynamics Simulations and Experiments." *J. Hydraul. Eng.*, 129(3), 177-186.
- Colby, B. R. (1964). "Practical computations of bed-material discharge." *J. Hydraul. Div.*, ASCE, 90 (2), 217-246.
- Coleman, S. E., and Nikora, V. I. (2008). "A unifying framework for particle entrainment." *Water Resour. Res.*, 44, W04415, doi:10.1029/2007WR006363
- Copeland, R. R. (1983). "Bank protection techniques using spur dikes." Miscellaneous Paper No. HL-83-1, U.S. Army Waterways Experiment Station, Vicksburg, Miss.
- Dargahi, B. (1987). "Flow field and local scouring around a pier." *Bulletin No. TRITA-VBI-137*, Hydraulic Laboratory, Royal Institute of Technology, Stockholm, Sweden.
- Dey, S., and Barbhuiya, A. K. (2005). "Flow field at a vertical-wall abutment." *J. Hydraul. Eng.*, 131(12), 1126–1135.
- Dey, S., and Lambert, M. F. (2005). "Reynolds stress and bed-shear in non-uniform unsteady open-channel flow." *J. Hydraul. Eng.*, 131(7), 610–614.
- Duan, J. G. (2009). "Mean flow and turbulence around an experimental spur dike." *J. Hydraul. Eng.*, 134 (3), 315-327.
- Duan, J.G. (2005). "Analytical approach to calculate the rate of bank erosion." *J. Hydraul. Eng.*, 131(11), 980-990.
- Duan, J. G., and Barkdoll, B. D. (2008). "Surface-based fractional transport predictor: Deterministic or stochastic." *J. Hydraul. Eng.*, ASCE, 134(3), 350-353.
- Duan, J. G., He, L., Wang, G., and Fu, X. (2009). "Mean flow and turbulence in a scoured hole around an experimental spur dike." *Advance in Water Resource*, 32(12), 1717-1725.
- DuBoys, M. P. (1879). "Le Rhone et les Rivieres a Lit affouillable." *Annales de Ponts et Chausses*, 18(5), 141-195.
- Einstein, H. A. (1950). "The bed-load function for sediment transportation in open channel flows." *Technical Bulletin No. 1026*, U. S. Department of Agriculture, Soil Conservation Service., 70 pp.

- Einstein, H. A., and Chien, N. (1954). "Second approximation to the solution of suspended-load theory." University of California, Institute of Engineering Research No.3.
- Engelund, F., and Hansen, E. (1967). "A monograph on sediment transport in alluvial streams." *Teknisk Forlag.*, Technical Press, Copenhagen, Denmark, 62 pp.
- Ettema, R., Melville, B. W., and Barkdoll, B. (1998). "Scale effect in pier-scour experiments." *J. Hydraul. Eng.*, 124(6), 639–642.
- Ferguson, R. I., Parsons, D. R., Lane, S. N., and Hardy, R. J. (2003). "Flow in meander bends with recirculation at the inner bank." *Water Resour. Res.*, 39(11), 1322–1334.
- Ferro, V. (2003). "ADV measurements of velocity distributions in a gravel-bed flume." *Earth Surface Processes and Landforms*, 28(7), 707-722.
- Flow Science, Inc. (2009). *FLOW-3D user's manual*, 9.4 edition, Flow Science, Inc., Santa Fe, N.M.
- García, C. M., Cantero, M. I., Nino, Y., and García, M. H. (2005). "Turbulence measurements with acoustic Doppler velocimeters." *J. Hydraul. Eng.*, 131(12), 1062–1073.
- Garde, R. J., Subramanya, K., and Nambudripad, K. D. (1961). "Study of scour around spur-dikes." *J. Hydraul. Div.*, ASCE, 87(6), 23–37.
- Garde, R. J., and Ranga Raju, K. G. (1977). "Mechanics of sediment transportation and alluvial stream problems," *Wiley Eastern Limited*, New Delhi, India.
- Gilbert, G. K. (1914). "The transportation of debris by running water." *U. S Geological Survey, Professional Paper 86*, Washington D.C., U.S.
- Gill, M. A. (1972). "Erosion of sand beds around spur dikes." *J. Hydraul. Div.*, ASCE, 98(9), 1587–1602.
- Goring, D. G., and Nikora, V. I. (2002). "Despiking acoustic Doppler velocimeter data." *J. Hydraul. Eng.*, 128(1), 117–126.
- Graf, W. H. (1971). *Hydraulics of sediment transport problems*. New York: McGraw-Hill.
- Graf, W. H., and Yulistiyanto, B. (1998). "Experiments on flow around a cylinder; the velocity and vorticity fields." *J. Hydraul. Res.*, 36(4), 637–653.

- Graf, W. H., and Istiarto, I. (2002). "Flow pattern in the scour hole around cylinder." *J. Hydraul. Res.*, 40(1), 13–20.
- Griffith, A.R., Rutherford, J. H., Alavi, A., Moore, D.D., and Groeneveld, J. (2007). "Stability review of the Wanapum spillway using CFD analysis." *Bulletin*, Canadian Dam Association., 16–26.
- Haltigin, T. W., Biron, P. M., and Lapointe, M. F. (2007). "Predicting equilibrium scour-hole geometry near angled stream deflectors using a three-dimensional numerical flow model." *J. Hydraul. Eng.*, 133(8), 983–988.
- HEC (2010). "HEC-RAS River analysis system." Hydraulic Reference Manual (Version 4.1), U.S. Army Corps of Engineers, Hydrologic Engineering Center, Davis, California.
- Hirt, C. W., and Nichols, B. D. (1981). "Volume of fluid (VOF) method for the dynamics of free boundaries." *J. Comput. Phy.*, 39, 201-225.
- Istiyato, I., and Graf, W. H. (2001). "Experiments on flow around a cylinder in a scoured channel bed." *Int. J. Sediment Res.*, 16(4), 431–444.
- Jain, S. C. (1981). "Maximum clear-water scour around circular piers." *J. Hydraul. Div., Am. Soc. Civ. Eng.*, 107(5), 611–626.
- Jia, Y., and Wang, S. S. Y. (1993). "3D numerical simulation of flow near a spur dike." *Adv. Hydrosci.*, 1, 2150–2156.
- Jia, Y., and Wang, S. S. Y. (1996). "A modeling approach to predict local scour around spur dike-like structures." *Proc., 6th Federal Interagency Sedimentation Conf.*, Subcommittee on Sedimentation, Interagency Advisory Committee on Water Data. II, 90–97.
- Julien, P.Y. (1995). "Erosion and Sedimentation," Cambridge University Press, Cambridge, UK.
- Kim, S. C., Friedrichs, C.T., Maa, J. P.Y., and Wright, L. D. (2000). "Estimating bottom stress in tidal boundary layer from acoustic Doppler velocimeter data." *J. Hydraul. Eng.*, 126(6), 399–406.
- Klingeman, P. C., Kehe, S. M., and Owusu, Y. A. (1984). "Streambank erosion protection and channel scour manipulation using rockfill dikes and groins." *WRR- 98*, Water Resources Research Institute, Oregon State University, Corvallis, Oregon. 169 pp.
- Koken, M., and Constantinescu, G. (2008). "An investigation of the flow and scour mechanisms around isolated spur dikes in a shallow open channel: 1. Conditions

corresponding to the initiation of the erosion and deposition process.” *Water Resour. Res.*, 44, W08406.

Kraus, N. C., Lohrmann, A., and Cabrera, R. (1994). "New Acoustic Meter for Measuring 3D Laboratory Flows." *J. Hydraul. Eng.*, 120(3), 406-412.

Kuhnle, R. A., Alonso, C. V., and Shields, D. F. (2002). “Local scour associated with angled spur dikes.” *J. Hydraul. Eng.*, 128(12), 1087–1093.

Kuhnle, R. A., Jia, Y., and Alonso, C.V. (2008). “Measured and simulated flow near a submerged spur dike.” *J. Hydraul. Eng.*, 134(7), 916–924.

Kwan, T. F., and Melville, B. W. (1994). “Local scour and flow measurements at bridge abutments.” *J. Hydraul. Res.*, 32(5), 661–673.

Lane, E. W., Kalinske, A.A. (1941). “Engineering calculations of suspended sediment.” *Transactions of the American Geophysical Union.*, 20(3),603-607.

Lauder, B. E., and Spaulding, D. B. (1972). *Mathematical models of turbulence*. Academic Press, New York, N.Y.

Laursen, E. M. (1963). “Analysis of relief bridge scour.” *J. Hydraul. Div., Am. Soc. Civ. Eng.*, 89(3), 93–118.

Lim, S. Y. (1997). “Equilibrium clearwater scour around an abutment.” *J. Hydraul. Eng.*, 123(3), 237–243.

Maddock, T., Jr. (1976). "Equations for resistance to flow and sediment transport in alluvial channels." *Water Resour. Res.*, 12(1), 11-21.

Mayerle, R., Toro, F. M., and Wang, S. S. Y. (1995). “Verification of a three-dimensional numerical model simulation of the flow in the vicinity of spur dikes.” *J. Hydraul. Res.*, 33(2), 243–256.

McCoy, A., Constantinescu, G., and Weber, L. (2007). “A numerical investigation of coherent structures and mass exchange processes in channel flow with two lateral submerged groynes.” *Water Resour. Res.*, 43, W05445, doi: 10.1029/2006WR005267.

Melville, B. W. (1975). “Local scour at bridge sites.” *Rep. No. 117*, Dept. of Civil Engineering, School of Engineering., Univ. of Auckland, Auckland, New Zealand.

Melville, B. W. (1992). “Local scour at bridge abutments.” *J. Hydraul. Eng.*, ASCE, 118(4), 615–631.

- Melville, B. W., and Raudkivi, A. J. (1996). "Effects of foundation geometry on bridge pier scour." *J. Hydraul. Eng.*, 122(4), 203–209.
- Melville, B. W., and Raudkivi, A. J. (1977). "Flow characteristics in local scour at bridge piers." *J. Hydraul. Res.*, 15(4), 373-380.
- Mendoza-Cabrales, C. (1993). "Computation of flow past a cylinder mounted on a flat plate." *Proc., Hydraul. Eng.*, ASCE Reston, Va., 899-904.
- Meyer-Peter, E., and Muller, R. (1948). "Formulas for bed load transport." *Proceedings, second Meeting of International Association for Hydraulic Structures Research*, Stockholm, 26 pp.
- Michiue, M., and Hinokidani, O. (1992). "Calculation of 2-dimensional bed evolution around spur-dike." *Ann. J. Hydraul. Eng.*, 36, 61–66.
- Nagata, N., Hosoda, T., Nakato, T. and Muramoto, Y. (2005). "Three-Dimensional Numerical Model for Flow and Bed Deformation around River Hydraulic Structures." *J. Hydraul. Eng.*, 131(12), 1074-1087.
- Nikora, V. I., and Goring, D. G. (1998). "ADV measurements of turbulence: can we improve their interpretation?" *J. Hydraul. Eng.*, 124(6), 630–634.
- Nikora, V. I., and Goring, D. G. (2000). "Flow turbulence over fixed and weakly mobile gravel beds." *J. Hydraul. Eng.*, 126 (9), 679–690.
- Olsen, N.R.B., and Melaan, M.C. (1993). "Three dimensional calculation of scour around cylinders". *J. Hydraul. Eng.*, ASCE, 119(9), 1048-1054.
- Olsen, N. R. B., and Kjellesvig, H. M. K. (1998). "Three-dimensional numerical flow modeling for estimation of maximum local scour depth." *J. Hydraul. Res.*, 36(4), 579–590.
- Ouillon, S., and Dartus, D. (1997). "Three-dimensional computation of flow around groyne." *J. Hydraul. Eng.*, 123(11), 962–970.
- Pope, N. D., Widdows, J., and Brinsley, M. D. (2006). "Estimation of bed shear stress using turbulent kinetic energy approach – a comparison of annular flume and field data." *Cont. Shelf Res.*, 26, 959–970.
- Posey, C. J. (1949). "Why bridges fail in floods." *Civ. Eng. (N.Y.)*, 19, 42–90.

- Rahman, M. M., Nagata, N., Muramoto, Y., and Murata, H. (1998). "Effect of side slope on flow and scouring around spur-dike-like structures." *Proc., 7th Int. Symp. on River Sedimentation*, Hong Kong, China, 165–171.
- Rajaratnam, N., and Nwachukwu, B. A. (1983). "Flow near groin-like structures." *J. Hydraul. Eng.*, 109(3), 463–480.
- Raudkivi, A. J. (1986). "Functional trends of scour at bridge piers." *J. Hydraul. Eng.*, 112(1), 1–13.
- Raudkivi, A. J. (1990). *Loose boundary hydraulics*, 3rd Ed., Pergamon, New York.
- Raudkivi, A. J., and Ettema, R. (1977). "Effect of sediment gradation on clear water scour." *J. Hydraul. Div., Am. Soc. Civ. Eng.*, 103(10), 1209–1213.
- Raudkivi, A. J., and Ettema, R. (1985). "Scour at cylindrical bridge piers in armored beds." *J. Hydraul. Eng.*, 111(4), 713–731.
- Richardson, J. E., and Panchang, V. G. (1998). "Three-Dimensional Simulation of Scour-Inducing Flow at Bridge Piers." *J. Hydraul. Eng.*, 124(5), 530-540.
- Rodi, W (1980). *Turbulence models and their application in hydraulics: A state of the art Review*. IAHR.
- Roulund, A., Sumer, B. M., Fredsoe, J., and Michelsen, J. (1998). "3D mathematical modelling of scour around a circular pile in current." *Proc., 7th Int. Symp. on River Sedimentation*, Hong Kong, China, 131–137.
- Salaheldin, T. M., Imran, J., and Chaudhry, H. (2004). " Numerical modeling of three-dimensional flow field around circular piers." *J. Hydraul. Eng.*, 130(2), 91-100.
- Shaw, C. T. (1992). *Using computational fluid dynamics*. Prentice Hall, New York, N.Y.
- Shen, H. W., Schneider, V. R., and Karaki, S. (1969). "Local scour around bridge piers." *J. Hydraul. Div., Am. Soc. Civ. Eng.*, 95(6), 1919–1940.
- Shields, F. D., Jr., Cooper, C. M., and Knight, S. S. (1995). "Experiment in stream restoration." *J. Hydraul. Eng.*, 121(6), 494–502.
- Shields, F. D., Bowie, A. J., and Cooper, C. M. (1995a). "Control of stream bank erosion due to bed degradation with vegetation and structure." *Water Resources Bulletin*, 31(3), 475- 489.

Shen, H. W., and Hung, C. S. (1972). "An engineering approach to total bed material load by regression analysis." *Proc., of the Sedimentation Symposium*, Berkeley, Calif., Chap.14, 14.1-14. 7.

Sicilian, J. M., Hirt, C. W., and Harper, R. P. (1987). "FLOW-3D: Computational modeling power for scientists and engineers." *Rep. FSI-8700- 1*, Flow Science, Los Alamos, N.M.

Smith, H. D., and Foster, D. L. (2005). "Modeling of flow around a cylinder over a scoured bed." *Journal of Waterway, Port, Coastal, and Ocean Engineering*, 131(1), 14-24.

Song, T., and Chiew, Y. M. (2001). "Turbulence Measurement in Nonuniform Open-Channel Flow Using Acoustic Doppler Velocimeter (ADV)." *J. Eng. Mech.*, 127(3), 219-232.

SonTek (2001). "Acoustic Doppler velocimeter (ADV) principles of operation." *SonTek ADV Technical Manual*, SonTek, San Diego.

Stevens, M. A., Gasser, M. M., and Saad, M. B. A. M. (1991). "Wake vortex scour at bridge piers." *J. Hydraul. Eng.*, 117(7), 891–904.

Tanaka, T., and Eaton, J. K. (2008). "Classification of turbulence modification by dispersed spheres using a novel dimensionless number." *Phys.l Rev. Letters*, 101, 114502.

Tominaga, A., and Matsumoto, D. (2006). "Diverse riverbed figuration by using skew spur-dike groups." *River Flow 2006–1: Proc. Int. Conf. Fluv. Hydraul.*, Taylor and Francis Group, London, 2006.

Tywoniuk, N. (1972). "Sediment discharge computation procedures." *Journal of the Hydraulics Division*, ASCE, 98(3), 531-5380.

Uijtewaal, W. S. J. (2005). "Effects of groyne layout on the flow in groyne fields: laboratory experiments." *J. Hydraul. Eng.*, 131(9), 782–791.

Vanoni, V. A. (1971). "Sediment Transportation Mechanics: H. Sediment Discharge Formulas." *J. Hydraul. Div.*, ASCE, 97(4), 523-567.

Velikanov, M. A. (1954). "Gravitational theory for sediment transport." *Journal of Science of the Soviet Union, Geophysics*, Vol. 4.

Wahl, T. L. (2000). "Analyzing data using WinADV." *2000 Joint Conf. on Water Resour. Eng. and Water Resour. Planning and Management*, 1–10.

Weitbrecht, V., Uijtewaal, W., and Jirka, G. H. (2003). "2D particle tracking to determine transport characteristics in rivers with dead zones." *Proc., Int. Symp. Shallow Flows*, Delft, the Netherlands, 103–110.

Willis, J.C. (1979). "Suspended load from error-function Models." *J. Hydraul. Div.*, ASCE, 105(7), 801-816.

Yaeger, M.A. (2009). "Mean flow and turbulence around two series of experimental dikes." *MS Thesis*, Department of Hydrology and Water Resources, The University of Arizona, Tucson, AZ, 100 pp.

Yakhot, V., and Orszag, S. A. (1986). "Renormalization group analysis of turbulence." *J. Sci. Comp.*, 1(1), 3.

Yang, C. T. (1973). "Incipient motion and sediment transport." *J. Hydraul. Div.*, ASCE, 99(10), 1679-1704.

Yang, C. T. (1979). "Unit stream power Equations for total load." *Journal of Hydrology*, 40(1-2), 123-138.

Yang, C. T. (1996). *Sediment transport theory and practice*. The McGraw-Hill Companies, Inc., New York.

Yang, C, T., and Molinas, A. (1982). "Sediment transport and unit stream power function." *J. Hydraul. Div.*, ASCE, 108(6), 774-793.

Yang, C. T., and Kong, X. (1991). "Energy dissipation rate and sediment transport." *J. Hydraul. Res.*, 29(4), 457-474.

Yang, S. Q., and Lim, S. Y. (2003). "Total load transport formula for flow in alluvial channels." *J. Hydraul. Eng.*, ASCE, 129(1), 68-72.

Yu, G. L., Lim, S. Y., and Tan, S. K. (2002). "Flow and scouring in main channel due to abutments." *Proc., 1st Int. Conf. on Scour and Erosion*, Tex., 785–794.

Zhang, H., Nakagawa, H., Ishigaki, T, and Muto, Y. (2005). "Prediction of 3D flow field and local scouring around spur dikes." *Ann. J. Hydraul. Eng.*, 49, 1003–1008.

Zhang, H. and Nakagawa, H.(2008). "Scour around spur dyke: recent advances and future researches." *Annals of the Disaster Prevention Research Institute*, Kyoto University.

APPENDICES

APPENDIX A: A UNIFIED TOTAL SEDIMENT LOAD FORMULA

A Unified Total Sediment Load Formula

Anu Acharya¹ and Jennifer G. Duan²

Abstract

Predicting the total sediment load in rivers has been a challenge to river engineers for decades. Although numerous formulae have been developed, none of them is universal for all the rivers. Consequently, engineers have to compare several formulas with field observations to select an appropriate one for a given river reach. To overcome this difficulty, this study evaluated 31 commonly used formulae for predicting the total sediment load which include the early work of *Einstein* [1950], *Yang* [1973], *Brownlie* [1981], and many recent published equations, such as *Molinas and Wu* [2001], *Yang and Lim* [2003], etc. It is well known, at a given flow and sediment condition, the results from these formulae deviate significantly from each other. This study attributed these deviations to the stochastic properties of bed shear stresses. The Monte Carlo simulation was applied to each equation by assuming the bed shear stress obeys the log-normal distribution. Then, at any given bed shear stress, a set of bed shear stresses were randomly generated based on the log-normal distribution. The total sediment loads were calculated by applying all the equations based on these series of bed shear stresses. The statistical properties of the resultant total sediment loads (e.g. standard deviation, mean) at each given bed shear stress were calculated. Then, a unified total sediment load equation is obtained based on the mean value from all the equations. The results showed the mean of all the equations is a power function of dimensionless bed shear stress. 6,999 sets of laboratory and field data were used to verify this statistically derived equation. Reasonable agreements with

¹ Graduate Student, Department of Civil Engineering, the University of Arizona, 1209 E. 2nd Street, Tucson, AZ 85721.

² Assistant Professor, Department of Civil Engineering, the University of Arizona, same address.

measurements demonstrated that this unified equation is more accurate than any individual equation for predicting the total sediment load.

Introduction

The accurate prediction of sediment load in rivers is essential to manage reservoirs, operate dams, and design instream hydraulic structures. Sediment transport rate is a function of flow intensity and sediment properties, such as size, gradation, and density. Since 1914 [Gilbert, 1914], many sediment transport equations were derived for predicting the transport rate of single or multi-grain sized sediment in steady uniform open channel flow. Some of these equations are for the total sediment load that does not differentiate bed load and suspended load, and some only for bed load or suspended load. Among them, the total load equations are the most frequently used by engineering practitioners. For example, the newly developed sediment model in HEC-RAS 4.1 included five total load transport equations and two bed load equations [HEC, 2010]. Although all of the equations were verified and tested by using series of laboratory and field data, results from those equations can be order-of-magnitude different. The inconsistent predictions from those sediment transport formulae indicated that the understanding of sediment transport is still incomplete, especially how instantaneous flow turbulence entrain and transport sediment and how instantaneous bed shear stresses affect sediment motion. Therefore, predicting the total sediment load in rivers is still a challenge to river engineers, which requires a universal equation that unifies the existing equations and gives accurate predictions of existing measurements.

Up to date, the total sediment load equations are based on laboratory and field data collected from steady uniform or gradually varied open channel flows. This study chose 31 commonly used formulae for a single grain-sized sediment, which include the original and modified ones, such as that by *Einstein* [1950], *Velikanov* [1954], the modification of *Einstein's* relationship [Colby and Hembree, 1955], the modification of *Laursen's* relationship [Copeland and Thomas, 1989], *Colby* [1964], *Chang et al.* [1965], *Egiazaroff* [1965], *Bishop et al.* [1965], *Engelund and Hansen* [1967], *Graf et al.* [1968, 1987], *Bagnold* [1966], *Toffaleti* [1969], *Ackers-White* [1973], *Vittal et al.* [1973], the modification of *Ackers-White's* relationship [HR Wallingford, 1990], *Yang* [1973, 1979, 1984, 1996], *Maddock* [1976], the modification of *Engelund and Hansen* [1967] relationship [Vanoni, 1975; *Raudkivi*, 1976], *Brownlie* [1981] and his modified one [Brownlie, 1983], *Ranga Raju et al.* [1981], *Karim and Kennedy* [1982], *Moore and Burch* [1986], *Wu et al.* [2000], *Molinas and Wu* [2001], *Yang and Lim* [2003]. Most of these equations calculated the total sediment load directly, but a few formulas [*Einstein*, 1950; *Colby and Hembree*, 1955; *Chang et al.*, 1965; *Bagnold*, 1966; *Toffaleti*, 1969; *Wu et al.*, 2000] calculated the bed load and suspended load separately and then added them together. Regardless, the total sediment load is the bed material load equals to the sum of bed load and suspended load if calculated separately.

This study attributed the different results from those equations to stochastic characteristics of bed shear stresses [*Duan and Scott*, 2007; *Duan and Barkdoll*, 2008]. All the thirty-one formulae were used to predict the total load for sediment sizes ranging from 0.125 mm to 28 mm and dimensionless bed shear stresses, also called as the Shields parameter, ranging from 0.01 to 25.0. The bed shear stress in each formula is treated as a random variable that satisfies the log-normal distribution. The statistical mean of the total sediment loads from all the formulae is used to

define a unified total load transport formula. This unified equation was tested and verified by using 6,999 sets of measurements consisting of all the original data points used for those formulas.

Methodology

The total sediment load formulae are classified into three categories according to their theoretical basis: formulae based on the advection-diffusion equations; empirical equations based on the regression analysis and graphical methods; formulae based on the energy concept [Julien, 1995]. Not all the existing sediment transport equations can be used for computing the total sediment load because some of them were developed for computing bed load only while others for suspended load only. Table 1 summarized the applicable ranges of sediment size, flow depth, channel slope for those selected equations.

All of the selected formulae are for single-grain sized sediment transported in steady uniform or gradually varied flows. The sediment transport rate is calculated as a function of flow parameters, such as the mean flow velocity, bed shear stress, and sediment properties (e.g. mean size, size gradation, and density). For fully developed turbulent flows, flow velocity relates to the shear velocity through the logarithmic law. Therefore, only the dimensionless shear stress is needed for quantifying flow intensity. Many researchers [Vittal *et al.*, 1973; Engelund and Hansen, 1967; Graf and Acoraglu, 1968; Ranga Raju *et al.*, 1981; Einstein, 1942] suggested calculating the dimensionless sediment transport rate from the dimensionless shear stress. Although it is unlikely to find a common mathematical expression for all the equations, all the equations were converted into a function between a dimensionless sediment transport rate and the dimensionless shear stress. In this study, the Einstein parameter [Einstein, 1942; Meyer-Peter

and Muller, 1948; Wu et al., 2000] denoted as q_s^* was adopted to quantify the dimensionless total sediment transport rate. The Einstein parameter is defined as

$$q_s^* = q_s / [\sqrt{(\gamma_s / \gamma - 1)gd^3}] \quad (1)$$

where q_s is the volumetric sediment transport rate per unit width; γ_s and γ are the specific weights of sediment and water, respectively; d is the sediment size; and g is the gravitational acceleration. The dimensionless shear stress, known as Shields parameter is written as:

$$\Phi = \frac{\tau_0}{(\gamma_s - \gamma)d} \quad (2)$$

where Φ is the dimensionless shear stress; τ_0 is the actual shear stress. The functional relation between the Einstein parameter and the Shields parameter formulate the unified total sediment load equation as follows:

$$q_s^* = f(\Phi, d) \quad (3)$$

where $f(\Phi, d)$ is a function relation that needs to be determined. From Eq.3, only one total load transport rate should be predicted for a sediment size at a given shear stress. However, the results from the existing total sediment load equations vary by orders of magnitude. Those large deviations in results were caused by the stochastic properties of bed shear stresses that resulted in the randomness of sediment transport rate. Therefore, this study assumed that the bed shear stress is a random variable of a log-normal distribution so that the calculated total sediment load from those equations is a random variable. Monte Carlo simulation of each transport equation was then performed at given sediment size and bed shear stress. The total sediment load data generated from each Monte Carlo realization of all the equations are assembled to represent the samples of total sediment load predicted from all the equations. Then, at a given flow, statistical analysis was performed to obtain the mean sediment transport rate of all the samples.

Monte Carlo Simulation

This study assumed the sediment is uniform, and its size varies from 0.125mm to 28mm to be in consistent with available experimental and field data. The bed shear stress is a stochastic variable due to turbulence fluctuations on bed surface, which was found to be either normally [Einstein, 1950] or log-normally distributed [Lopez and Garcia, 1999; Cheng and Law, 2003]. Previous studies [Cheng and Chiew, 1998; Chiew et al., 1998; Miyagi et al., 2000] suggested that the log-normal distribution can be used as an approximation of the probability density function of bed shear stress. The Cheng and Law [2003] experimental study indicated that the log-normal distribution converged to a Gaussian distribution when the relative intensity of bed shear stress, denoted as the ratio between the deviation and mean of bed shear stress, is small. Therefore, this study adopted the assumption that bed shear stress satisfies a standard log-normal distribution as in Cheng and Law [2003] and Duan and Barkdoll [2008]. For the random variable bed shear stress (τ), E_τ and $E_{\ln\tau}$ denote the mean values of τ and $\ln\tau$, respectively. In addition, σ_τ and $\sigma_{\ln\tau}$ denote the standard deviations of τ and $\ln\tau$, respectively. The PDFs for a standard log-normally distributed random variable, bed shear stress (τ), can be expressed as

$$f(\tau : E_{\ln\tau}, \sigma_{\ln\tau}) = \begin{cases} \frac{1}{\sqrt{2\pi}\sigma_{\ln\tau}\tau} \exp\left[\frac{-(\ln\tau - E_{\ln\tau})^2}{2\sigma_{\ln\tau}^2}\right] & \tau \geq 0 \\ 0 & \tau < 0 \end{cases} \quad (4)$$

where the mathematical expectation and standard deviation of τ are written as

$$E_\tau = e^{\frac{E_{\ln\tau} + \frac{\sigma_{\ln\tau}^2}{2}}}, \quad \sigma_\tau = E_\tau \sqrt{e^{\sigma_{\ln\tau}^2} - 1} \quad (5)$$

If $I_\tau = \frac{\sigma_\tau}{E_\tau}$ represents the relative intensity of bed shear stress, the relations between the

mathematical expectation and standard deviation of $\ln\tau$ can be written as follows,

$$\sigma_{\ln \tau} = \sqrt{\ln(1 + I_{\tau}^2)} \text{ and } E_{\ln \tau} = \ln \frac{E_{\tau}}{\sqrt{1 + I_{\tau}^2}} \quad (6)$$

Duan and Barkdoll [2008] derived an empirical relation of the relative intensity of bed shear stress based on the data in *Cheng and Law* [2003] as follows:

$$I_{\tau} = \alpha (R_e)^{\beta} \quad R_e \geq 1,000 \quad (7)$$

where $R_e = \frac{uh}{\nu}$ is the flow Reynolds number, in which u is flow velocity, h is flow depth, and ν is kinetic viscosity; $\alpha = 150.0$ and $\beta = -0.671$ are constant coefficients based on the best curve fitting of the experimental data. At low Reynolds number, I_{τ} decreases rapidly as flow Reynolds number increases. At high Reynolds number, $R_e > 100,000$, I_{τ} reaches to a constant value of 0.05 [*Duan and Barkdoll*, 2008]. I_{τ} ranges from 0.04 to 0.12 for *Wilcock* (1992) experiments where Re value ranged from 40,000 to 200,000 [*Duan and Barkdoll*, 2008]. This study assumes $I_{\tau} = 0.05$ because most of the available experimental and field data measurements are obtained at fully turbulent flows with Reynolds number greater than 100,000.

Because the dimensionless shear stress is an independent stochastic variable in each individual equation, the Monte Carlo simulation was carried on for each equation in which the bed shear stress is considered as a random variable with PDF expressed in Eq.4. At a given sediment size and shear stress, 1,000 samples were selected for shear stresses so that a total of 1,000 realizations were obtained from each equation. Therefore, at each bed shear stress and sediment size, each sediment formula yielded 1,000 total sediment load predictions. A total of 31,000 total load transport rates were predicted from the 31 equations. The realizations are sufficient because additional realizations did not change the statistic properties of the output, the total sediment load.

Results

The statistical properties (e.g. mean, standard deviation) of total sediment load at each sediment size and bed shear stress were calculated using 31,000 samples. Figure 1 shows the relationship between the mean dimensionless shear stress (Φ) and the mean dimensionless sediment transport parameter (q_s^*). The least square curve fitting gives an empirical relation as follows:

$$q_s^* = 10.69\Phi^{3.08} \quad (8)$$

Eq.8 is based on the statistical mean of predicted total sediment load from all the 31 equations that unifies the predictions from each individual equation, hereafter is called the unified total load equation. The correlation coefficient between the dimensionless shear stress and the dimensionless transport rate is 0.99, indicating the mean total load transport rate highly depends on the mean dimensionless shear stress.

The statistically derived equation, Eq.8, is compared with several original total sediment load equations. To avoid cloudy overlapped lines, only some of the equations are shown in Fig. 2. *Yang and Lim* [2003], *Maddock* [1976], *Graf et al.* [1968, 1987], and *Velikanov* [1954] are the closest ones to the unified equation. *Vittal et al.* [1973], *Bishop et al.* [1965], *Yang* [1973, 1996], *Moore and Burch* [1986], *Ackers and White* [1973] systematically over-predict the total sediment load. *Colby* [1964], *Yang* [1984] and *Chang et al.* [1965], also over-predict the total sediment load at low shear stresses whereas under-predict at high shear stresses. *Karim and Kennedy* [1981], and *Bagnold* [1966] under-predict the equation at low shear stress whereas over-predict at high shear stresses.

Einstein [1950], *Colby and Hembree* [1955], *Engelund and Hansen* [1967], *Ranga Raju et al.* [1981], *Copeland and Thomas* [1989], *Vanoni and Raudkivi* [1975, 1976], *Toffaleti* [1969], and

Egiazaroff [1965] generally under-predict the sediment load. *Rottner* [1959], *Molinas and Wu* [2001], *HR Wallingford* [1990], *Yang* [1979], *Brownlie* [1983] over-predict the equation at low shear stresses but are in good agreements with Eq.8 at high bed shear stresses.

The unified total load equation is also verified by using 6,999 sets of laboratory and field data in canals and natural rivers, having a wide range of sediment and stream characteristics. These data cover sediment sizes ranging from 0.011 mm to 76.113 mm, flow depth from 0.0091m to 17.28 m, velocity from 0.086 m/s to 6.180 m/s, channel slope from 0.000003 to 0.0367. Details of these data sources and relevant flow and sediment ranges are summarized in Table 2. Eq.8 was used to calculate the total sediment load using measured flow velocity and sediment size. At first, the shear velocity was calculated from the depth-averaged velocity using the logarithmic law,

$$\frac{V}{u_*} = 5.75 \log\left(\frac{12.27R}{K_s}\right) \quad (9)$$

in which V is depth-averaged flow velocity, u_* is shear velocity given as: $u_* = \sqrt{\frac{\tau_0}{\rho}}$, in which ρ is the density of water, R is the hydraulic radius, and K_s is the roughness height that varies from d_{50} to $3.5d_{90}$ depending on bed material composition [*Chien and Wan*, 1999]. Since the sediment is uniform, $K_s = d$ suggested by *Einstein* [1950] was used in this study. Secondly, the dimensionless shear stress was calculated by $\Phi = \frac{\tau_0}{(\gamma_s - \gamma)d}$. Thirdly, Eq.8 was used to calculate the total load transport rate. Results from Eq.8 were then compared with the measured total sediment load shown in Figure 3. With the exception of some of the measured points, the computed results agreed very well with 6,999 measurements from flume and natural rivers. The

root mean square error (RMSE), mean absolute error (MAE), bias (%) and Nash-Sutcliffe efficiency (E) were calculated as follows to determine the accuracy of the unified equation.

$$RMSE = \sqrt{\frac{1}{n} \sum_{i=1}^n (O_i - P_i)^2}, MAE = \frac{1}{n} \sum_{i=1}^n |O_i - P_i|, E = 1 - \frac{\sum_{i=1}^n (O_i - P_i)^2}{\sum_{i=1}^n (O_i - \bar{O})^2} \quad (10)$$

where O_i and P_i are the observed and predicted values, respectively; \bar{O} is the mean of the observed data; and n is the number of observations. The root mean square error of the calculated and measured total sediment load is approximately 1490 parts per million (ppm). The mean absolute error is 710 ppm. Since $MAE < RMSE$, the errors at each individual measured point could vary significantly. The Nash-Sutcliffe efficiency is 0.82, nearly a unit, indicating Eq.8 is more accurate than any individual equation for this data set. The standard deviation of the difference between the measured and calculated total sediment concentrations is approximately 1300 ppm. Over 75% of measured data fell within 95% confidence interval of Eq.8.

Discussion

This study is an attempt to unify the existing total sediment transport formulae by the Monte Carlo simulations. The authors believe the different results from individual total load equation are outcomes of stochastically distributed bed shear stresses. The analysis assumed the bed shear stresses satisfy the log-normal distribution. The proposed unified equation (Eq.8) is obtained by using the statistical mean of total load predictions from 31 of the commonly used formulae. Although several existing total load transport formulae are very close to Eq.8 at a given range of shear stresses, none of the formulae matches Eq.8 for the entire range of shear stresses. Therefore, Eq.8 can be considered as a general representation of all the existing equations.

On the other hand, results from Eq.8 were compared with 6,999 sets of laboratory and field data. More than 75% of the observed data fall in the 95% confidence interval of Eq.8. The Nash-Sutcliff coefficient and RMSE both showed the high accuracy of the proposed unified equation. However, the bias indicates that the unified equation still over-predicts the measurements. Further examinations of individual equation and inclusions of more data sets are needed to improve the accuracy of Eq.8.

Up to date, no universal sediment transport equation exists. The unified equation (Eq.8) is averaging the predictions from all the equations. This unified equation predicted the mean value of the possible results from all the equation, which is much accurate than any individual equation. This unified equation can be used for river engineers to estimate the total sediment load without examining individual equation, especially when field data is available. It is extremely beneficial to sediment transport models in which many sediment transport formulae have to be programmed [*Duan and Julien, 2010; Duan and Nanda, 2006*]. A hydrodynamic and sediment transport analysis does not have to run with each individual sediment transport formula, but this unified equation. Unless flow and sediment compositions are unique in a given river reach, this study believe the unified equation will give better predictions than any individual formula.

Conclusions

This study aims to formulate a general relation between the dimensionless sediment transport parameter and the dimensionless bed shear stress. To achieve this, the bed shear stress is treated as a random variable having a log-normal distribution. Monte Carlo simulations were applied to each existing sediment transport formula at a given flow and sediment size to obtain sufficient samples of sediment load predictions. Then, the mean value of all the predictions was correlated with the dimensionless shear stress to formulate a unified total load transport formula.

Comparisons of the unified equation with a total of 6,999 sets of laboratory and field data indicated that the statistically derived equation yielded excellent agreements with measurements.

This unified formula has advantages over existing formulae because it is not only the average of results from many existing formulae but also the most accurate one for this intensive data set. The unified formula will be an excellent choice to river engineers if no sediment measurement is available. This formula is limited to sediment size of 0.0125mm to 28mm, dimensionless shear stress defined as the Shields parameter from 0.01 to 25. However, due to the limitations and assumptions adopted in each individual transport equation, this study has not found an appropriate probability density distribution function to represent the distribution of each sediment load prediction. Future analysis will examine individual sediment transport equations for sediment mixture of non-uniform size.

Notation

The following symbols are used in this paper:

d	= sediment size (mm);
d_{50}, d_{90}	= sediment sizes in which 50% and 90% sediments are finer (mm);
E_{τ} and $E_{\ln \tau}$	= mean values of τ and $\ln \tau$, respectively;
$f(\Phi, d)$	= function relation;
h	= flow depth (m);
$I_{\tau} = \frac{\sigma_{\tau}}{E_{\tau}}$	= relative intensity of bed shear stress;
g	= gravitational acceleration (m/s^2);
K_s	= roughness height (mm);

n	= number of observations;
O_i	= observed value;
\bar{O}	= mean of the observed data;
P_i	= predicted value;
q_s	= volumetric sediment transport rate per unit width (m^2/s);
q_s^*	= dimensionless total sediment transport rate;
R	= hydraulic radius (m);
R_e	= flow Reynolds number;
u	= flow velocity (m/s);
u_*	= shear velocity (m/s);
V	= depth-averaged flow velocity (m/s);
Φ	= dimensionless shear stress;
$\alpha = 150.0$ $\beta = -0.671$	= constant coefficients;
γ_s and γ	= specific weights of sediment and water, respectively (N/m^3);
ν	= kinetic viscosity (m^2);
ρ	= density of water (kg/m^3);
σ_τ and $\sigma_{\ln \tau}$	= standard deviations of τ and $\ln \tau$, respectively;
τ_0	= actual shear stress (Pa);
τ	= random variable bed shear stress (Pa).

References

- Abdel-Aal, Farouk, M. (1969) "Extension of bed load formula to high sediment rates." *PhD Thesis*, University of California, Berkeley.
- Ackers, P., and White, W. R. (1973). "Sediment transport: New approach and analysis." *J. Hydraul. Div.*, ASCE, 99(11), 2041-2060.
- Bagnold, R. A. (1966). "An approach to the sediment transport problem from General Physics." *U. S. Geological Survey Professional Paper 4221*, U.S. Government Printing Office, Washington, D.C.
- Barton, J. R., and Lin, P.N. (1955). "A study of the sediment transport in alluvial channels." *Report No. CEF 55JRB2*, Colorado State University, Fort Collins, Colorado, 41 pp.
- Bishop, A. A., Simons, D. B., and Richardson, E.V. (1965). "A total bed-material transport." *J. Hydraul. Div.*, ASCE, 91(2), 175-191.
- Borgardi, J., and Yen, C. H. (1939). "Traction of pebbles by flowing water." *PhD Thesis*, State University of Iowa, 66 pp.
- Brownlie, W. R. (1981). "Prediction of flow depth and sediment discharge in open channels." *W. M. Keck Laboratory of Hydraulics and Water Resources*, Report No. KH-R-43A, Division of Engineering and Applied Science, California Institute of Technology, Pasadena, California, 232 pp.
- Brownlie, W. R. (1982). "Prediction of flow depth and sediment discharge in open channels." *PhD Thesis*, California Institute of Technology, Pasadena, California, 423.
- Brownlie, W. R. (1983). "Flow depth in sand-bed channels." *J. Hydraul. Eng.*, ASCE, 109(7), 959-990.

- Casey, H.J. (1935). "Uber Geschiebebewegung." Preuss. Versuchsanst. für Wasserbau und Schiffbau, Berlin, Mitt., 19, 86 pp. (Translation on file at U.S. Soil Conservation Service, Washington, D.C.).
- Chang, F. M., Simons, D. B., and Richardson, E. V. (1965). "Total bed-material discharge in alluvial channels." *U. S. Geological Survey Water-Supply Paper* 1498-I.
- Chaudhry, H. M., Smith, K. V. H. and Vigil, H. (1970). "Computation of sediment transport in irrigation canals." *Proc. Institution of Civil Engineers*, 45, 79-101.
- Cheng, N. S., and Chiew, Y.M. (1998). "Pick-up probability for sediment entrainment." *J. Hydraul. Eng.*, ASCE, 124(2), 232-235.
- Cheng, N. S., and Law, A. W. K. (2003). "Fluctuations of turbulent bed shear stress." *Journal of Engineering Mechanics*, ASCE, 129(1), 126-130.
- Chien, N., and Wan, Z. (1999). "Mechanics of sediment transport." ASCE, Reston, Virginia, 913 pp.
- Chiew, Y. T., Khoo, B. C., Lim, P.C., and Teo, C. J. (1998). "Dynamic response of a hot-wire anemometer. Part II: A flush-mounted hot-wires and hot-film probes for wall shear stress measurements." *Mes. Sci. Technol.*, 9, 764-778.
- Chitales, S. V. (1966). "Hydraulics of stable channels." Tables 13 and 17, Government of India, Ministry of Irrigation and Power, Central Water and Power Commission.
- Chyn, S.D. (1935). "An experimental study of the sand transporting capacity of the flowing water on sandy bed and the effect of the composition of the sand." *MS. Thesis*, Massachusetts Institute of Technology, Cambridge, Massachusetts, 33 pp.
- Colby, B. R. (1964). "Practical computations of bed-material discharge." *J. Hydraul. Div.*, ASCE, 90(2), 217-246.

- Colby, B. R. and Hembree, C.H. (1955). "Computation of total sediment discharge, Niobrara River near Cody, Nebraska." *U. S. Geological Survey Water-Supply Paper* 1357, 187 pp.
- Copeland, R. R. and Thomas, W. A. (1989). "Corte Madera Creek sedimentation study." *Technical Report HL 89-6.*, USACE, Waterways Experiment Station, Vicksburg, MS.
- Costello, W.R. (1974). "Development of bed configuration in coarse sands." *Report 74-1*, Department of Earth and Planetary Science, Massachusetts Institute of Technology, Cambridge, Massachusetts.
- Culbertson, J.K., Scott, C. H. and Bennett, J. P. (1972). "Summary of alluvial-channel data from Rio Grande conveyance channel, New Mexico, 1965-69." *Professional Paper 562-J*, United States Geological Survey, Washington, D.C., 49 pp.
- Davies, T. R. (1971). "Summary of experimental data for flume tests over fine sand." Department of Civil Engineering, University of Southampton.
- Duan, J. G., and Barkdoll, B. D. (2008). "Surface-based fractional transport predictor: Deterministic or stochastic." *J. Hydraul. Eng.*, ASCE, 134(3), 350-353.
- Duan, J. G. and Julien, P. Y. (2010). "Numerical simulation of meandering evolution." *Journal of Hydrology*, in press.
- Duan, J. G. and Nanda, S. K. (2006). "Two-dimensional depth-averaged model simulation of suspended sediment concentration distribution in a groyne field." *Journal of Hydrology*, 327 (3-4), 426-437.
- Duan, J. G. and Scott, S. (2007). "Selective bed-load transport in Las Vegas Wash, a gravel-bed stream." *Journal of Hydrology*, 342 (3-4), 320-330.

- East Pakistan Water and Power Development Authority (1966, 1967, 1968, 1969). "Flume studies of roughness and sediment transport of movable bed of sand." Annual Report of Hydraulic Research Laboratory for 1966, 1967, 1968-1969, Dacca.
- Egiazaroff, I. V. (1965). "Calculation of non-uniform sediment concentrations." *J. Hydraul. Div.*, ASCE, 91(4), 225–247.
- Einstein, H.A. (1942). "Formulas for the transportation of bed load." *Transactions of the ASCE*, 107, 561-573.
- Einstein, H.A. (1944). "Bed load transportation in Mountain Creek," *U.S. Soil Conservation Service*, SCS-TP-55, 50 pp.
- Einstein, H. A. (1950). "The bed-load function for sediment transportation in open channel flows." *Technical Bulletin No. 1026*, U. S. Department of Agriculture, Soil Conservation Service., 70 pp.
- Einstein, H. A. and Chien, N. (1955). "Effects of heavy sediment concentration near the bed on velocity and sediment distribution." MRP Series No. 8, University of California, Institute of Engineering Research and U.S. Army Engineering Division, Missouri River Corps of Engineers, Omaha, Nebraska.
- Engelund, F., and Hansen, E. (1967). "A monograph on sediment transport in alluvial streams." *Teknisk Forlag.*, Technical Press, Copenhagen, Denmark, 62 pp.
- Foley, M. G. (1975). "Scour and fill in ephemeral streams." *W. M. Keck Laboratory Report No. KH-R-33*, California Institute of Technology, Pasadena, California.
- Franco, J. J. (1968). "Effects of water temperature on bed-load movement." *Journal of Waterways and Harbors Division*, ASCE, 94(WW3), Proc. Paper 6083, 343-352.

- Gibbs, C. H., and Neill, C. R. (1972). "Interim report on laboratory study of basket-type bed-load samplers." Research Council of Alberta in association with Department of Civil Engineering, University of Alberta, No. REH/72/2.
- Gilbert, G. K. (1914). "The transportation of debris by running water." *U. S Geological Survey, Professional Paper 86*, Washington D.C., U.S.
- Graf, W. H., and Acaroglu, E.R. (1968). "A physical model for sediment transport in conveyance systems." *Bull., Int. Assoc. Scient. Hydrology.*, 13(3).
- Graf, W.H., and Suszka, L. (1987). "Sediment transport in steep channels." *J. Hydrosoc. and Hydr. Eng.*, 5 (1).HR Wallingford (1990). Sediment transport, the Ackers and White theory revised, Report SR237, England.
- Guy, H. P., Simons, D. B. and Richardson, E. V. (1966). "Summary of alluvial channel data from flume experiments, 1956-61." *U.S. Geological Survey, Professional Paper 462-1*, 96 pp.
- Hill, H. M., Srinivasan, V.S., and Unny, T. E., Jr. (1969) "Instability of flat bed in alluvial channels." *J. Hydraul. Div., ASCE*, 95(5), 1545-1558.
- Ho, P. Y. (1939) "Abhängigkeit der geschiebebewegung von der kornform und der temperature." *Preuss. Versuchsanst. für Wasserbau and Schiffbau*, Berlin, Mitt., 37,43 pp.
- Hubbell, D. W. and Matejka, D. Q. (1959). "Investigation of sediment transportation, Middle Loup River at Dunning, Nebraska." *U.S. Geological Survey, Water Supply Paper No. 1476*.
- HR Wallingford (1990). "Sediment transport, the Ackers and White theory revised." *Report SR237*, England.
- Johnson, J. W. (1943). "Laboratory investigations on bed-load transportation and bed roughness." *U.S. Soil Conservation Service, SCS-TP-50*.

- Jorissen, A. L. (1938). "Etude experimentale du transport solide des cours d'eau." *Revue Universelle des Mines, Belgium*, 14(3), 269-282.
- Julien, P.Y. (1995). "Erosion and Sedimentation," Cambridge University Press, Cambridge, UK.
- Karim, F. M., and Kennedy, J. F. (1981). "Computer-based predictors for sediment discharge and friction factor of alluvial streams." *Report No. 242, Iowa Inst.of Hydraul. Res.*, Univ. of Iowa, Iowa City, Iowa.
- Kennedy, J. F. (1961). "Stationary waves and anti-dunes in alluvial channels." *Report KH-R-2, W. M. Keck Laboratory of Hydraulics and Water Resources*, California Institute of Technology, Pasadena, California.
- Kennedy, J. F. and Brooks, N. H. (1963). "Laboratory study of an alluvial stream of constant discharge." *Proceedings, Federal Inter-Agency Sediment Conference, Misc. Pub. 970*, U.S. Department of Agriculture, 320-330.
- Knott, J.M. (1974). "Sediment discharge in the Trinity River basin, California," *Water-Resources Investigations 49-73, U. S. Geological Survey*, 62 pp.
- Lopez, F., and Garcia, M. H. (1999). "Wall Similarity in Open Channels: Universal value of the Normalized Vertical Flux of Turbulent Kinetic Energy." *Journal of Engineering Mechanics, Special issue on turbulence, ASCE*, 125(7), 789-796.
- MacDougall, C. H. (1933). "Bed-sediment transportation in open channels," *Transactions of the Annual Meeting 14, American Geophysical Union*, 491-495.
- Mahmood, K., et al. (1979). "Selected equilibrium-State data from ACOP Canals." *Civil, Mechanical and Environmental Engineering Department Report No. EWR-79-2*, George Washington University, Washington, D.C., 495 pp.

- Maddock, T., Jr. (1976). "Equations for resistance to flow and sediment transport in alluvial channels." *Water Resour. Res.*, 12(1), 11-21.
- Mavis, F. T., Liu, T., and Soucek, E. (1937) "The transportation of Detritus by flowing water - II." *Iowa University Studies in Engineering, Bulletin 11*, 28 pp.
- Meyer-Peter, E., and Muller, R. (1948). "Formulas for bed load transport." *Proceedings, second Meeting of International Association for Hydraulic Structures Research*, Stockholm, 26 pp.
- Milhaus, R.T. (1973). "Sediment transport in a gravel-bottomed stream," *PhD Thesis*, Oregon State University, 232 pp.
- Miyagi, N., Kimura, M., Shoji, H., Saima, A., Ho, C. M., Tung, S., and Tai, Y. C. (2000). "Statistical analysis on wall shear stress of turbulent boundary layer in a channel flow using micro-shear stress imager." *Int. J. Heat Fluid Flow*, 21, 576-581.
- Molinas, A., and Wu, B. (2001). "Transport of sediment in large sand-bed rivers." *J. Hydraul. Res.*, 39 (2), 135-146.
- Moore, I.D., and Burch, G.J. (1986). "Sediment transport capacity of sheet and rill flow: application of unit stream power theory." *Water Resour. Res.*, 22(8), 1350-1360.
- Mutter, D. G. (1971). "A flume study of alluvial bed configurations." *Master Thesis*, Faculty of Graduate Studies, University of Alberta.
- National Research Council (1950). "Flume studies on bed movement of Fraser River model." Unpublished Report, Experiments conducted at University of British Columbia, Vancouver, Canada.
- NEDECO (1973). "Rio Magdalena and Canal del Dique project, Mission Tecnica Colombo-Holandesa." NEDECO Report, NEDECO, Hague.

- Nordin, C. F., Jr. (1976). "Flume studies with fine and coarse sands." Open File Report 76-762, *U.S. Geological Survey*, Washington, D.C., 18 pp.
- Nordin, C. F., and Beverage, J. P. (1965). "Sediment transport in the Rio Grande, New Mexico." Professional Paper 462-F, *U.S. Geological Survey*, Washington, D.C., 35 pp.
- O'Brien, M. P. (1936). "Notes on the transportation of silt by streams." Transactions of the Annual Meeting 17, *American Geophysical Union*, 431-436.
- Onishi, Y., Jain, S. C., and Kennedy, J. R. (1976). "Effects of meandering in alluvial channels." *J. Hydraul. Div.*, ASCE, 102(7), 899-917.
- Peterson, A. W., and Howells, R. F. (1973). "A compendium of solids transport data for mobile boundary channels." *Report No. HY-1973-ST3*, Department of Civil Engineering, University of Alberta, Canada.
- Pratt, C. J. (1970). "Summary of experimental data for flume tests over 0.49 mm sand." Department of Civil Engineering, University of Southampton.
- Ranga Raju, K. G., Garde, R. J. and Bhardwaj, R. (1981). "Total load transport in alluvial channels." *J. Hydraul. Div.*, ASCE, 107(2), 179-191.
- Raudkivi, A. J. (1976). "Loose boundary hydraulics," 2nd ed., Pergamon press Ltd., Oxford, United Kingdom, 397 pp.
- Rottner, J. (1959). "A formula for bed-load transport." *La Houille Blanche*. 3, 301-307.
- Samide, G. W. (1971). "Sediment transport measurements." *Master's Thesis*, University of Alberta.
- Sato, S., Kikkawa, H. and Ashida, K. (1958). "Research on the bed load transportation." *Journal of Research*, Public Works Research Institute, Research Paper 3, Construction Ministry, Tokyo, Japan, 3, 21 pp.

- Seitz, H. R. (1976). "Suspended and bed-load sediment transport in the Snake and Clearwater Rivers in the vicinity of Lewiston, Idaho." File Report 76-886, *U. S. Geological Survey*, Boise, Idaho, 77 pp.
- Shen, H. W., Mellema, W. J. and Harrison, A.S. (1978). "Temperature and Missouri river stages near Omaha." *J. Hydraul. Div.*, ASCE, 104(1), 1-20.
- Shinohara, K., and Tsubaki, T. (1959). "On the characteristics of sand waves formed upon beds of the open channels and rivers." Reprinted from reports of Research Institute of Applied Mechanics, Kyushu University, VII(25).
- Simons, D. B. (1957). "Theory of design of stable channels in alluvial materials," *PhD Thesis*, Colorado State University.
- Singh, B. (1960). "Transport of bed-load in channels with special reference to gradient form," *PhD Thesis*, University of London, London, England.
- Soni, J. P. (1980). "Short statistical analysis of total load concentration." *J. Hydraul. Div.*, ASCE, 106(8), 1383-1389.
- Stein, R. A. (1965). "Laboratory studies of total load and apparent bed load." *Journal of Geophysical Research*, 70(8), 1831-1842.
- Straub, L. G. (1954). "Transportation characteristics Missouri River sediment." *M.R.D. Sediment Series* No. 4, St. Anthony Falls Hydraulic Laboratory, Minneapolis, Minnesota.
- Straub, L. G., Anderson, A. G. and Flammer, G. H. (1958). "Experiments on the influence of temperature on the sediment load." *M.R.D. Sediment Series* No. 10, St. Anthony Falls Hydraulic Laboratory, Minneapolis, Minnesota.

- Taylor, B. D. (1971). "Temperature effects in alluvial streams." *W. M. Keck Laboratory of Hydraulics and Water Resources Report KH-R-27*, California Institute of Technology, Pasadena, California, 204 pp.
- Toffaleti, F. B. (1968). "A procedure for computation of the total river sand discharge and detailed distribution, bed to surface." *Technical Report No. 5*, Committee on Channel Stabilization, U. S. Army Corps of Engineers Waterways Experiment Station, Vicksburg.
- Toffaleti, F. B. (1969). "Definitive computations of sand discharge in Rivers." *J. Hydraul. Div.*, ASCE, 95(1), 225-246.
- United States Army Corps of Engineers, U.S. Waterways experiment station, Vicksburg, Mississippi (1935a). "Studies of river bed materials and their movement with special reference to the lower Mississippi River." Paper 17, 161 pp.
- United States Army Corps of Engineers, U.S. Waterways experiment station, Vicksburg, Mississippi (1935 b). "Effect of turbidity on sand movement." unpublished report of experiments.
- United States Army Corps of Engineers, U.S. Waterways experiment station, Vicksburg, Mississippi (1936a). "Flume tests made to develop a synthetic sand which will not form ripples when used in movable-bed models." *Technical Memorandum 99-1 (unpublished)*, 21 pp.
- United States Army Corps of Engineers, U.S. Waterways experiment station, Vicksburg, Mississippi (1936 b). "Flume tests of synthetic sand mixtures (sand No. 10)." *Technical Memorandum 95-1 (unpublished)*, 21 pp.
- United States Army Corps of Engineers, U.S. Waterways experiment station, Vicksburg, Mississippi (1936 c). "Studies of light-weight materials, with special reference to their

- movement and use as model bed material," *Technical Memorandum 103-1* (unpublished), 56 pp.
- United States Department of the Interior, Bureau of Reclamation (1958). "Interim report, total sediment transport program, Lower Colorado River Basin," 175 pp.
- U.S. Army Corps of Engineers (2010). "HEC-RAS River analysis system." Hydraulic Reference Manual (Version 4.1), Hydrologic Engineering Center, Davis, California.
- Vanoni, V. A. (1975). "ASCE Manuals and Reports on Engineering Practice." *Sedimentation Engineering*, 54, 745pp.
- Vanoni, V. A., and Brooks, N. H. (1957). "Laboratory studies of the roughness and suspended load of alluvial streams." *M.R.D. Sediment Series No. 11*, California Institute of Technology Sedimentation Laboratory, 121 pp.
- Vanoni, V. A., and Hwang, L. S. (1967). "Relation between bed forms and friction in streams." *J. Hydraul. Div.*, ASCE, 93, (3), Proc. Paper 5242, 121-144.
- Velikanov, M. A. (1954). "Gravitational theory for sediment transport." *Journal of Science of the Soviet Union, Geophysics*, Vol. 4 (in Russian).
- Vittal, N., Ranga Raju, K. G., and Garde, R. J. (1973). "Sediment transport relations using concept of effective shear stress." *Proceedings., International Association for Hydraulic Research, International Symposium on River Mechanics*, Bangkok, Thailand, 489-499.
- West Bengal, Government of. (1965). "Study on the critical tractive force various grades of sand." Annual Report of the River Research Institute, West Bengal, Publication No. 26 (I), 5-12.

- Wilcock, P. R. (1992). Experimental investigation of the effect of mixture properties on transport dynamics, in *Dynamics of Gravel-Bed Rivers*, edited by P. Billi et al., 109–130, John Wiley, New York.
- Williams, G. P. (1970). "Flume width and water depth effects in sediment transport experiments." *U. S. Geological Survey*, Professional Paper 562-H.
- Willis, J. C. (1979). "Suspended load from error-function Models." *J. Hydraul. Div.*, ASCE, 105(7), 801-816.
- Wu, W., Wang, S. S., and Jia, Y. (2000). "Non-uniform sediment transport in alluvial rivers." *J. Hydraul. Res.* 38 (6), 427–434.
- Yang, C, T. (1973). "Incipient motion and sediment transport." *J. Hydraul. Div.*, ASCE, 99(10), 1679-1704.
- Yang, C, T. (1979). "Unit stream power Equations for total load." *Journal of Hydrology*, 40(1-2), 123-138.
- Yang, C.T. (1984). "Unit stream power and sediment transport." *J. Hydraul. Eng.*, ASCE, 110 (12), 1783–1797.
- Yang, C. T. (1996). "Sediment transport theory and practice." The McGraw-Hill Companies, Inc., New York.
- Yang, C. T., Molinas, A., and Wu, B. (1996). "Sediment transport in the Yellow River." *J. Hydraul. Eng.*, ASCE, 122(5), 237-244.
- Yang, S. Q. and Lim, S. Y. (2003). "Total load transport formula for flow in alluvial channels." *J. Hydraul. Eng.*, ASCE, 129(1), 68-72.

Znamenskaya, N. S. (1963). "Experimental study of the dune movement of sediment."
Transactions of the State Hydrologic Institute (Trudy GGI), 108, 89-111. Translated by L. G.
Robbins.

Table 1. Applicable Ranges of Total Sediment Load Transport Equations

Number	Sediment Function	Sediment size (mm)	Mean size (mm)	Specific gravity	Velocity (m/s)	Flow depth (m)	Channel slope (S x1000)	Channel width (m)	Water temperature (°F)
1	Ackers -White (1973)	0.040-7.00	NA	1.00-2.70	0.021-2.164	0.003-0.427	0.060-37.000	0.070-1.220	46-89
2	Engelund - Hansen (1967)	NA	0.19-0.93	2.65	0.198-1.933	0.058-0.405	0.055-0.019	2.44	45-93
3	Copeland - Lausen (1989)	0.011-290.000	NA	0.70-9.40	0.009-1.097	0.00007-0.008	0.250-25.000	0.076-1109.756	32-93
4	Tofaletti (1969)	0.062-4.000	0.09-0.91	2.65	0.213-2.378	0.021-17.287	0.140-19.000	0.244-1109.756	32-93
5	Yang (1972)	0.150-7.000	NA	2.65	0.243-1.951	0.012-15.244	0.043-29.000	0.134-533.537	32-94
6	Bagnold (1966)	0.120-200.000	NA	2.65	0.244-2.134	0.091-2.287	12.400-25.800	0.235-6.548	35-86
7	Bishop et al. (1965)	0.190-0.930	0.37	1.87-2.65	0.200-1.897	0.030-0.405	0.055-19.280	0.610-2.439	44-94
8	Brownlie (1981)	0.062-0-76.000	0.08-2.80	2.65	0.008-3.719	0.009-17.282	0.002-36.700	0.021-1109.000	32-146
9	Brownlie (1983)	0.062-76.000	0.08-2.80	2.65	0.008-3.719	0.009-17.282	0.0021-36.700	0.021-1109.000	32-146
10	Chang et al. (1965)	NA	0.19-0.93	2.65	0.091-0.305	0.019-0.488	1.000-15.000	2.439	34-100
11	Colby (1964)	0.100-0.800	0.20-0.30	2.65	0.030-3.049	0.030-30.488	0.010-18.000	0.267-2.439	40-80
12	Einstein (1950)	NA	0.06-8.00	2.65	0.020-0.063	0.152-3.049	1.000-1.050	1.524-198.171	32-95
13	Egiazaroff (1965)	0.050-20.000	0.07-0.77	2.65	NA	NA	0.900-11.000	NA	36-96
14	Karim- Kennedy (1981)	NA	0.13-28.65	2.65	0.300-2.700	0.030-5.900	0.080-24.300	0.610-2.440	33-100
15	Graf et al. (1968)	0.010-30.000	0.30-1.70	2.65	0.198-2.134	0.091-0.400	0.500-1.000	0.065-3.865	35-90
16	Graf et al. (1987)	0.010-28.000	0.30-1.70	2.65	0.152-2.350	0.065-0.500	0.300-1.900	0.700-5.090	35-90
17	Colby- Hembree (1955)	0.031-28.600	0.19-4.00	2.65	0.268-2.220	0.108-2.134	12.400-25.800	21.341-36.585	35-85
18	Vanoni -Raudkivi (1975,1976)	NA	0.19-0.93	2.65	0.198-1.933	0.058-0.405	0.055-19.000	2.439-2.500	45-93
19	Maddock (1976)	0.001-100.000	0.40-2.35	2.65	0.622-0.878	0.183-0.200	0.600-3.200	0.305-1.341	35-86
20	HR Wallingford (1990)	0.040-7.000	NA	1.00-2.70	0.021-2.165	0.003-0.427	0.060-37.000	0.070-1.220	46-89
21	Yang (1979)	0.062-2.000	0.15-1.71	2.65	0.230-1.970	0.010-15.198	0.043-27.900	0.116-532.012	32-94
22	Yang (1984)	3.170-7.010	NA	2.65	0.221-1.549	0.009-0.226	0.120-13.400	0.200-0.400	32-94
23	Yang et al. (1996)	0.007-0.091	NA	2.65	0.260-5.470	0.509-11.290	0.010-0.100	55.000-1500.000	87-88
24	Yang-Lim (2003)	0.400-7.650	0.83-3.54	2.65	0.150-0.733	0.020-0.220	0.500-1.000	0.061-1.000	34-111
25	Moore-Burch (1986)	0.100-10.000	0.06-2.00	2.65	0.183-2.134	0.010-16.250	1.000-40.000	0.105-4.000	50-69
26	Velikanov (1954)	0.033-3.250	NA	2.65	0.150-2.845	0.010-4.635	0.010-32.500	NA	NA

Number	Sediment Function	Sediment size (mm)	Mean size (mm)	Specific gravity	Velocity (m/s)	Flow depth (m)	Channel slope (S x1000)	Channel width (m)	Water temperature (°F)
27	Vittal et al. (1973)	0.009-12.652	0.01-7.36	2.65	0.091-4.350	0.020-11.260	0.080-18.735	0.070-260.583	32-96
28	RangaRaju et al. (1981)	0.007-9.856	0.01-3.60	2.65	0.126-2.500	0.017-10.000	0.090-16.000	0.067-253.963	32-98
29	Wu et al. (2000)	0.010-128.000	0.06-2.37	2.65	0.140-2.800	0.030-4.400	0.110-16.200	0.204-558.130	42-96
30	Molinas-Wu (2001)	0.090-1.300	0.10-0.90	2.65	0.230-1.670	0.056-1.496	0.930-12.700	0.260-46.630	33-77
31	Rottner (1959)	0.150-7.000	NA	2.65	0.198-2.546	0.003-14.924	0.060-30.568	0.020-35.625	40-95

Table 2. Details of Experimental and Field Data of Total Sediment Load

No (1)	Source Description (2)	No. of data points (3)	Size of sediment (mm) (4)	Width (m) (5)	Flow depth (m)		Velocity (m/s)		Slope (S x 1000)	
					Min (6)	Max (7)	Min (8)	Max (9)	Min (10)	Max (11)
1	Abdel-Aal, F. M. (1969)	10	0.11	0.31	0.09	0.14	0.38	0.89	1.70	2.50
2	Barton, J.R., Lin, P. N. (1955)	28	0.18	1.22	0.09	0.42	0.23	1.09	0.44	2.10
3	Government of West Bengal (1965) ¹	18	0.32	0.46	0.01	0.16	0.14	0.29	0.20	1.00
4	Bogardi, J., Yen, C. H. (1939)	48	10.34	0.82	0.04	0.20	0.29	0.99	10.90	24.80
5	Vanoni, V.A., and Brooks, N. H., (1957) ¹	21	0.15	0.27	0.05	0.09	0.25	0.65	1.30	3.50
6	Casey, H. J. (1935)	92	2.46	0.40	0.01	0.22	0.22	0.75	1.19	5.19
7	Chyn, S.D. (1935)	32	0.79	0.61	0.05	0.10	0.37	0.59	1.11	3.00
8	Costello, W. R. (1974)	28	0.51	0.92	0.14	0.16	0.29	0.50	0.05	1.01
9	Davies, T. R. (1971)	79	0.15	1.37	0.08	0.30	0.22	0.79	0.11	2.67
10	Einstein, H. A., Chien, N. (1955)	16	0.27-1.30	0.31	0.11	0.14	1.87	2.22	12.40	25.80
11	E. Pakistan Water and Power (1967) ¹	68	0.16-0.44	1.22	0.09	0.31	0.24	0.71	0.14	3.80
12	Gov. of E. Pakistan (1966,1968,1969) ¹	56	0.15	1.22	0.11	0.39	0.19	0.86	0.05	3.00
13	Foley, M. (1975)	12	0.29	0.27	0.03	0.05	0.39	0.80	3.74	10.63
14	Franco, J. J. (1968)	19	0.23	0.91	0.13	0.16	0.26	0.45	0.23	1.69
15	Gibbs, C. H., Niell, C. R. (1972)	9	4.37	1.22	0.17	0.18	0.75	0.95	2.90	5.00
16	Gilbert, G. K. (1914) ¹	889	0.30-7.01	0.07-0.60	0.01	0.23	0.23	1.55	0.12	31.00
17	Gilbert, G. K. (1914) ¹	125	0.30-1.71	0.20-0.60	0.02	0.17	0.52	1.37	0.30	24.30
18	Gilbert, G. K. (1914) ¹	62	0.30-0.79	0.20-0.60	0.02	0.18	0.34	0.97	1.12	13.38
19	Guy, H. P., et al. (1966)	339	0.19-0.93	0.61-2.44	0.06	0.41	0.20	1.90	0.06	19.28
20	Hill, H. M., et al. (1969)	46	0.09-0.31	0.61	0.16	0.26	0.59	1.17	0.52	2.68
21	Ho, P. (1939) ¹	80	1.40-6.28	0.40	0.08	0.26	0.21	1.02	0.99	5.04
22	Jorissen, A. L. (1938) ¹	26	0.60-0.91	0.61	0.02	0.10	0.26	0.57	1.11	3.33
23	Karim, F., Kennedy, J.F.(1981)-0.19mm	29	0.19	8.00	0.49	1.09	1.04	4.74	0.43	9.50

No (1)	Source Description (2)	No. of data points (3)	Size of sediment (mm) (4)	Width (m) (5)	Flow depth (m)		Velocity (m/s)		Slope (S x 1000)	
					Min (6)	Max (7)	Min (8)	Max (9)	Min (10)	Max (11)
24	Karim, F., Kennedy, J.F.(1981)-0.27mm	17	0.27	8.00	0.45	1.13	1.33	4.93	0.65	10.22
25	Karim, F., Kennedy, J.F.(1981)-0.28 mm	32	0.28	8.00	0.30	1.07	1.04	4.93	0.63	10.00
26	Karim, F., Kennedy, J.F.(1981)-0.32 mm	29	0.32	2.00	0.54	0.74	1.24	5.73	0.86	16.20
27	Karim, F., Kennedy, J.F.(1981)-0.45 mm	27	0.45	8.00	0.19	1.00	1.30	6.18	0.78	10.10
28	Karim, F., Kennedy, J.F.(1981)-0.93 mm	23	0.93	8.00	0.38	1.11	1.80	5.86	1.30	12.60
29	Karim, F., Kennedy, J.F.(1981)-1.35 mm	24	1.35	8.00	0.29	0.52	1.54	3.49	1.33	10.88
30	Kennedy, J. F. (1961)	41	0.23-0.55	0.26-0.85	0.02	0.11	0.41	1.42	1.70	27.20
31	Kennedy, J. F., Brooks, N. H. (1965)	9	0.14	0.85	0.07	0.17	0.28	0.67	0.56	2.50
32	Mavis, F. T., et al. (1937)	293	1.41-4.18	0.82	0.01	0.13	0.29	0.86	1.25	10.10
33	MacDougal, C. H. (1933) ¹	74	0.26-1.26	0.61	0.02	0.16	0.32	0.68	1.11	3.33
34	Meyer-Peter, E., Muller, R. (1948)	135	0.34-28.65	2.00	0.01	1.09	0.38	2.88	0.42	22.70
35	Mutter, D.G. (1971)	28	0.26	1.22	0.01	0.10	0.13	0.79	0.75	7.50
36	National Research Council (1950) ²	16	0.18-0.80	0.50	0.05	0.14	0.36	0.97	1.18	6.20
37	Neill, C. R. (1967) ¹	51	3.99-20.00	0.89-0.91	0.03	0.18	0.11	1.07	1.20	27.00
38	Nomicos, G. (1957) ¹	30	0.09-0.15	0.27	0.07	0.09	0.25	0.81	1.90	3.90
39	Nordin, C. F. (1976)	62	0.25-1.14	2.38	0.24	0.86	0.37	2.02	0.14	5.77
40	O'Brien, M. P. (1936)	83	0.36-0.36	0.91	0.08	0.33	0.21	0.95	0.29	3.23
41	Onishi, Y., et al. (1972)	14	0.25	0.91	0.08	0.14	0.34	0.59	1.09	2.67
42	Pratt, C. J. (1970)	60	0.48	1.37	0.08	0.46	0.14	0.70	0.02	2.87
43	Sato, S., et al. (1958)	243	1.03-4.58	0.76-0.78	0.11	0.52	0.22	1.53	0.22	3.03
44	Singh, B. (1960)	305	0.62	0.25-0.75	0.01	0.20	0.23	0.87	1.00	14.00
45	Soni, J. P. (1980)	23	0.32	0.20	0.02	0.10	0.22	0.61	2.07	7.00
46	Stein, R. A. (1965)	56	0.40	1.22	0.09	0.37	0.42	1.84	0.61	16.95
47	Straub, L. G. (1954, 1958)	24	0.16-0.19	0.30-0.91	0.03	0.24	0.34	0.84	0.56	7.35
48	Taylor, B. D. (1971)	39	0.14-2.81	0.26-0.85	0.06	0.18	0.20	3.72	0.25	3.72
49	US Waterways Exp. Sta. (1935A) ¹	330	0.18-4.10	0.74	0.01	0.21	0.15	0.73	1.00	4.50

No (1)	Source Description (2)	No. of data points (3)	Size of sediment (mm) (4)	Width (m) (5)	Flow depth (m)		Velocity (m/s)		Slope (S x 1000)	
					Min (6)	Max (7)	Min (8)	Max (9)	Min (10)	Max (11)
50	US Waterways Exp. Sta. (1936A) ¹	102	0.95	0.70	0.03	0.20	0.34	0.58	1.00	2.00
51	US Waterways Exp. Sta. (1936C) ¹	298	0.83-0.96	0.31	0.04	0.21	0.28	0.51	0.50	1.50
52	US Waterways Exp. Sta. (1936B) ¹	313	0.35-1.20	0.31	0.07	0.28	0.28	0.57	1.00	1.00
53	US Waterways Exp. Sta. (1935B) ¹	23	0.50	0.06-0.15	0.06	0.15	0.35	0.51	1.00	1.00
54	Vanoni, V. A. , Brooks, N. H. (1957)	15	0.14	0.85	0.06	0.17	0.23	0.77	0.39	2.80
55	Vanoni, V. A., Hwang, L.S. (1965) ¹	16	0.21-0.23	0.26-1.10	0.07	0.37	0.19	0.56	0.46	2.90
56	Willis, J. C. (1979)	32	0.54	0.36	0.10	0.15	0.33	1.20	0.83	8.58
57	Williams, G. P. (1970)	177	1.35	0.07-1.19	0.03	0.22	0.33	2.35	0.60	36.70
58	Znamenskaya, N. S. (1963)	36	0.18-0.80	0.50	0.04	0.20	0.22	0.98	1.18	8.00
^a 59	ACOP Canal, Mahmood, K., et al. (1979)	151	0.08-0.33	35.36-135.94	0.76	3.72	0.35	1.29	0.05	0.15
^a 60	American Canal, Simons, D. B. (1957)	11	0.09-7.00	3.20-22.19	0.80	2.59	0.42	0.77	0.06	0.33
^a 61	Atchafalaya River, Toffaleti, F. B. (1968)	72	0.08-1.00	304.80-503.20	6.10	14.75	0.21	2.03	0.00	0.05
^a 62	Canal Data, Chitale, S. V. (1966)	32	0.02-0.08	4.30-79.10	0.67	3.56	0.38	1.05	0.06	0.16
^a 63	Chop Canals, Chaudhry, et al. (1970)	66	0.09-0.31	23.77-121.62	1.31	3.41	0.69	1.60	0.05	0.25
^a 64	Colorado River, U. S. Bureau of Reclamation (1958)	131	0.15-0.69	91.44-254.55	0.85	3.89	0.36	1.29	0.04	0.41
^a 65	Elkhorn River data ³	23	0.23	NA	2.05	6.19	1.60	6.00	0.29	0.47
^a 66	HII River, Shinohara, K., Tsubaki, T. (1959)	38	0.21-1.46	0.35-8.00	0.02	0.73	0.14	0.93	0.84	11.30
^a 67	River Data, Leopold, L. B. (1969) ²	72	0.14-0.81	88.69-250.55	0.85	4.11	0.36	1.32	0.04	0.35
^a 68	Middle Loup River, Hubbell, D., Matejka, D. (1959)	38	0.21-0.43	37.49-46.63	0.25	0.41	0.59	1.12	0.93	1.57
^a 69	Mississippi River, Toffaleti, F. B. (1968)	165	0.16-1.13	455.98-1109.50	4.66	17.28	0.62	2.42	0.01	0.13
^a 70	Missouri River, Shen, H. W., et al. (1978)	25	0.19-0.27	194.34-223.54	2.77	5.00	1.29	1.76	0.12	0.17

No (1)	Source Description (2)	No. of data points (3)	Size of sediment (mm) (4)	Width (m) (5)	Flow depth (m)		Velocity (m/s)		Slope (S x 1000)	
					Min (6)	Max (7)	Min (8)	Max (9)	Min (10)	Max (11)
^a 71	Mountain Creek, Einstein, H. A. (1944)	100	0.28-0.90	3.29-4.33	0.04	0.44	0.37	1.35	1.36	3.15
^a 72	Niobrara River , Colby, B.R., Hembree, C. H. (1955)	40	0.21-0.36	21.03-21.95	0.40	0.59	0.62	1.27	1.14	1.80
^a 73	North Saskatchewan Riv. & Elbow Riv., Samide, G. W. (1971)	55	13.60-76.11	3.04-6.09	0.73	2.74	1.78	3.32	1.53	7.45
^a 74	Oak Creek, Oregon, Milhous, R. T. (1973)	17	8.20-27.00	4.22-5.91	0.31	0.53	0.81	1.12	9.70	12.60
^a 75	Portugal Rivers, Da Cunha, L. V. (1969) ²	219	2.20-2.60	69.60-188.94	0.46	2.44	0.64	1.44	0.54	0.97
^a 76	Red River , Toffaleti, F. B.(1968)	30	0.09-0.22	130.45-182.88	3.00	7.38	0.37	1.14	0.06	0.08
^a 77	Rio Grande Conveyance Channel, Culbertson, J. K., et al. (1976)	33	0.16-0.28	16.76-22.86	0.39	1.51	0.51	1.69	0.45	0.80
^a 78	Rio Grande River, Nordin, C.F., Beverage, C.P. (1965)	293	0.17-10.96	7.92-121.92	0.16	3.12	0.19	2.38	0.69	2.46
^a 79	Rio Grande near Bernalillo, N.M., Toffaleti, F. B. (1968)	38	0.20-0.37	40.53-196.60	0.33	1.46	0.62	2.38	0.74	0.89
^a 80	Rio Magdalena and Canal del Dique, NEDCO (1973)	113	0.10-1.08	27.00-845.00	1.32	13.28	0.09	1.89	0.00	0.62
^a 81	Snake and Clearwater River, Seitz, H.R. (1976)	21	0.40-33.00	137.16-198.12	4.02	5.91	1.68	3.00	0.25	1.21
^a 82	Trinity River, Knott, J. M. (1974)	4	3.40-11.80	30.18	0.66	1.20	1.27	2.18	2.60	3.00

^aRiver and Canal data.

¹Data source: Brownlie(1982).

²Data source: Peterson and Howells (1973).

³Data Source: Karim and Kennedy(1981).

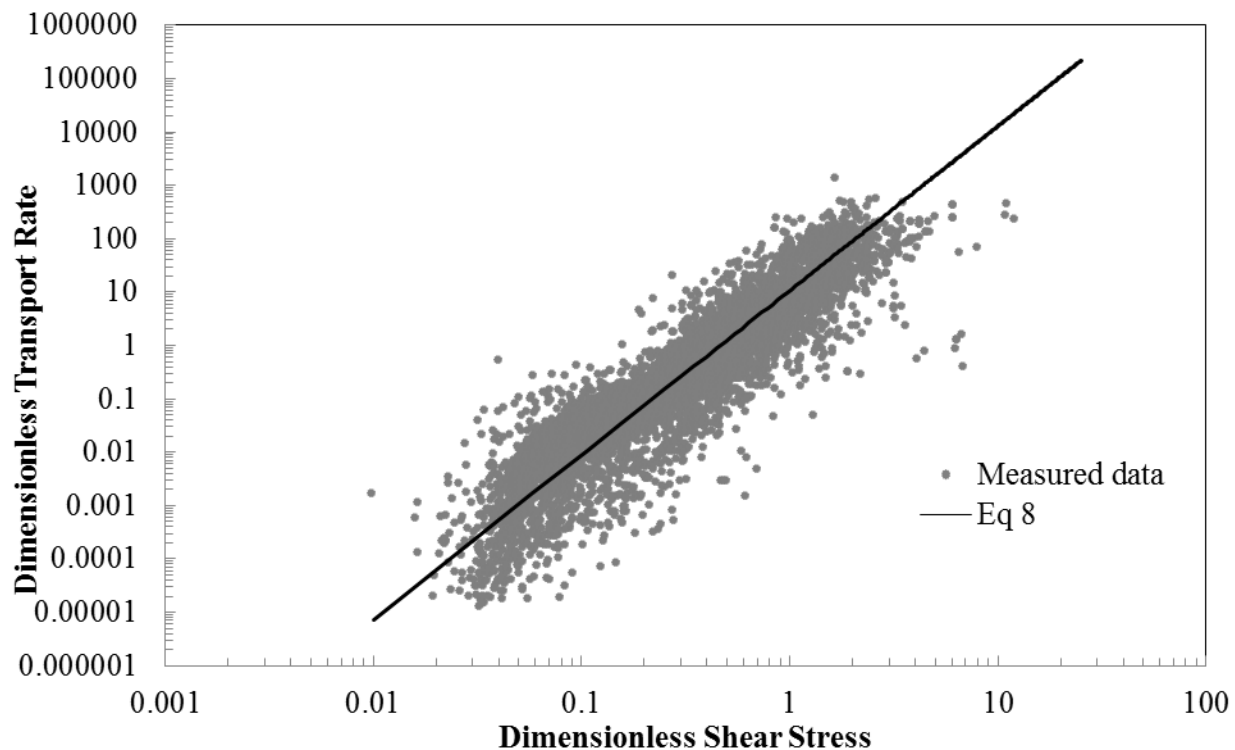


Fig. 1. Mean dimensionless total load vs dimensionless shear stress

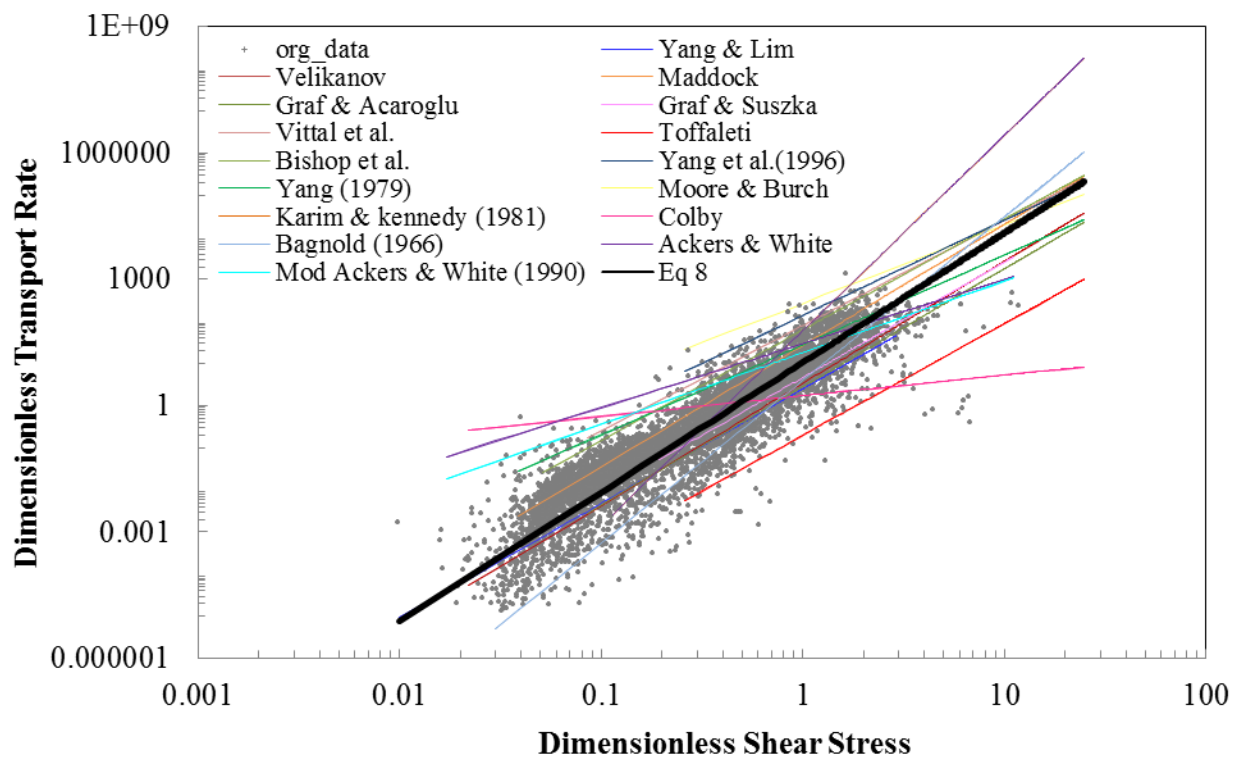


Fig.2. Comparison of Eq.8 with other total load equations

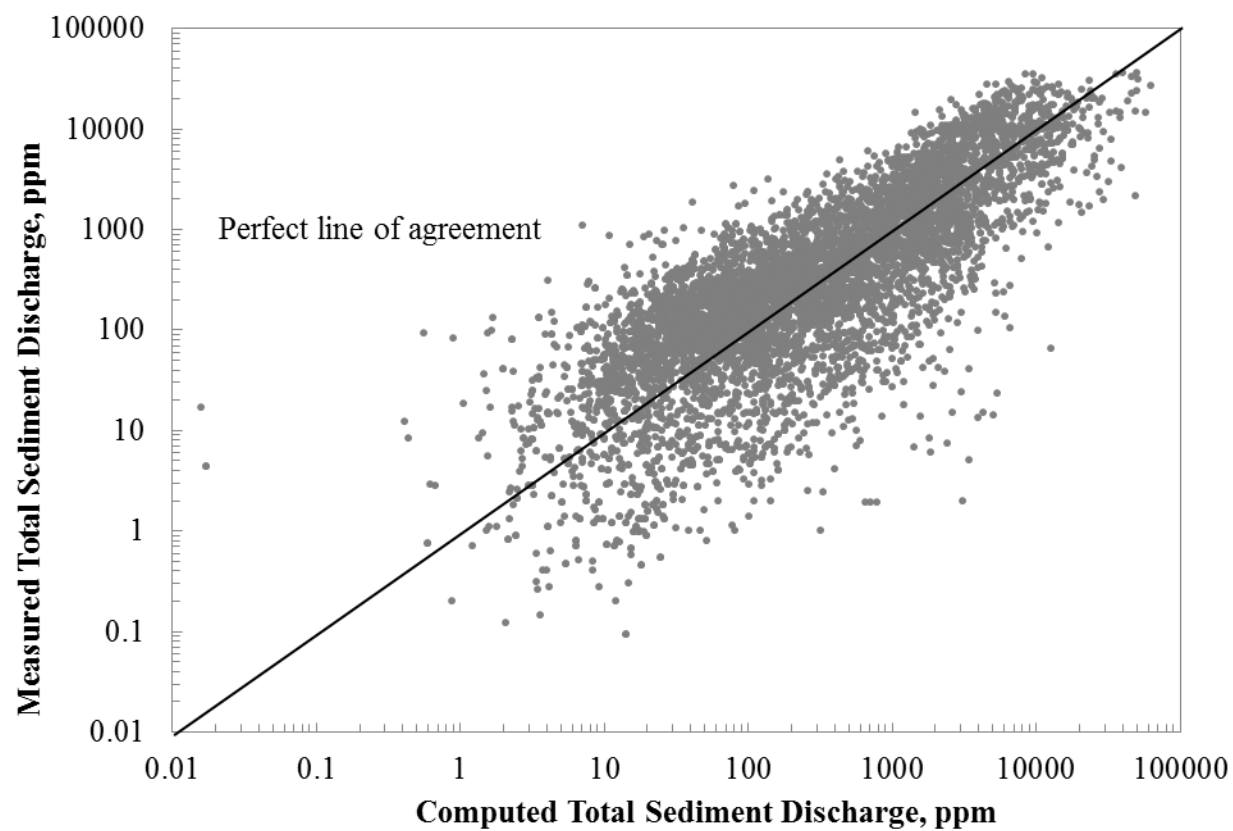


Fig. 3. Comparison of calculated and measured total sediment load

APPENDIX B: NEAR-BED TURBULENCE AND LOCAL SCOUR
AROUND SERIES OF THREE DIKES

Near-Bed Turbulence and Local Scour around Series of Three Dikes

Jennifer G. Duan¹, Mary A. Yaeger², and Anu Acharya³

Abstract

Predicting scour around a series of dike structures in open channel flow has challenged river engineers for decades. Flow turbulence around structures initiates erosion and facilitates the development of local scour. However, the influence of turbulence flow properties, bed shear stress, and sediment transport on the scour depth has not been fully understood. Additionally, there is no consensus on which mean or turbulence flow property determines the scour depth, and whether or not the scour depth is proportional to bed shear stress. Therefore, an experimental study of near-bed turbulence and bed shear stress distributions around a series of three dikes was conducted in a fixed and then a mobile bed laboratory flume. A micro-Acoustic Doppler Velocimeter (ADV) was used to measure velocities near the bed in all three spatial directions and then the turbulence intensities and Reynolds stresses were calculated from these measurements. Results showed the maximum bed shear stress, occurring at the tip of the second dike in the three-dike series, does not correspond to the maximum scour. Rather the local scour develops around the first dike where the mean vertical flow \bar{w} is the largest toward the bed and the turbulence intensity, w' is the largest away from the bed in the series. The results showed that higher shear stresses can transport more bed load, but not necessarily result in local scour. The

¹Assistant Professor, Department of Civil Engineering and Engineering Mechanics, Univ. of Arizona, Tucson, Arizona.

²Graduate Student, Department of Civil and Environmental Engineering, Univ. of Illinois, Urbana-Champaign, Illinois

³Graduate Student, Department of Civil Engineering and Engineering Mechanics, Univ. of Arizona, Tucson, Arizona.

turbulence intensity together with the mean velocity in the vertical direction measured at the fixed, flat bed determines the scour depth.

Subject headings: Reynolds stress, local scour, Spur dike, Turbulence, Bed Shear Stress

Introduction

Erosion of the banks and bed of natural and manmade channels is a common problem in water resources management (Duan 2005). Spur dikes in rivers and streams such as the Mississippi River are used to prevent bank erosion and to keep the main channel navigable. These structures extend from the bank into the stream flow, perpendicularly or at some angle. Most are emergent from the water surface only during low flows, becoming submerged during flood events (Duan and Nanda 2006). Scour around these and other structures such as bridge piers can be a serious problem, weakening structural stability. To understand the mechanism of scour around such hydraulic structures, the questions of what are the turbulence distributions around these structures and how the turbulent flow field affects sediment transport must be answered. In addition, it is important to determine which turbulence properties are more important in predicting the local scour as well as the sediment transport rate. Better understanding of these processes will aid river engineers in designing better embankments for preventing bank erosion and scour. This knowledge will also benefit river restoration projects, as areas around these embankments and dikes are often habitats for vegetation and fish (Hildrew 1996).

Theoretical studies have derived equations describing the bed shear stress in turbulent flows (Dey and Lambert, 2005; McLean and Nikora, 2006; Coleman and Nikora, 2008; Tanaka

and Eaton, 2008). Many modeling studies using large eddy simulations (LES) have determined the location and amount of scour that will occur around embankments, abutments, dikes, piers and other obstructions to flow (Zhang, et al, 2005; Yossef and Rupprecht, 2006; Haltigin, et. al, 2007; Koken and Constantiescu, 2008; McCoy, et al, 2007). Often these theoretical and numerical studies are validated with experimental observations using dye tracers. LES simulated results shed light on the detailed turbulence vorticity field near structures, which has not been measured in the laboratory. In addition, experiments have been carried out in laboratory flumes to determine the effects of engineering structures on the flow (Uijttewaal 2005). Laser visualization techniques, particle image velocimetry (PIV), and instruments such as acoustic Doppler velocimeters (ADV), have been used extensively in recent years to determine flow fields around spur dikes, abutments, and the like. Three-dimensional measurements of velocity can then be used to determine turbulence intensities, Reynolds stresses and shear stress. Studies using fixed, flat beds often measure Reynolds stresses and bed shear stress in an attempt to predict where scour will take place if the bed were mobile. Dey and Barbhuiya (2005) used an ADV to examine the turbulent flow field around a short rectangular abutment oriented 90° to the flow, starting with the fixed rough plane bed condition, and ending with the equilibrium scour hole condition. It was determined from the two experiments that the maximum bed shear stresses were about 3.2 times that of the incoming flow. Because the bed shear stress τ_b was greater than that of the critical shear stress τ_c of the sand forming the bed, the majority of the plane bed would have scoured had it been mobile. A later study by Kuhnle et al (2008) used an ADV to examine the three-dimensional flow field around a submerged spur dike with sloped sides, oriented 90° from the bank. An amplification factor of three was found for the bed shear stresses around this

dike, compared to earlier studies of emergent, straight-sided dikes, which had amplification factors of about 3 to 5 times that of the incoming flow. A third flume experiment using similar techniques was done by Duan (2009) and Duan et al. (2009) in which a single dike (a flat rectangular metal plate) was placed 90° to the wall of a flume with a fixed, flat bed. In this case, the bed shear stress calculated from the Reynolds stresses was 2–3 times that of the incoming flow. In spite of the differences in dike shape and flow Reynolds number, all three studies showed similar amplification factors of bed shear stress.

Dikes angled in the direction of flow (oriented with a downstream skew) attract the flow towards the banks. Dikes angled against the direction of flow (oriented with an upstream skew) repel the flow, directing it towards the main channel. Dikes oriented perpendicular to the flow deflect it, similar to the upstream-skewed dikes, but with less vorticity near the tip (Zhang and Nakagawa, 2008). Several studies have been done on the effects of orientation angle on the amount of scour around a spur dike. One such study examined the effects of three different orientation angles on scour around spur dikes (Kuhnle et al, 2002) for the purposes of creating scour holes for aquatic habitats while at the same time minimizing bank erosion. A series of flume experiments was performed using a short, angled, submerged spur dike with sloped sides. Results indicated that the least bank erosion occurred when the dike was oriented 90° from the bank, and the greatest amount of scour occurred near the 135° dikes (45° from the bank, upstream skew) with only a little more bank erosion occurring than for the 90° dikes. Similar results were seen by Tominaga and Matsumoto (2006) in an experiment using flat slabs of wood as model spur dikes in a sand bed flume. The dikes were arranged in alternating series of three, on both sides of the flume, and remained submerged throughout the experiment. For both the

135° case and the 90° case, the maximum scour was mainly seen around the dike tips, with some deposition on the sides, and with the greatest scour occurring in the upstream skew dikes. For submerged dikes in series, the maximum scour was located around the tip of the first dike. Biron et al (2005) also examined the effects of orientation angle on turbulent flow. The study included both emerged and submerged flow, and plane bed and mobile bed. Results also showed that the location of maximum shear stress in the plane bed runs did not spatially coincide with the location of the maximum scour in the mobile bed runs. The maximum bed shear stress was located downstream of the dikes, with a maximum amplification factor of 12 to 15. The 90° oriented dikes produced the highest bed shear stresses, both for emerged and submerged flows; with the 135° emerged dikes having slightly smaller bed shear stress amplification.

In the present experimental study, the flow field was measured around two series of three spur dikes installed at an open channel with flat and mobile bed surfaces by using a SonTek 16-MHz micro-ADV. Time histories for velocities in all three spatial dimensions were recorded near the bed at cross sections perpendicular to the walls of the flume. These measurements were used to study the turbulent flow field and bed shear stress distributions around series of dikes of different alignments and the correlations between near-bed turbulence and scour depth. These results, which include flow turbulence, locally increased bed-shear stress, and scour depth, will be used to explain the initiation and progression of local scour.

Experimental Set-up

An experimental study was conducted in a 0.6 m wide, 12.2 m long flume with a flat, fixed bed (Figure 1). The left wall of the flume was painted metal and the right wall of the flume

was painted metal with a 3 m long smooth glass observation section roughly in the middle of its length. A 10 cm high broad-crested weir was installed at the end of the flume to measure volumetric discharge. The weir equation $Q = KLH^{1.5}$, where L is the crest length in meter, H is the height of water flowing over the weir in meter, and K is a constant, was used. For this study, $K = 6678$ (for units of m^3/hr).

This study chose a 16 MHz SonTek micro-ADV to measure the instantaneous velocities in the three spatial directions in the flume at a sampling rate of 25 Hz. The sampling volume was about 5 cm below the probe tip, thus allowing for unimpeded sampling of the flow. The sample volume is a cylinder of diameter 4.0 mm and height of 5.6 mm. Micro- ADVs have been used in many recent experiments of turbulent flow either in flume studies as mentioned earlier or in the field (Nikora and Goring, 2000; Sukhodolov et al. 2004; Tritico and Hotchkiss, 2005; Stone and Hotchkiss, 2007). The accuracy of ADVs for various turbulence applications has been well-documented (Voulgaris and Trowbridge, 1998; Nikora and Goring, 1998; Gratiot et al, 2000; McLelland and Nicholas, 2000; Garcia et al, 2005; Abad and Garcia, 2009). Research into new data filtering methods to assure ADV data quality is ongoing. Goring and Nikora (2002) proposed a phase-space de-spiking algorithm for ADV data, and this method has been incorporated into the publicly available WinADV data processing program used in this study (Wahl, 2000). Recently, Cea et al (2007) developed a new filtering process for ADV data gathered in highly turbulent flows, but after comparing the method to available ones found that the SNR as a filter is not good because it varies with the flow properties. Finelli et al (1999) evaluated the spatial resolution of the ADV for near-bed flows, found that the system incorrectly calculated the transmitter-to-bed distance, and therefore underestimated the near-bed velocities.

Therefore, careful monitoring of signal quality is required to assure proper placement of the ADV probe for near-bed applications. In this study, about 5,000 measurements were taken to ensure at least 1,000 good measurements for the near bed nodes. According to the manufacturer, the signal-to-noise ratio is a function of turbidity, i.e. the amount of particulate matter in the flow. For high-frequency measurements ($> 25\text{Hz}$), a signal-noise-ratio (SNR) > 15 decibels (db) is recommended. When the three-dimensional velocity measurements are to be used to determine turbulence properties, an SNR > 15 db is required. In addition, the manufacturer also recommends a correlation score (COR) between 70% and 100%. However, highly turbulent or aerated flows can cause the COR to be much lower than this recommended range. This phenomenon was noticed in this study, especially at nodes around the dikes and when the flow was particularly aerated at the highest flow. When only the mean velocity properties are desired, a COR of near 30% is considered sufficient (SonTek, 2001).

In this study, the publicly available WinADV software from SonTek was used for the post-processing of the raw data. The filtering criteria used was SNR > 15 db, as well as the Nikora-Goring despiking algorithm (Wahl, 2000) incorporated into the software. For the smallest flow, SNR > 10 had to be used, since the flow velocity was so small that an insufficient amount of data points had SNR > 15 . The averaged COR is from 60 to 80 for all the filtered data.

Experimental Procedure

To study the effects of dike placement and the relation between flow turbulence and the local scour, three sets of experimental runs were performed: one with a series of three deflecting dikes perpendicular to the direction of flow on a fixed flat bed; the second with three repelling dikes angled into the direction of flow on the same flat bed; and the third with the same angled

dikes but on a mobile bed. Each model dike was made of 40 cm tall, 15 cm long, and 4 mm thick metal plate. The model dikes were placed a distance of 30 cm apart, and protruded 15 cm into the flow, about $\frac{1}{4}$ the width of the flume. The second set was for three dikes skewed toward upstream at 30° to the left wall, which are modeled as three metal plates 40 cm tall, 30 cm long and 4 mm thick (Figure 2). In the second set of experimental runs, the dikes were spaced 30 cm apart and protruded into the channel the same distance (15 cm) as the straight dikes, but at a different angle (Figure 2). This study chose the dike deflection angle of 30° to mimic dikes used in the Spanish Creek Restoration design (Weller, 2005), which is different from the 45° deflecting angle in other experiments (Biron et al. 2004). The first two sets of experiment consisted of three runs with discharges of $0.013\text{m}^3/\text{s}$, $0.035\text{m}^3/\text{s}$ and $0.065\text{m}^3/\text{s}$, respectively. The third experiment was performed on a mobile bed having three angled dikes at a discharge of $0.035\text{m}^3/\text{s}$. Table 1 summarizes flow parameters (e.g. discharge, velocity, flow depth) of the experimental runs.

Flow properties of the approaching flow were measured at the unaffected flow reach upstream of the first dike. A full velocity profile consisting of 5 verticals starting about 5 mm from the bed and extending at 1 cm intervals to 5 cm from the water surface was measured at a distance greater than $2l$ upstream from the first dike, where l is the length of a dike. This was 33 cm for the 90° dikes and 63 cm for the 150° dikes. This was done in order to establish the mean and unaffected flow properties in the flume. The mean flow velocity and the shear velocity of the approaching flow, obtained through a linear regression analysis and summarized in Table 1, were then used to non-dimensionalize the near-bed velocities, turbulence intensities and Reynolds stresses.

The turbulent flow field around the dikes was measured in a grid, at 5 mm from the bed and starting 10 cm from the left wall and extending to 10 cm from the right wall, as seen in Figure 2. The ADV was mounted on an instrument carriage, held in place by a specially made milled-aluminum vise. The size of the vise was such that measurements closer than 10 cm to the walls of the flume were prohibited. The vise was raised and lowered and moved side to side manually to allow for proper placement of the ADV at each of the nodes. The carriage itself was mounted on wheels on a track that extended most of the length of the flume, thus allowing for movement of the ADV both horizontally and vertically.

The measurement grid was arranged such that the nodes were denser around the dikes and becoming sparser away from the dikes (Figure 2). 167 near-bed nodes for the 90° dikes and 295 near-bed nodes for the 150° dikes were arranged around the dikes. Around the dike tips, 10 cm from the wall to the center of the flume the resolution was 3 cm by 3 cm, with two lower resolution rectangular arcs of 5 cm by 5 cm and one of 10 cm by 10 cm at the outskirts of the area of interest. Raw data was collected using the ADV probe and the Horizon ADV software. Time series of velocities in three spatial directions measured at each node at a depth $z = 5\text{mm}$ from the bed were used to calculate the turbulence intensities and Reynolds stresses.

After completing the fixed bed experiments, the flume was filled up with 10 cm of well-sorted sand and gravel mixture having a median diameter of 0.85 mm. The mobile bed experiment was only performed for the series of angled dikes at a discharge of $0.035\text{m}^3/\text{s}$. The mean flow velocity and the shear velocity of the approaching flow, obtained through a linear regression analysis are 29.10 cm/s and 1.30 cm/s, respectively (Table 1). The critical shear stress for the sediment mixture is 0.066 Pa based on the Shields diagram. Sediment starts to transport at

the approaching flow section. The scour hole was formed around the first dike of the series. After about 24 hrs, the scour hole reaches equilibrium and the scour depth remains unchanged. Fig.3 is a picture of the equilibrium scour hole, and Fig.4 is the contour lines of scoured bed surface. Water surface elevations and flow velocities were measured at the same grid as the one for the fixed bed shown in Fig.2.

Data Processing

In the data analysis, the x , y , and z axes were oriented along the main flow longitudinally, to the left bank in the transverse direction, and toward the water surface in vertical with instantaneous velocity components denoted as u , v , and w , respectively. Processed data was directly used by a calculation program to output the desired information in a text file to be used by visualization software. The measured velocities in the processed data file were used to calculate the following turbulence characteristics: (a) mean velocities in the longitudinal, transverse, and vertical directions denoted as \bar{u} , \bar{v} , \bar{w} , respectively; (b) Reynolds stresses, $-\rho\overline{u'v'}$, $-\rho\overline{u'w'}$, and $-\rho\overline{v'w'}$ in which ρ is flow density, and u' , v' , and w' are turbulence fluctuations in the longitudinal, transverse, and vertical directions, respectively; (c) turbulent kinetic energy (TKE), calculated as $\frac{1}{2}(u'^2 + v'^2 + w'^2)$.

From the measurements of the complete velocity profile of unaffected flow, the mean horizontal velocity, where $V_x = \sqrt{\bar{u}^2 + \bar{v}^2}$, and vertical (\bar{w}) velocities at each node were calculated; \bar{w} was nearly zero and orders of magnitude smaller than V_x . The mean horizontal velocity was plotted against $\log(\frac{z}{h})$ where z is the distance from the bed surface, and h is the

flow depth. Linear regression analysis was then used to fit the data in a semi-logarithmic scale plot and from this the friction velocity for each vertical profile, u_* , was obtained. Shear stresses of the approaching flow calculated using the measured mean velocity profile was summarized in Table 2. Bed shear stresses can be calculated by four different methods as discussed in the results section. Table 2 also listed the shear stresses calculated by those methods. The shear velocity calculated from those four methods varies by a factor of 2 to 5. The shear stresses calculated by the total turbulent kinetic energy (TKE) was found to be the best approximation of bed shear stresses (Biron et al. 2005). However, to be consistent with other turbulence studies, this study scaled the turbulence properties by using the shear velocity determined from the velocity profile of the incoming flow.

Experimental Results

Mean flow

The experimental results of dimensionless mean flow velocities in three directions at the discharge of $0.035\text{m}^3/\text{s}$ were shown in Fig.5a, 5b, and 5c, respectively. Results at other discharges were not shown to be concise. For the flow $Q = 0.035\text{ m}^3/\text{s}$, corresponding to a 0.20 m flow depth at the weir, the dimensionless near-bed mean longitudinal flow velocity was about the same for the straight and the angled dikes (Fig.5a). The straight dikes showed a patch of high velocity directly across from the first two dikes. The angled dikes showed this pattern as well, but to a lesser degree. As expected, areas between the dikes showed relatively low velocities. The time-averaged velocities in the transverse and vertical directions at the flat bed were nearly zero with the maximum \bar{v} at the front of the first dike, and the maximum \bar{w} near the tip of the

second dike (Fig.5b and 5c). As for the mobile bed, the mean longitudinal velocity considerably reduced around the first dike, while only a small area of high velocity occurred near the tip of the second and the third dike (Fig.5a). Fig.5b showed the mean velocities in the transverse direction, reduced near the second dike, but not significantly. Fig.5c showed the vertical mean velocities increased at the tip of the first dike towards the bed surface at the flat bed whereas away from the bed in the scoured zone (Fig.5c). This means that the mean near-bed vertical velocity was towards the bed surface prior to the scour, and changed to away from the bed after the formation of equilibrium scour.

Turbulence intensities

Fig.6a, 6b, and 6c showed measured turbulence intensities from all three experimental runs. At the flat bed, both the straight and angled dikes showed the same ranges of u' and v' values regardless of measurement locations, Reynolds number, or alignment of dikes. However, the w' component was consistently nearly three times smaller than u' or v' . There was little difference at the bed between the turbulence intensities for the straight and angled dikes, except in the spatial distribution shown in Figure 6a and 6b where the maximum values were much more spread out in the angled dike case. In general, the magnitudes of u' and w' were larger for the angled dike series, but only by about 1.5 times that of the straight dike series. The increase was not concentrated on any one turbulence intensity, although u' had a slightly larger increase over v' and w' when the dikes were angled upstream.

As the Reynolds number increased, turbulence intensities u' , v' and w' generally increased. The dimensionless values of u' , v' and w' were obtained by dividing the individual velocity fluctuations by the shearing velocity of the incoming flow, u_{*0} . The mean amplification across

the domain was nearly the same for both the straight and angled dike series. The maximum dimensionless u' and v' were located at the tip of the second and the third dike, while the maximum dimensionless w' are found at the first dike for both experiments at the fixed, flat bed.

When the scour reached equilibrium, all three components of dimensionless turbulence intensities reduced as shown in Fig.6c. The high turbulence intensities, u' and v' , have spread out of the second dike. But, a small area of high u' and v' still hovered between the first and the second dike. The turbulence intensity w' significantly reduced at the first dike where the scour hole resides. This indicates the reduction of the turbulence intensity in the vertical direction is most remarkable as the scour develops, which is also accompanied by the changes in the mean vertical velocity.

Reynolds stresses

As the Reynolds number increased, $-\overline{\rho u'v'}$, $-\overline{\rho u'w'}$ and $-\overline{\rho v'w'}$ in general increased as well. When they were non-dimensionalized by the shear stresses of the approach flow, the mean amplification of the time-averaged Reynolds stresses was nearly the same for both angled and straight dikes at the flat bed. When comparing the three components of Reynolds stresses, the component, $-\overline{\rho u'v'}$ had a much greater magnitude than the other two components, $-\overline{\rho u'w'}$ and $-\overline{\rho v'w'}$. The latter two components were of roughly the same magnitude in each case, both for straight and angled dikes.

The spatial distributions of the dimensionless Reynolds stress components at the flat bed were shown in Figure 7a and 7b in which the angled dikes had higher magnitudes of both positive and negative values of the Reynolds stresses than the straight dikes. For the straight

dikes, the area of highest $-\overline{\rho u'v'}$ resides at the tip of the second dike; whereas for the angled dikes, the largest magnitude of $-\overline{\rho u'v'}$ was just downstream of it. For $-\overline{\rho u'w'}$, for both the straight and angled dikes, the highest magnitudes were positive, and each series showed a zone of positive $-\overline{\rho u'w'}$ circulating near the tip of the first dike. Since the highest magnitudes of $-\overline{\rho u'w'}$ were positive, sweeps and ejections perhaps are the dominant turbulent burst events around the tip of the first dike. Sediment transport is closely associated with sweep events, and less sediment motion was observed in the events of outward and inward interactions (Nelson et al. 1995). For the straight dike series, the zone of high $-\overline{\rho u'w'}$ was located just upstream of the first dike, while for the angled dikes it was located just downstream of the tip of the first dike. This indicates that the scour hole will initiate from the upstream face of the straight dikes, while the tip or slightly downstream of the angled dikes. The highest $-\overline{\rho u'w'}$ values perhaps correspond to the largest scour depth.

Although very large values of $-\overline{\rho u'v'}$ were observed in this study and around a complex bridge pier (Behesti and Ataie-Ashtiani, 2010), no study have examined the role of $-\overline{\rho u'v'}$ component on sediment transport. This study showed that the larger $-\overline{\rho u'v'}$ values shown in Fig.7b do not correspond to the location of scour zone shown in Fig.4. How $-\overline{\rho u'v'}$ influence sediment transport requires further examinations. Fig.7c showed the dimensionless Reynolds stresses after the local scour has reached equilibrium. All three components of Reynolds stresses considerably reduced, especially at and around the first dike. Inside the scour zone, the Reynolds stresses are much smaller than those at the fixed flat bed. Higher Reynolds stresses existed between the first and the second dike, perhaps due to sediment deposition.

Bed Shear Stresses

For non-uniform and unsteady flows in open channels or natural rivers, bed shear stress is important for estimating sediment transport rate. Therefore, many methods to calculate bed shear stresses are available in the literature. Among them, civil engineers (Beheshti and Ataie-Ashtiani 2010) often adopt the Reynolds stresses method in Dey and Barbhuiya (2005). If using the near-bed Reynolds stresses to approximate bed shear stress, τ_b , the mathematical equation is $\tau_b = \sqrt{(\tau_b^x)^2 + (\tau_b^y)^2}$, where $\tau_b^x = -\rho(\overline{w'u'} + \overline{v'u'})|_{bed}$ and $\tau_b^y = -\rho(\overline{w'v'} + \overline{v'u'})|_{bed}$, ρ = density of water. An alternate method to calculate bed shear stress uses only the w' component, and the equation becomes simply $\tau_b = -\rho(\overline{u'w'} + \overline{v'w'})$ if both streamwise and transverse turbulence velocities are considered. Since turbulence intensity in the transverse direction is significant in this study, this form was often used instead of the one in Biron et al. (2004), where $\tau_b = -\rho(\overline{u'w'})$.

Another common method of calculating the bed shear stress involves the turbulent kinetic energy (TKE). This method uses the turbulent fluctuations in the three spatial directions, u' , v' , and w' . In this case, $\tau_b = C_1[\frac{1}{2}\rho(u'^2 + v'^2 + w'^2)]$, where C_1 is a proportionality constant equal to 0.19 (Kim, et al., 2000, Pope, et al., 2006). Because the instrument noise error associated with vertical velocity fluctuations is smaller than that associated with the horizontal fluctuations, bed shear stress can also be calculated using only w' , and the equation becomes simply $\tau_b = C_2\rho(w'^2)$ and where $C_2 = 0.9$. The total bed shear stress

τ_b can be expressed in dimensionless form as $\hat{\tau}_b = \tau_b / \tau_0$, where τ_0 = the bed shear stress of approaching flow by the log law, ρu_*^2 .

These four methods of calculating bed shear stress were used in this study to determine which one would give the most satisfactory results. At first, the bed shear stress calculated by using the method in Dey and Barbhuiya (2005) was compared to the one calculated by using the TKE method as shown in Figure 8. Dey's and Barbhuiya's method yielded a bed shear stress nearly 2–4 times of those from the TKE method. As the Reynolds number increased, the correlation of bed shear stresses from these two methods became worse. Secondly, bed shear stresses obtained from only considering the Reynolds stresses associated with w' were also compared with the bed shear stresses from TKE method in Figure 8. The Reynolds stress method that only considers the w' component yielded much smaller bed shear stresses than the TKE method. Because turbulent flow around the dikes is three-dimensional, this excludes the use of this method. On the other hand, the accurate ADV measurements require the primary receiver pad to be aligned with the streamlines; measurements collected around the dike apparently were not able to be aligned with the curved streamlines. Many applications of ADVs (Kim, *et al.*, 2000; Huthnance, 2002; and Pope, *et al.*, 2006; McLelland and Nicholas 2000; Biron et al 2004; MacVicar and Roy 2007) concluded that the TKE method is the most reliable to estimate the bed shear stress. It is worthy to point out that Biron et al. (2004) compared these three methods for calculating bed shear stress and suggested that the method using w' is not appropriate for complex flow field around dikes (Biron et al. 2005). Therefore, this study employed the TKE method for calculating bed shear stress.

Bed Shear Stress Distributions

Dimensionless bed shear stress $\hat{\tau}_b$ was obtained using the bed shear stress τ_{b0} of the incoming flow, also calculated using the TKE method. The magnitudes of $\hat{\tau}_b$ reached a maximum of about 14.0 and 10.9 at the tip of the second dike for the straight and angled dikes, respectively. For all the fixed, flat bed experiments, the maximum bed shear stress was found at the tip of the second dike (Fig.9a and 9b).

As to the angled dikes (Fig.9b), the dimensionless bed shear stress around the angled dikes was slightly smaller than that around the straight dikes. The highest magnitude of bed shear stress was again seen near the tip of the second dike, although for the angled dikes it was located slightly downstream of the tip of the second dike. There was only a small area of high bed shear stress near the tip of the first dike. The bed shear stress near the tip of the second dike was 14.0 times that of the incoming flow for the straight dikes. These high amplifications were attributed to the turbulence induced by the upstream dikes. The experiments of Biron et al. (2005) measured an amplification of bed shear stress up to 25. The high amplifications of shear stress at high Reynolds numbers are common in air flows but not well studied in open channel flow. Therefore, more experimental data are needed to confirm the amplifications of bed shear stresses under various dike alignments and Reynolds numbers.

As to the mobile bed, the distribution of bed shear stress was shown in Fig.9c, in which bed shear stresses have reduced significantly at the first dike, while an area of large bed shear stresses were observed near the second dike. Comparing Fig.9c with Fig.4, one can find that the maximum shear stresses in Fig.9c do not correlate with the scour depth in Fig.4. Rather,

turbulence intensity, w' and Reynolds stresses $-\overline{\rho u'w'}$ measured at the flat bed closely relate to the scour depth.

Traditional hydraulic engineering methods determine shear stress by fitting velocity measurements using the logarithmic law. Acoustic sound and laser-based velocimeters can measure instantaneous velocities for calculating turbulence properties. Bottom shear stresses can then be determined directly from turbulence properties by several different techniques, such as Reynolds stresses (Dey and Barbhuiya, 2005), turbulent kinetic energy (Biron *et al.* 2005), and others. Prior studies (McLelland and Nicholas 2000; Biron *et al.* 2004; MacVicar and Roy 2007) as well as this study showed the turbulent kinetic energy method is an alternative for calculating bed shear stresses.

Correlation between Scour Depth and Flow Properties

A practical interest in the turbulent flow field around a series of spur dike is the need to predict location and geometry (e.g. size, depth) of the scour zone accurately. In alluvial channel beds composed of primarily of sand and gravels, scour is often developed because of non-equilibrium sediment transport, especially bed load. Because bed material is directly exposed to shear stress acting on the bed surface, the rate of bed-load transport is proportional to bed-shear stress. Fine sand, silt, and clay are transported as suspended sediment in a water column and settle where the turbulence intensity is weak.

Experimental results from the fixed, flat bed experiments showed that the maximum shear stress occurred at the tip of the second dike in the three dike series. This does not match the maximum scour depth observed at the first dike shown in Figure 4 from the mobile bed

experiment using the same flume, dikes, and flow conditions. On the other hand, except for the w' component in the case of angled dikes (Figure 5b), both u' and v' components have the maximum values around the second dike. In contrast, the w' component has the maximum values at the first dike regardless of dike alignments. As to the distribution of Reynolds stresses, the highest $-\rho \overline{u'v'}$ component was consistently located around the second dike, while the highest $-\rho \overline{u'w'}$ component was located at the first dike for both alignments. This implies that the scouring, defined as the removal of bed material from the bed surface, closely relates to the turbulence intensity in the vertical and the Reynolds stress $-\rho \overline{u'w'}$. Furthermore, the positive values of $-\rho \overline{u'w'}$ (Figure 6b) indicate the predominance of sweep or ejection burst events, which are perhaps responsible for the local scour.

Haltigin *et al.* (2007) hypothesized that the scour depth is closely correlated with the mean vertical velocity measured at the flat bed. Therefore, the correlations between the scour depth and the mean flow and turbulence properties including mean velocities, turbulence fluctuations, Reynolds stresses, and bed shear stresses were calculated and summarized in Table 3. The mean velocity and the velocity fluctuation in the vertical yielded correlation coefficients of -0.68 and 0.65, respectively, while other parameters had a correlation coefficient of less than 0.54. Since the scour depth is positive, a negative correlation factor with the mean vertical velocity indicates that a negative mean vertical velocity (towards bed surface) results in a larger scour depth. On the other hand, positive turbulence intensity (away from the bed) corresponds with a larger scour depth. The correlation between the scour depth and the Reynolds stress $-\rho \overline{u'w'}$ is 0.27, which implies that other Reynolds stresses other than $-\rho \overline{u'w'}$ also contributed to the local scour. After

the local scour has reached equilibrium, the maximum correlation coefficient is about 0.16, showing that none of the measured mean flow or turbulence properties has a strong correlation with the scour depth. These correlations of the scour depth and the mean vertical velocity and turbulence intensities in the vertical direction imply that the maximum scour depth depends on the maximum mean vertical velocity or the maximum turbulence intensity in the vertical direction. This may confirm the perception in Haltigin *et al.* (2007) that the scour depth should be predicted using the measured flow properties at the flat bed.

As the local scour develops, the zone of high turbulence intensity in the vertical, shown in Figures 6a and 6c shifts from the tip of the first dike to the tip of the second dike as the scour of the mobile bed surface gradually stretches downstream. The progression of the scour zone follows the contour lines of the w' turbulence intensity rather than the dimensionless bed shear stress, as shown in Figure 9b. McCoy *et al.* (2007) applied a large eddy simulation model and found that the high turbulent intensity and bed shear stresses are produced by the necklace vortices in the horseshoe vortices region. As the vortices transported to the downstream, loose bed material is entrained and transported in the zone of shear stress greater than the critical shear stresses of individual sized particles. This downstream progression of the scouring zone was also observed in large flume experiments to test riprap-apron performance (Morales *et al.*, 2008).

Conclusions

This study analyzed experimental results of turbulence properties, bed shear stresses and the scour depth. Results showed that the local scour was initiated and developed where the mean vertical velocity is toward the bed surface and the turbulence intensity in the vertical direction is the maximum. After the scour reached equilibrium, the near bed vertical velocity becomes

toward the water surface. Of the three turbulence intensities, although w' is much smaller than either of the other two components, it is closely correlated with the scour depth. In the case of the Reynolds stresses, the component $-\rho\overline{u'w'}$ has the distribution pattern similar to the developed scour hole. The sweeps and ejections events associated with u' and w' perhaps are the major mechanism of local scour development near dikes.

The highest magnitude of bed shear stress calculated by turbulent kinetic energy was consistently around the second dike in the series. However, the location of maximum scour was observed around the first dike in coincidence with the distribution of velocity fluctuation w' and mean velocity \bar{w} . This indicates that the initiation and development of local scour is determined by the turbulence intensity in the vertical rather than the bed shear stress. Large bed load transport due to bed shear stress may not initiate bed scouring, but turbulence bursts (e.g. sweeps and ejections) will entrain sediment from bed surface and develop the local scour. Therefore, the local scour will reach equilibrium when the turbulence intensity becomes insufficient to entrain sediment from the bed surface. However, the quantitative relation between local scour and turbulence intensity in the vertical still requires more experimental data. Further study will be done, using various sized sediment in the flume, to develop a quantitative relation between the turbulence strength and the depth of maximum equilibrium scour based on turbulence data obtained from the plane bed case, as well as information obtained from the mobile bed case.

Acknowledgements

This work is a result of research sponsored by the U.S. Department of Defense Army Research Office under Contract Number W911NF-07-1-0412 and NSF Award EAR-0846523. Thanks to Mr. Steve Albanese and Ms. Marika Klappert who assisted with the experiments.

Notations

The following symbols are used in this paper:

x = horizontal longitudinal direction

y = horizontal transverse direction

z = vertical direction

h = depth of water at the weir (m)

H = height of water flowing over the weir (m)

D = distance between two dikes at the base (cm)

Q = volumetric discharge ($\text{m}^3 \cdot \text{s}^{-1}$)

K = weir constant for discharge units $\text{m}^3 \cdot \text{hr}^{-1}$

L = weir crest length (cm)

l = dike length (cm)

V_x = velocity in horizontal direction ($\text{m} \cdot \text{s}^{-1}$)

u, v, w = instantaneous flow velocities ($\text{m} \cdot \text{s}^{-1}$)

$\bar{u}, \bar{v}, \bar{w}$ = mean flow velocities ($\text{m} \cdot \text{s}^{-1}$)

u', v', w' = turbulence intensities ($\text{m} \cdot \text{s}^{-1}$).

$-\overline{\rho u'v'}$, $-\overline{\rho u'w'}$, $-\overline{\rho v'w'}$ = Reynolds stresses ($\text{N}\cdot\text{m}^{-2}$)

τ_b = bed shear stress ($\text{N}\cdot\text{m}^{-2}$)

τ_{b0} = bed shear stress of the incoming flow

$\hat{\tau}_b$ = dimensionless bed shear stress

u_* = shear velocity ($\text{m}\cdot\text{s}^{-1}$).

u_{*0} = shear velocity of the incoming flow

ρ = density of water ($\text{kg}\cdot\text{m}^{-3}$)

References

Abad, J.D. and Garcia, M.H. (2009). “Experiments in a high-amplitude Kinoshita meandering channel: 1. Implications of bend orientation on mean and turbulent flow structure.” *Water Resour. Res.*, Vol. 45, W02401, doi: 10.1029/2008WR007016.

Beheshti and Ataie-Ashtiani, 2010, Experimental study of three-dimensional flow field around a complex bridge pier. *Journal of Engineering Mechanics*, ASCE, 136, 2, 143-154

Biron, P. M., Robson, C., Lapointe, M. F., and Gaskin, S. J. (2004). “Comparing different methods of bed shear stress estimates in simple and complex flow fields.” *Earth Surf. Process. Landforms*, 29, 1403-1415.

Biron, P. M., Robson, C., LaPointe, M. F., and Gaskin, S. J. (2005). "Three-dimensional flow dynamics around deflectors." *River Research and Applications*, 21, 961–975.

Cea L., Puertas, J., and Pena, L. (2007). "Velocity measurements on highly turbulent free surface flow using ADV." *Exp Fluids*, 42, 333–348.

Coleman, S. E. and Nikora, V. I. (2008). "A unifying framework for particle entrainment." *Water Resour. Res.*, 44, W04415, doi: 10.1029/2007WR006363

Dey, S. and Barbhuiya, A. K. (2005). "Flow field at a vertical-wall abutment." *J. Hydraul. Eng.*, 131(12), 1126–1135.

Dey S. and Lambert M. F. (2005). "Reynolds stress and bed-shear in non-uniform unsteady open-channel flow." *J. Hydraul. Eng.*, 131(7), 610–614.

Duan, J.G. (2005). "Analytical approach to calculate the rate of bank erosion." *J. Hydraul. Eng.*, 131(11), 980-990.

Duan, J.G. and Nanda, S.K. (2006) Two-dimensional depth-averaged model simulation of suspended sediment concentration distribution in a groyne field, *Journal of Hydrology*, 327(3-4), 426-437.

Duan, J. G. and He, L. Wang Guanxiang, Fu, Xudong (2009), Mean flow and turbulence in a scoured hole around an experimental spur dike, *Advance in Water Resource*, 32(12), 1717-1725.

Duan, J. G. (2009) Mean flow and Turbulence around an experimental spur dike, *J. Hydraul. Eng.*, 134(3), 315-327.

Finelli, C. M., Hart, D. D., and Fonseca, D. M. (1999). "Evaluating the spatial resolution of an acoustic Doppler velocimeter and the consequences for near-bed flows." *Limnol. Oceanogr.*, 44(7), 1793–1801.

García, C. M., Cantero, M. I., Niño, Y., and García, M. H. (2005). "Turbulence measurements with acoustic Doppler velocimeters." *J. Hydraul. Eng.*, 131(12), 1062–1073.

Goring, D. G. and Nikora, V. I. (2002). "Despiking acoustic Doppler velocimeter data." *J. Hydraul. Eng.*, 128(1), 117–126.

Gratiot, N., Mory, M., and Auchere, D. (2000). "An acoustic Doppler velocimeter (ADV) for the characterization of turbulence in concentrated fluid mud." *Continental Shelf Res.*, 20, 1551–1567.

Haltigin, T. W., Biron P. M., and Lapointe M. F. (2007). "Predicting equilibrium scour-hole geometry near angled stream deflectors using a three-dimensional numerical flow model." *J. Hydraul. Eng.*, 133(8), 983–988.

Huthnance, J. M., Humphery, J. D., Knight, P. J., Chatwin, P. G., Thomsen, L., and White, M. (2002). "Near-bed turbulence measurements, stress estimates, and sediment mobility at the continental shelf edge." *Progress in Oceanography*, 52, 17–194.

Hildrew, A. G. (1996). "Whole river ecology: spatial scale and heterogeneity in the ecology of running waters." *Archiv. Hydrobiol. Suppl.*, 113(10), 25-43.

Kim, S. C., Friedrichs, C.T., Maa, J. P.-Y., and Wright, L. D. (2000). "Estimating bottom stress in tidal boundary layer from acoustic Doppler velocimeter data." *J. Hydraul. Eng.*, 126(6), 399–406.

Koken, M. and Constantinescu, G. (2008). "An investigation of the flow and scour mechanisms around isolated spur dikes in a shallow open channel: 1. Conditions corresponding to the initiation of the erosion and deposition process." *Water Resour. Res.*, 44, W08406, doi:10.1029/2007WR006489.

Kuhnle, R. A., Alonso, C. V., and Shields, D.F. (2002). "Local scour associated with angled spur dikes." *J. Hydraul. Eng.*, 128(12), 1087–1093.

Kuhnle, R. A., Jia, Y., and Alonso, C.V. (2008). "Measured and simulated flow near a submerged spur dike." *J. Hydraul. Eng.*, 134(7), 916–924.

MacVicar, B. J. and Roy, A. G. (2007). "Hydrodynamics of a forced riffle pool in a gravel bed river: 1. Mean velocity and turbulence intensity." *Water Resour. Res.*, 43, W12401, doi: 10.1029/2006WR005272.

McCoy, A., Constantinescu, G. and Weber, L. (2007) A numerical investigation of coherent structures and mass exchange processes in channel flow with two lateral submerged groynes. *Water Resour. Res.*, 43, W05445, doi: 10.1029/2006WR005267.

McLean, S.R., and Nikora, V.I. (2006). "Characteristics of turbulent unidirectional flow over rough beds: Double-averaging perspective with particular focus on sand dunes and gravel beds." *Water Resour. Res.*, 42, W10409, doi: 10.1029/2005WR004708.

McLelland, S. J. and Nicholas, A. P. (2000). "A new method for evaluating errors in high-frequency ADV measurements." *Hydrol. Process.*, 14, 351–366.

Morales R., Ettema, R., and Barkdoll, B. (2008). "Large-scale flume tests of riprap-apron performance at a bridge abutment on a floodplain", *J. Hydraul. Eng.*, 134(6), 800-809.

Nelson, J. M., Shreve, R. L., Mclean, S. R., and Drake, T. G. (1995). "Role of near-bed turbulence structure in bed load transport and bed form mechanics." *Water Resour. Res.*, 31(8), 2071-2086.

Nikora, V. I. and Goring, D. G. (1998). "ADV measurements of turbulence: can we improve their interpretation?" *J. Hydraul. Eng.*, 124(6), 630–634.

Nikora, V. I. and Goring, D. G. (2000). "Flow turbulence over fixed and weakly mobile gravel beds." *J. Hydraul. Eng.*, 126 (9), 679–690.

Pope, N. D., Widdows, J., and Brinsley, M. D. (2006). "Estimation of bed shear stress using turbulent kinetic energy approach – a comparison of annular flume and field data." *Cont. Shelf Res.*, 26, 959–970.

SonTek (2001). "Acoustic Doppler velocimeter (ADV) principles of operation." *SonTek ADV Technical Manual*, SonTek, San Diego.

Stone M. C. and Hotchkiss R. H. (2007). "Turbulence descriptions in two cobble-bed river reaches." *J. Hydraul. Eng.*, 133(12), 1367–1378.

Sukhodolov, A., Engelhardt. C., Kruger, A. and Bungartz, H.(2004). "Case Study: Turbulent flow and sediment distributions in a groyne field." *J. Hydraul. Eng.*, 130(1), 1–9.

Tanaka, T. and Eaton, J. K. (2008). "Classification of turbulence modification by dispersed spheres using a novel dimensionless number." *Phys.l Rev. Letters*, 101, 114502. doi: 10.1103/PhysRevLett.101.114502.

Tominaga, A. and Matsumoto, D. (2006). "Diverse riverbed figuration by using skew spur-dike groups." *River Flow 2006-1: Proc. Int. Conf. Fluv. Hydraul.*, Taylor and Francis Group, London, 2006.

Tritico, H. M. and Hotchkiss R. H. (2005). "Unobstructed and obstructed turbulent flow in gravel bed rivers." *J. Hydraul. Eng.*, 131(8), 635–645.

Uijttewaal, W. S. J. (2005). "Effects of groyne layout on the flow in groyne fields: laboratory experiments." *J. Hydraul. Eng.*, 131(9): 782–791.

Voulgaris, G. and Trowbridge, J. H. (1998). "Evaluation of the acoustic Doppler velocimeter (ADV) for turbulence measurements." *J. Atmo. Oceanic Tech.*, 15, 272–289.

Wahl, T. L. (2000). "Analyzing data using WinADV." *2000 Joint Conf. on Water Resour. Eng. and Water Resour. Planning and Management*, 1–10.

Weller, J. (2005). "Predicting bed load transport for restoration of mountain streams." *MS Thesis*, University of Nevada, Reno, 132 pages.

Yossef, M. F. M. and Rupprecht, R. (2006). "Modeling flow and morphology in groyne fields." *River Flow 2006-2: Proc. Int. Conf. on Fluv. Hydraul.*, Taylor and Francis Group, London, 2006.

Zhang, H., Nakagawa H., Ishigaki, T, and Muto, Y. (2005). "Prediction of 3D flow field and local scouring around spur dikes." *Ann. J. Hydraul. Eng.*, 49, 1003–1008.

Zhang, H. and Nakagawa, H. (2008). "Scour around spur dyke: recent advances and future researches." *Annals of the Disaster Prevention Research Institute, Kyoto University*, (51B).

Table 1. Summary of Experimental Data




Bed Condition	Dike Alignment	Discharge (m ³ /s)	Approaching Flow Velocity (m/s)	Flow Depth (cm)	RE	Shear Velocity (cm/s)
Fixed		0.013	0.142	15	21325	0.42
		0.035	0.287	20	57414	0.79
		0.065	0.427	25	106627	0.88
		0.013	0.131	15	19650	0.59
		0.035	0.285	20	57000	0.81
		0.065	0.416	25	104000	1.09
Mobile		0.035	0.291	20	58200	1.30

Table 2. Shear Stresses of Approaching Flow Using Different Methods (Unit: Pa)

Alignment	Straight Dikes			Angled Dikes (fixed bed)			Angled Dikes (mobile bed)
	0.065	0.035	0.013	0.065	0.035	0.013	0.035
τ_0 by Dey et al	0.5918	0.1852	0.0437	0.1209	0.3742	0.2436	0.890
$\tau_0 = 0.19\rho(TKE)$	0.3285	0.1073	0.0271	0.2803	0.1931	0.1354	0.771
$\tau_0 = \rho u_*^2$	0.0775	0.0624	0.0178	0.0637	0.0650	0.0343	0.1687

Table 3. Correlation Coefficients between the Scour Depth and Flow Parameters

Parameters	Mean u	Mean v	Mean w	u'	v'	w'	$-\rho u'v'$	$-\rho u'w'$	$-\rho v'w'$	τ_b by TKE method	τ_b by Dey's method
Flat bed	-0.19	-0.33	-0.68	0.54	0.15	0.65	-0.17	0.27	-0.24	0.45	0.31
Scoured Bed	-0.16	-0.15	0.16	0.13	-0.12	0.12	0.12	-0.11	-0.15	0.01	-0.02

Figures

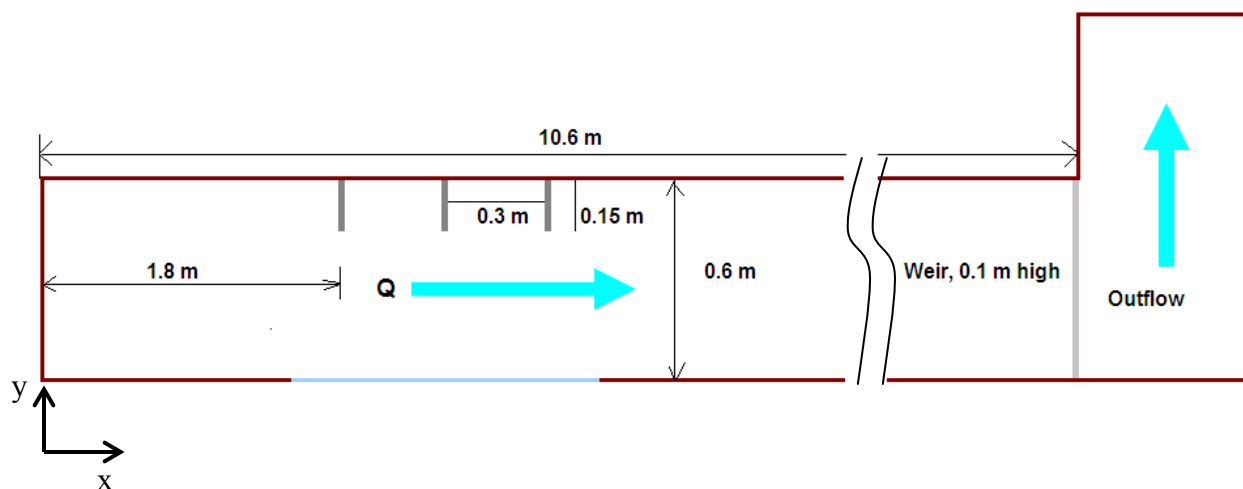


Figure 1: Plan view of the flume set up.

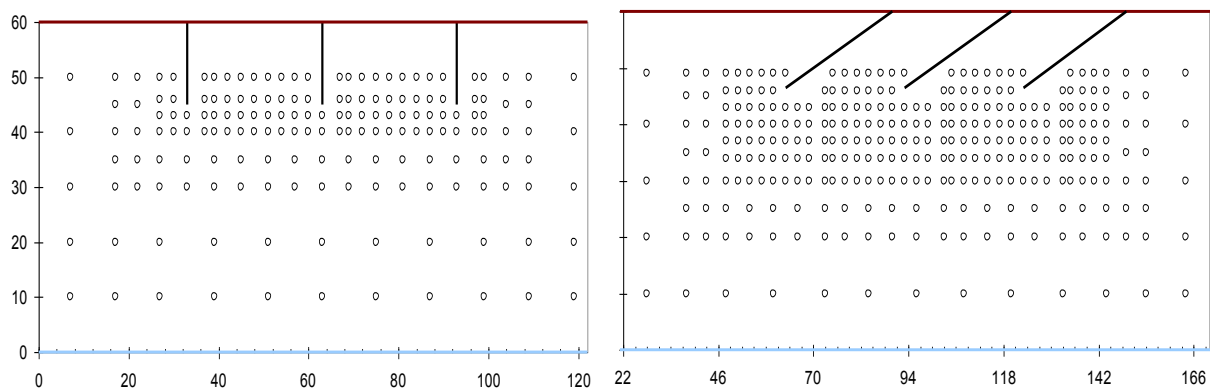


Figure 2: Measurement grid for the straight (*left*) and angled (*right*) dikes.



Figure 3. Picture of scoured bed surface

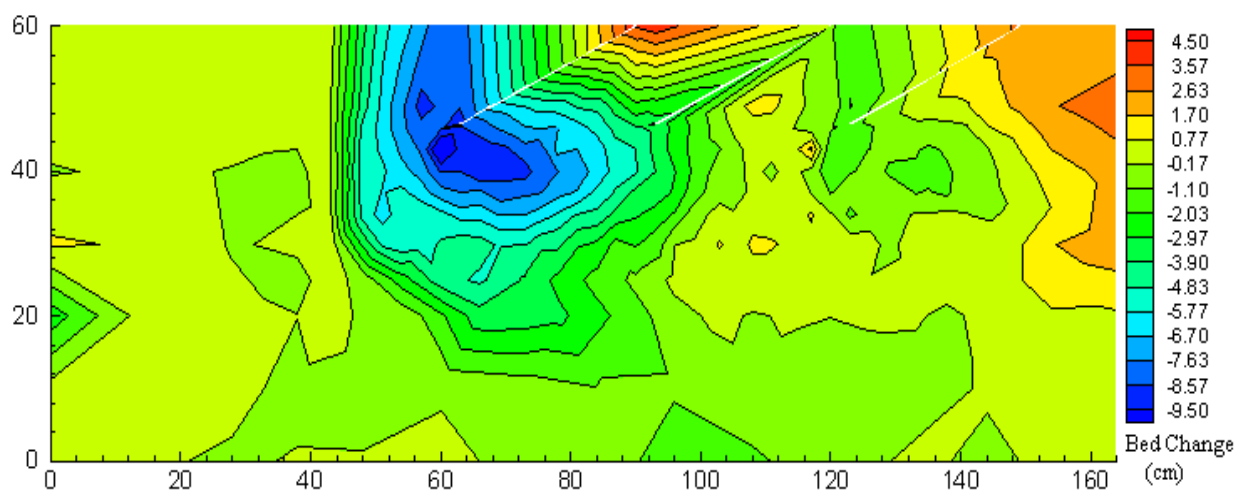


Figure 4: Bed bathymetry of the developed scour hole at $Q = 0.035 \text{ m}^3/\text{s}$

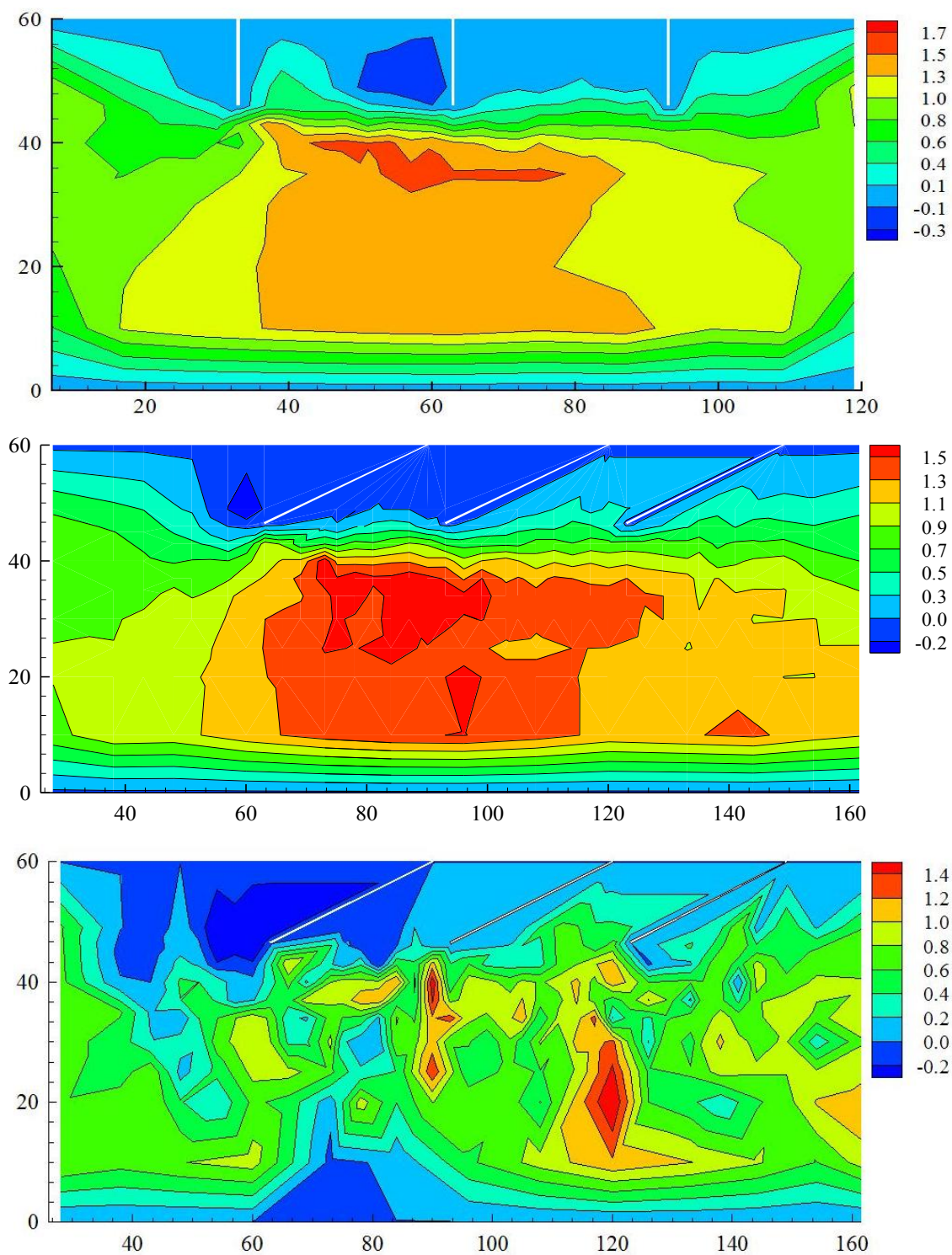


Figure 5a: Distribution of dimensionless mean longitudinal velocities for straight, angled dikes on flat bed and angled dikes on mobile bed at $Q = 0.035 \text{ m}^3/\text{s}$.

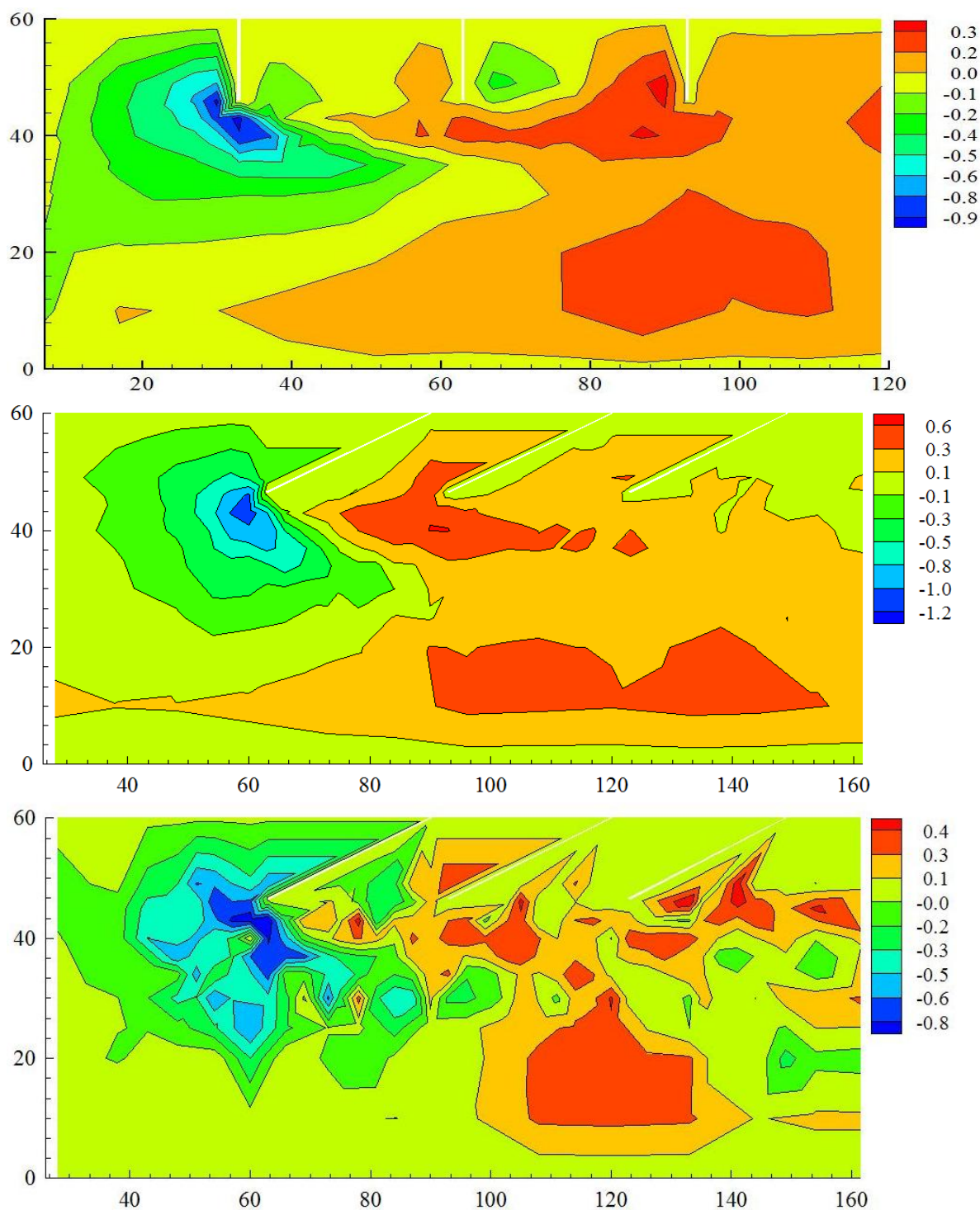


Figure 5b: Distribution of dimensionless mean transverse velocities for straight, angled dikes on flat bed and angled dikes on mobile bed at $Q = 0.035 \text{ m}^3/\text{s}$.

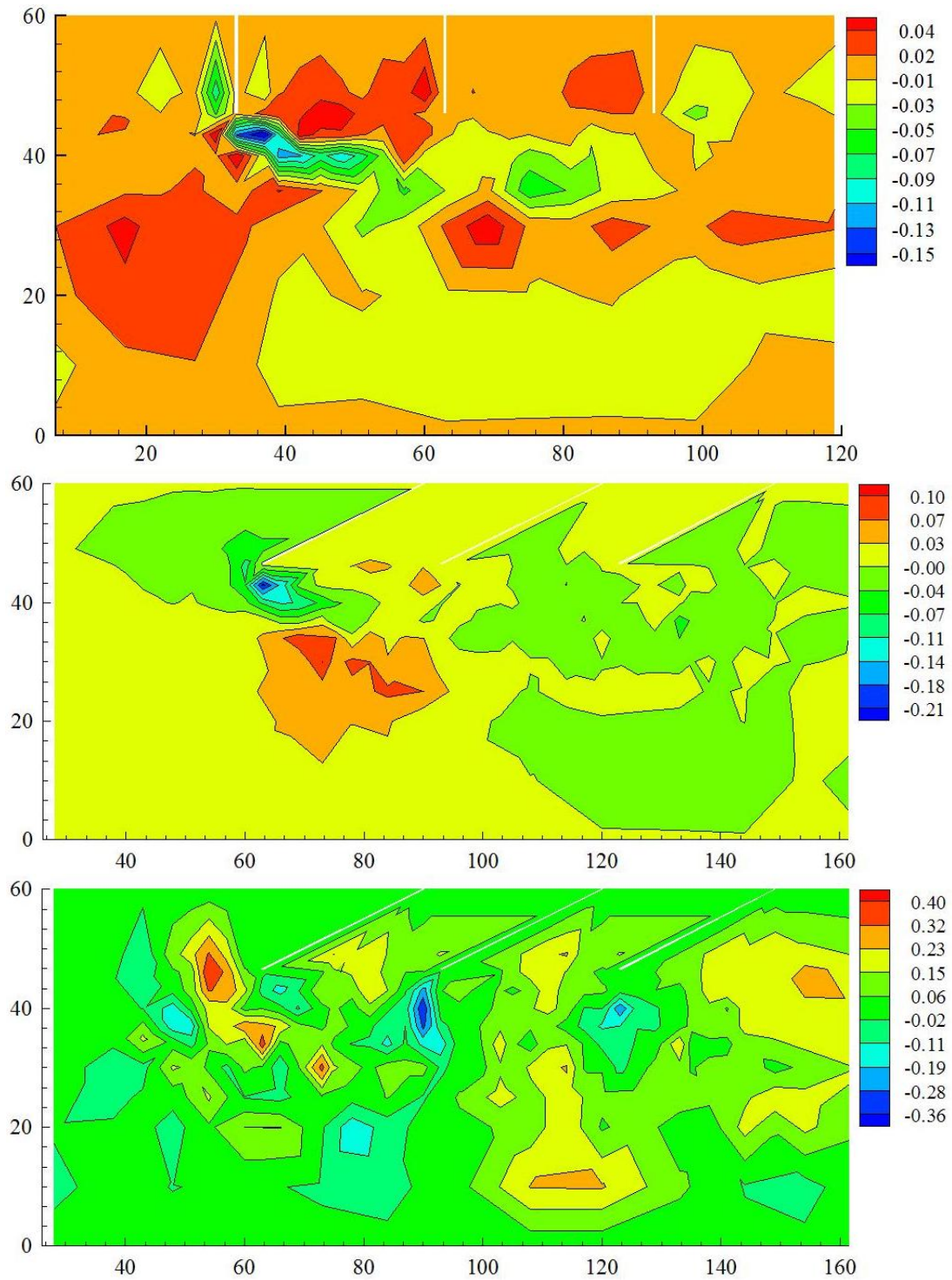


Figure 5c: Distribution of dimensionless mean vertical velocities for straight, angled dikes on flat bed and angled dikes on the mobile bed at $Q = 0.035 \text{ m}^3/\text{s}$

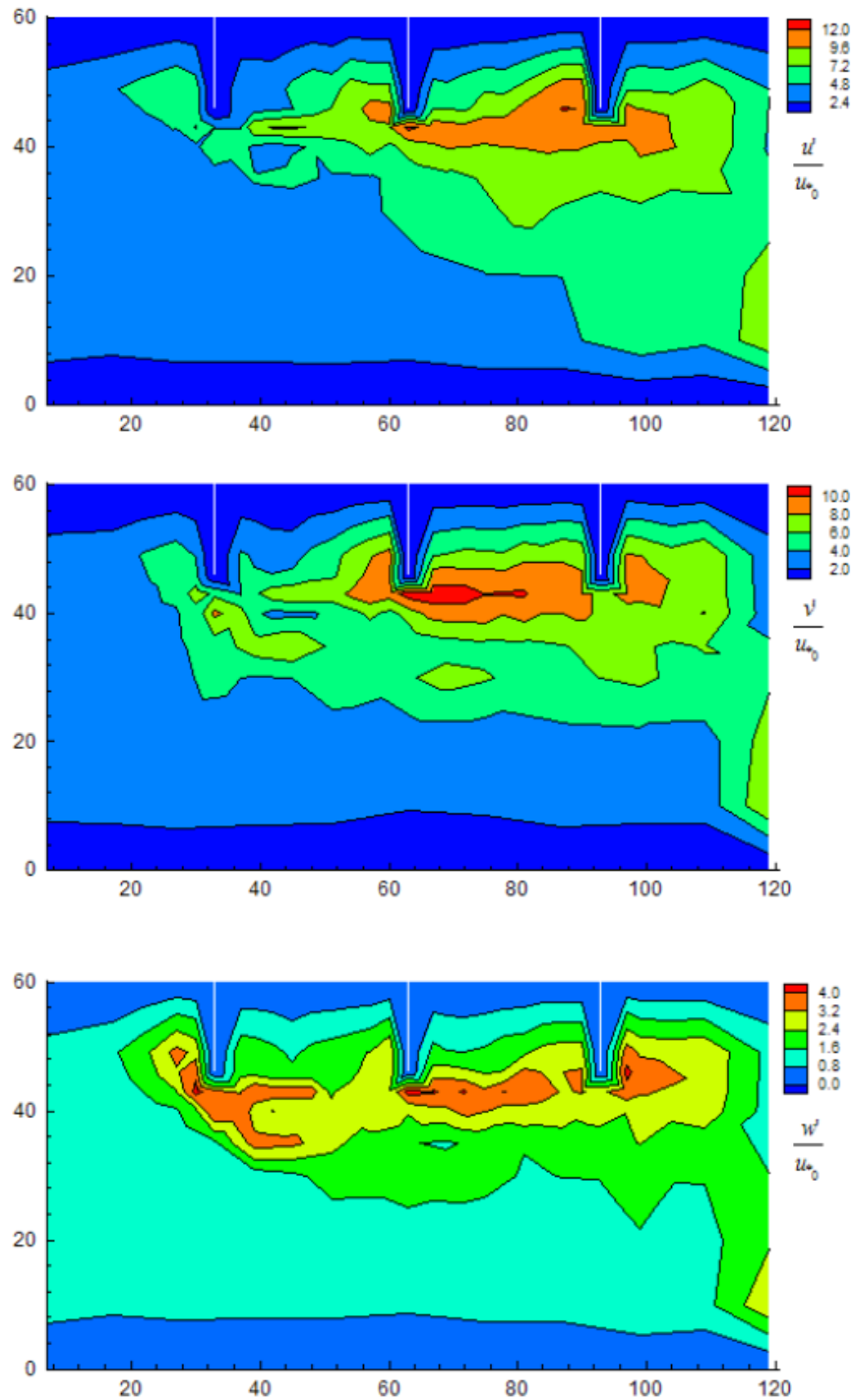


Figure 6a: Dimensionless turbulence intensities $\frac{u'}{u_{*0}}$ (*top*), $\frac{v'}{u_{*0}}$ (*center*), and $\frac{w'}{u_{*0}}$ (*bottom*) for straight dikes on the fixed bed at $Q = 0.035 \text{ m}^3/\text{s}$.

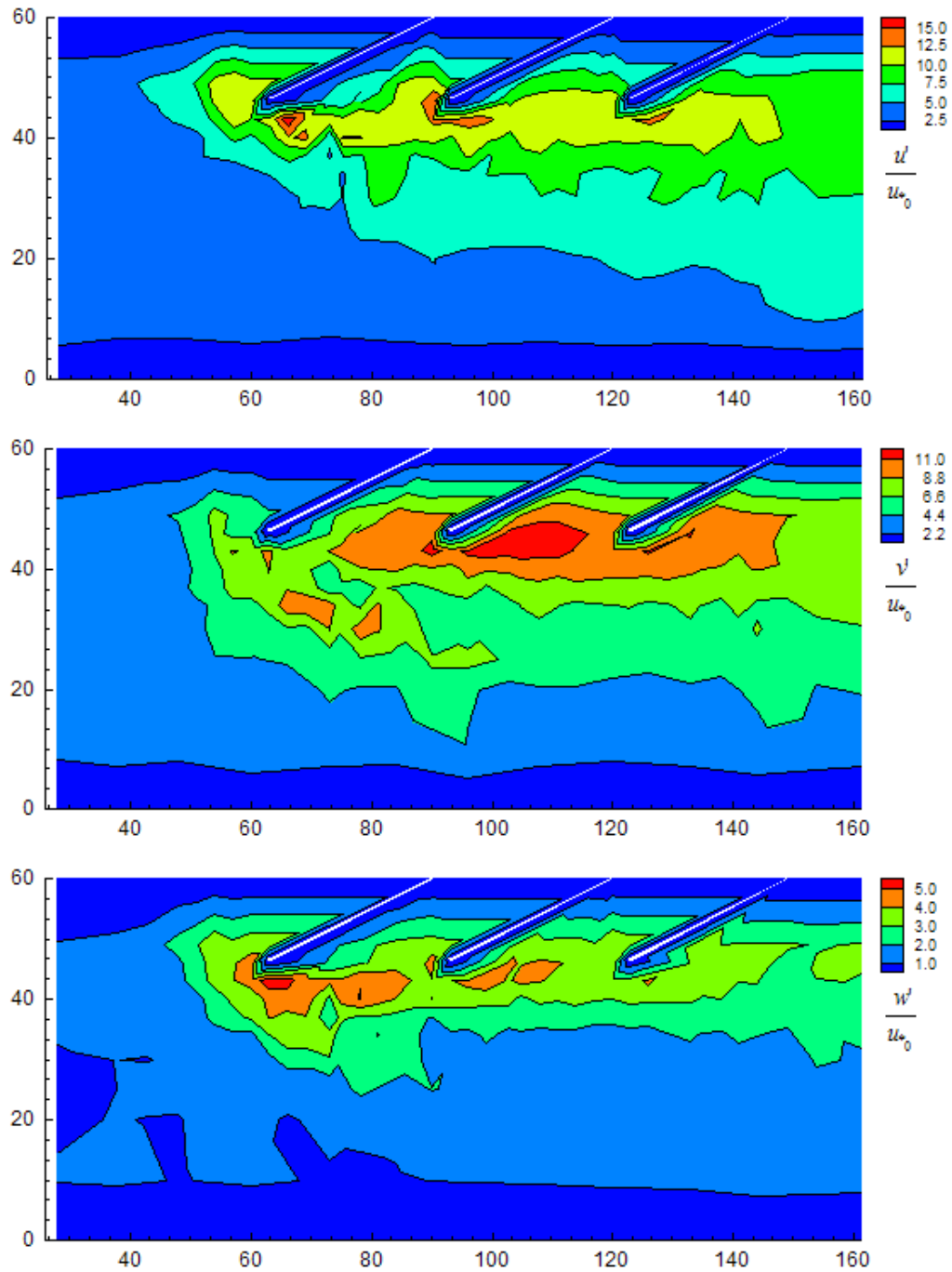


Figure 6b: Dimensionless turbulence intensities $\frac{u'}{u_{*0}}$ (top), $\frac{v'}{u_{*0}}$ (center), and $\frac{w'}{u_{*0}}$ (bottom) for angled dikes on the fixed bed at $Q = 0.035 \text{ m}^3/\text{s}$.

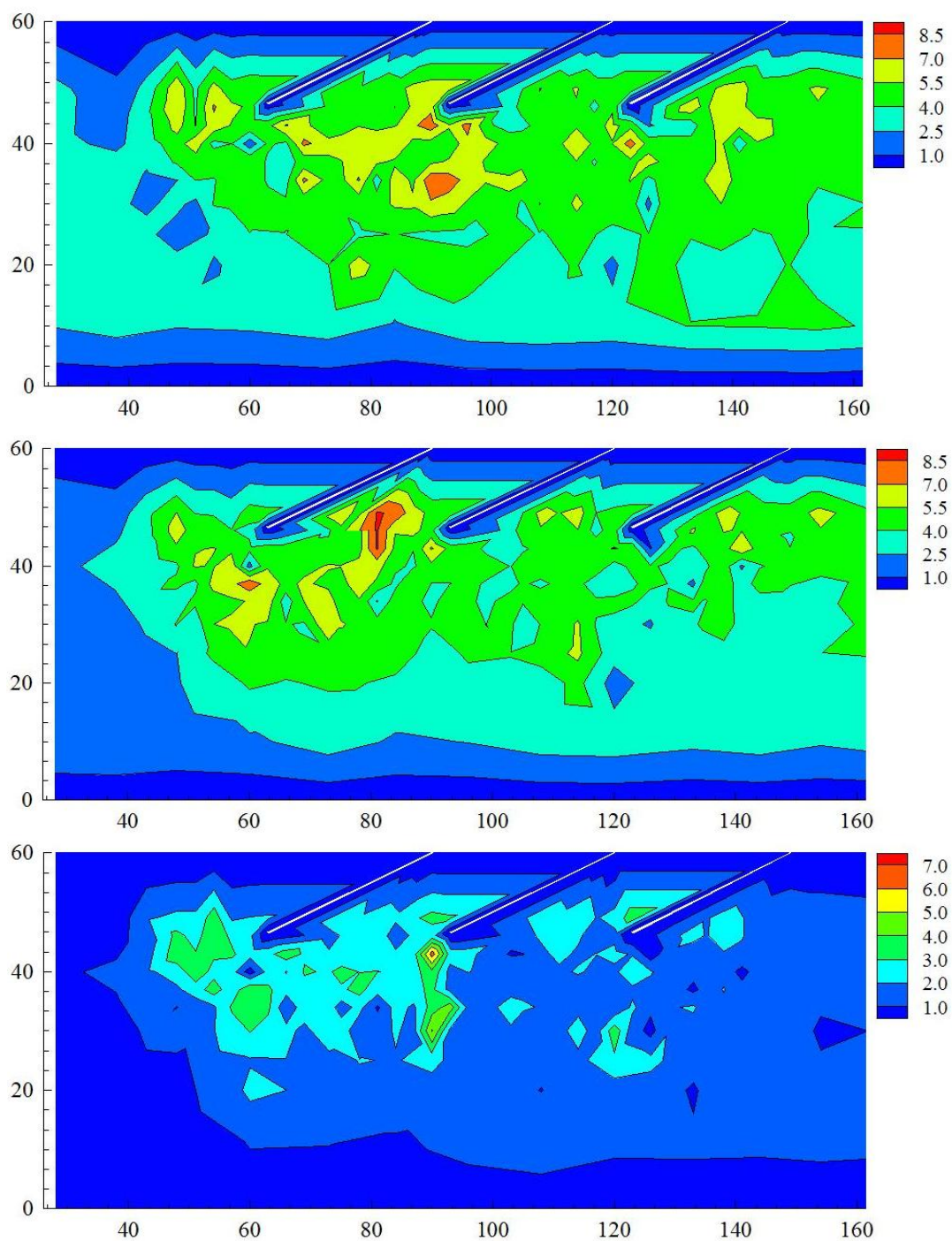


Figure 6c: Dimensionless turbulence intensities $\frac{u'}{u_{*0}}$ (*top*), $\frac{v'}{u_{*0}}$ (*center*), and $\frac{w'}{u_{*0}}$ (*bottom*) for angled dikes on the mobile bed at $Q = 0.035 \text{ m}^3/\text{s}$.

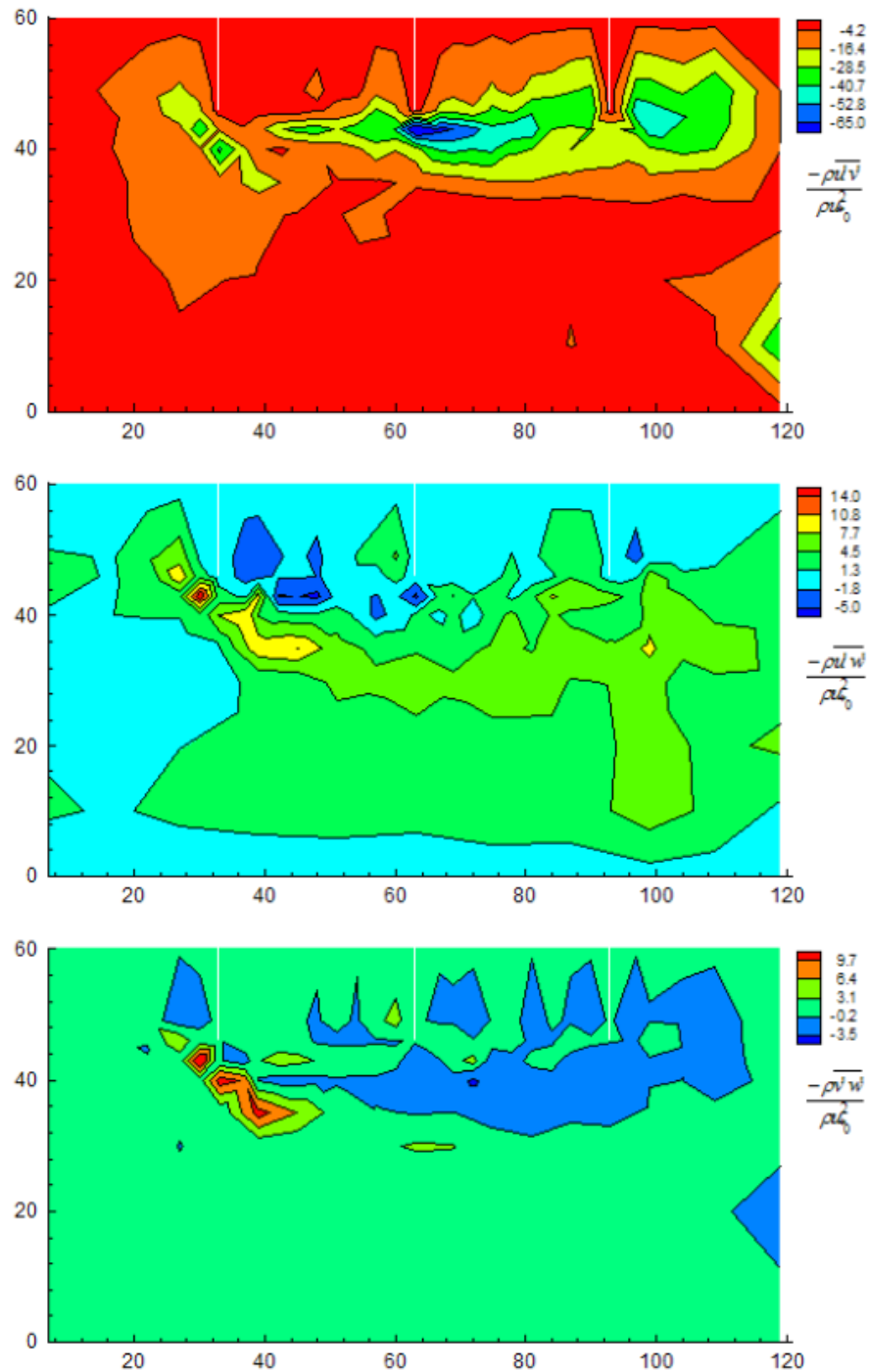


Figure 7a: Dimensionless Reynolds stresses $\frac{-\rho u'v'}{\rho u_{*0}^2}$ (top), $\frac{-\rho u'w'}{\rho u_{*0}^2}$ (center) and

$\frac{-\rho v'w'}{\rho u_{*0}^2}$ (bottom) for straight dikes on the fixed bed at $Q = 0.035 \text{ m}^3/\text{s}$.

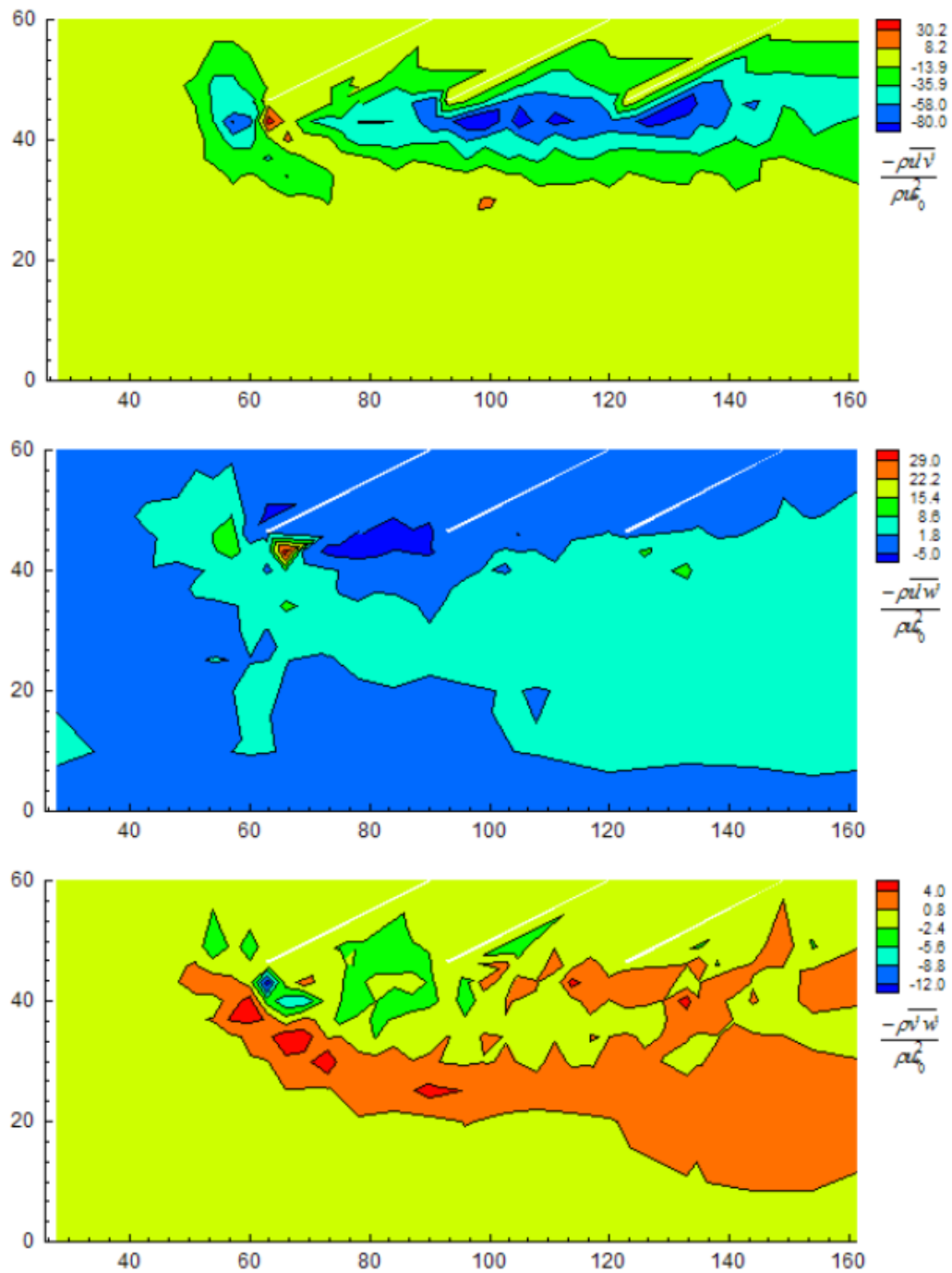


Figure 7b: Dimensionless Reynolds stresses $\frac{-\rho \overline{u'v'}}{\rho u_{*0}^2}$ (top), $\frac{-\rho \overline{u'w'}}{\rho u_{*0}^2}$ (center) and

$$\frac{-\rho \overline{v'w'}}{\rho u_{*0}^2} \text{ for angled dikes on the fixed bed at } Q = 0.035 \text{ m}^3/\text{s}.$$

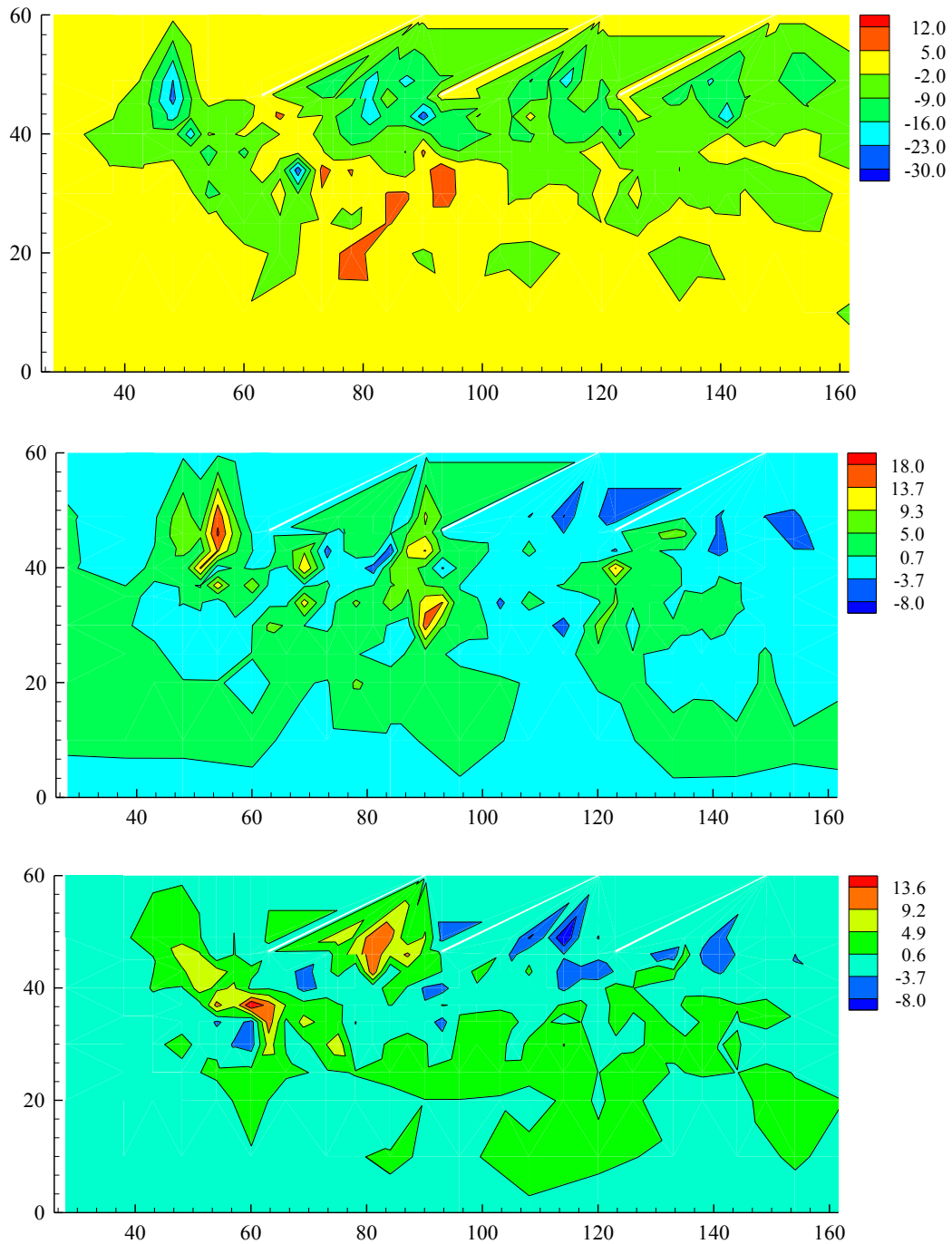
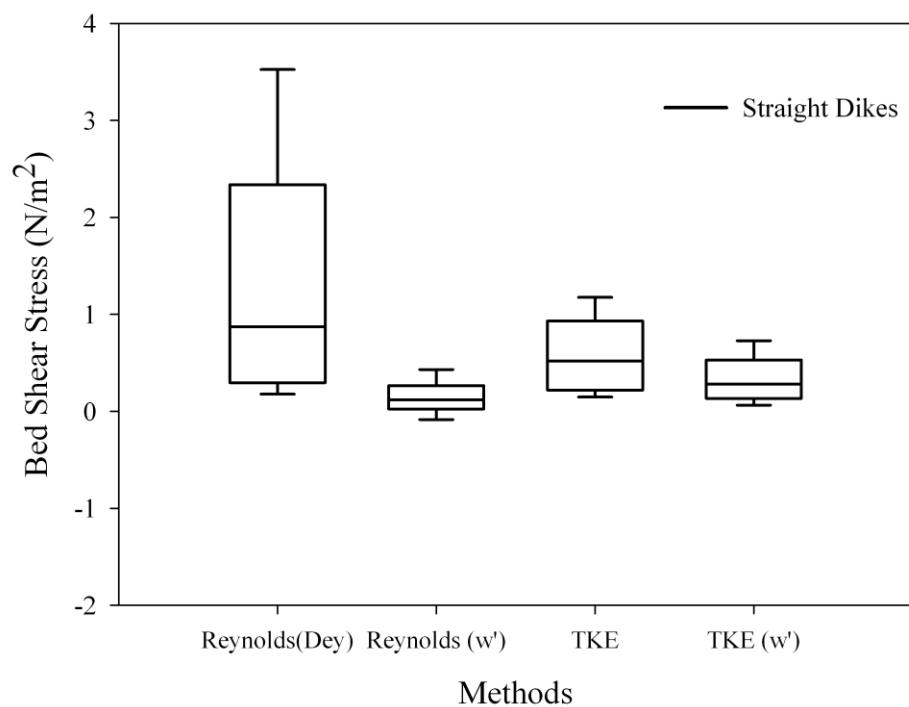
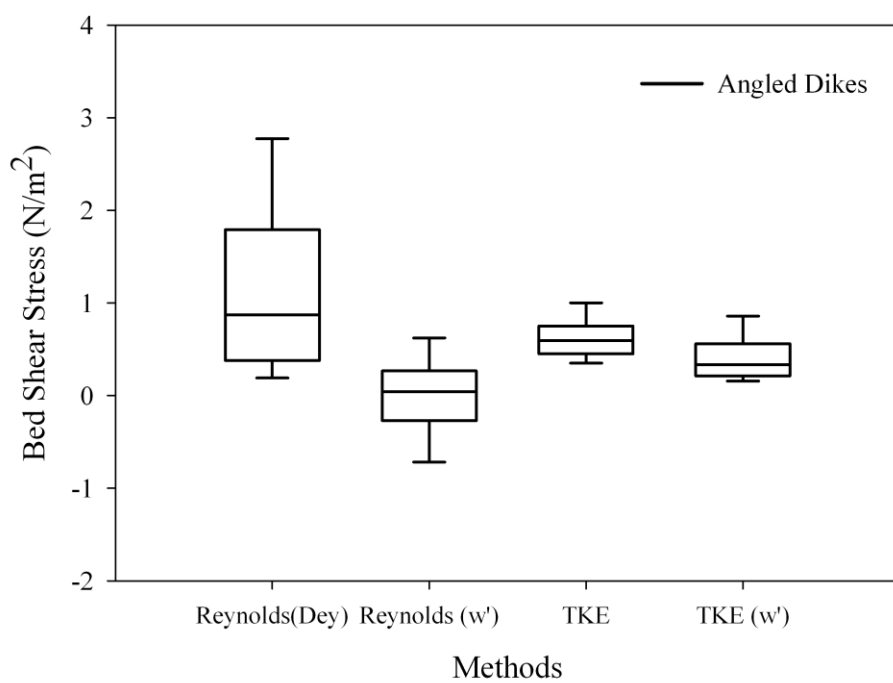


Figure 7c: Dimensionless Reynolds stresses $\frac{-\overline{\rho u'v'}}{\rho u_{*0}^2}$ (top), $\frac{-\overline{\rho u'w'}}{\rho u_{*0}^2}$ (center) and

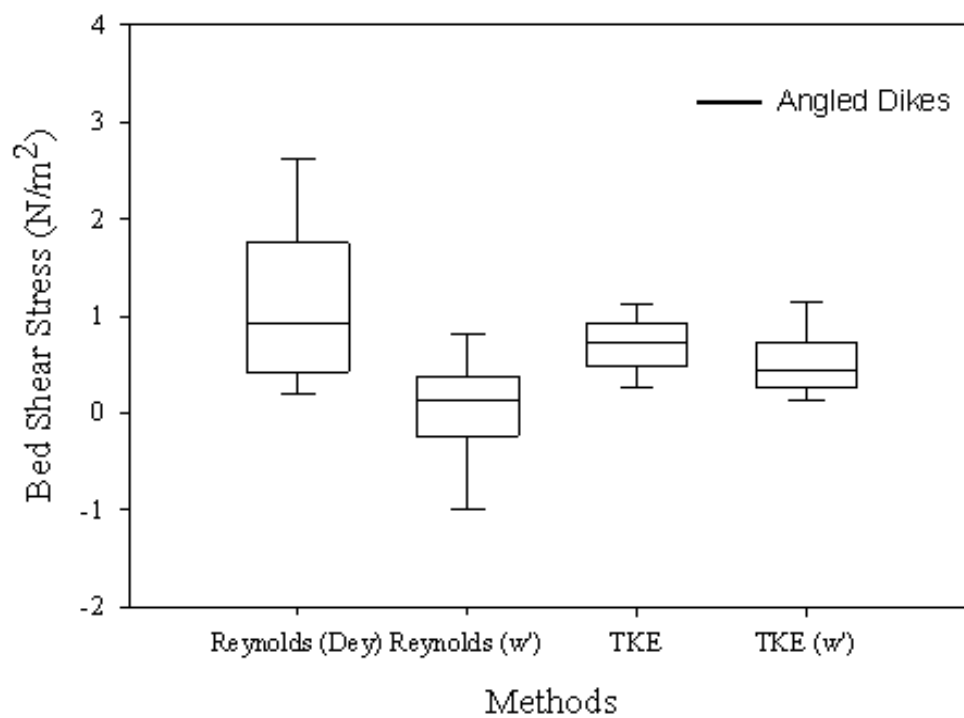
$$\frac{-\overline{\rho v'w'}}{\rho u_{*0}^2} \text{ for angled dikes on the mobile bed at } Q = 0.035 \text{ m}^3/\text{s}.$$



(a) Straight dikes on flat bed



(b) Angled dikes on flat bed



(c) Angled dikes on scoured bed

Figure 8: Comparison of different methods of calculating bed shear stresses for straight and angled dikes on the fixed and mobile bed

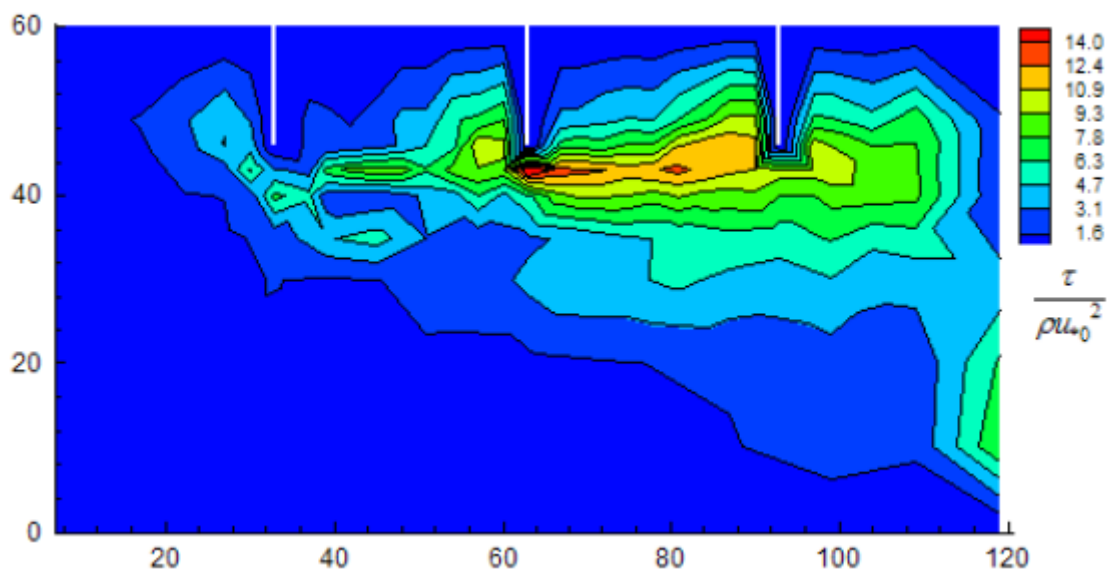


Figure 9a: Spatial distribution of dimensionless bed shear stress by the TKE method for straight dikes on the fixed bed at $Q = 0.035 \text{ m}^3/\text{s}$

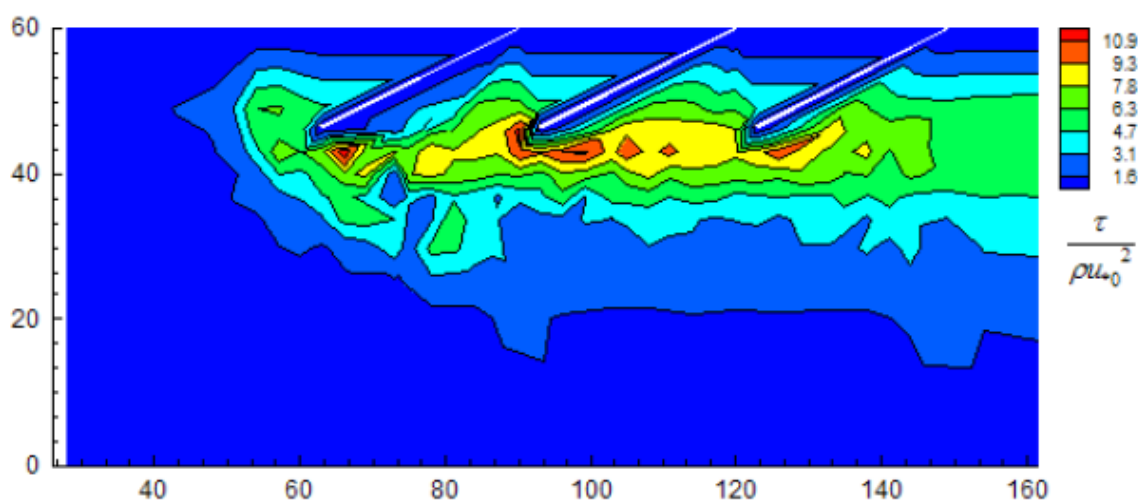


Figure 9b: Spatial distribution of dimensionless bed shear stress by the TKE method for angled dikes on the fixed bed at $Q = 0.035 \text{ m}^3/\text{s}$

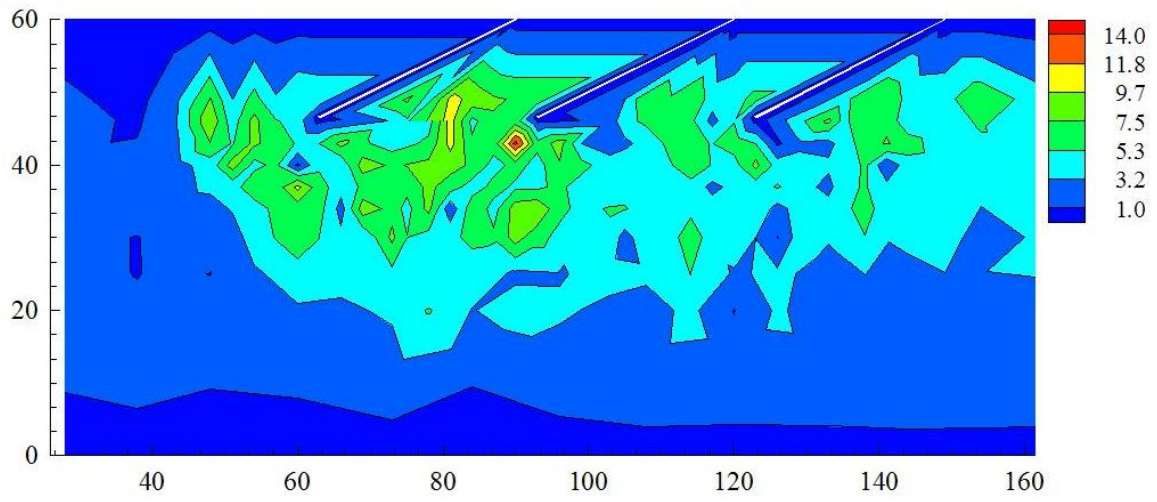


Figure 9c: Spatial distribution of dimensionless bed shear stress by the TKE method for angled dikes on the mobile bed at $Q = 0.035 \text{ m}^3/\text{s}$

APPENDIX C: THREE DIMENSIONAL SIMULATION OF FLOW
FIELD AROUND SERIES OF SPUR DIKES

Three Dimensional Simulation of Flow Field around Series of Spur Dikes

Anu Acharya¹, and Jennifer G. Duan²

Abstract

This paper presented a three-dimensional numerical simulation of turbulent flow field around a series of three experimental spur dikes in a flat and scoured bed surface using FLOW-3D software. At present, none of the turbulence closure model is valid for all cases of turbulent flow in open channels. Some turbulent closures offer advantages over others in specific turbulent flow fields depending on the nature of turbulence. This study examined one equation mixing length model, standard two-equation $k-\varepsilon$ model, Renormalization- Group (RNG) $k-\varepsilon$ model and Large Eddy Simulation (LES) model. Experimental data from a laboratory study of flow in a flat bed and scoured bed around a series of three dikes were used to verify the results from the numerical model. Although the simulated mean flow field is close to the experimental data for all the turbulence models, the simulated turbulence properties from different turbulent models deviate considerably. Modeling results of turbulent kinetic energy using the standard $k-\varepsilon$ model showed over 50% discrepancy from the measured. The RNG $k-\varepsilon$ model yielded better results of both mean flow field and turbulence kinetic energy for the flat bed surface and scoured bed surface. Based on these results, this study recommends the use of RNG $k-\varepsilon$ model for simulating mean flow field around dikes. Further improvements of FLOW-3D model is needed

¹Graduate Student, Department of Civil Engineering and Engineering Mechanics, Univ. of Arizona, Tucson, Arizona.

²Assistant Professor, Department of Civil Engineering and Engineering Mechanics, Univ. of Arizona, Tucson, Arizona.

for predicting turbulence properties (e.g. TKE) near this series of spur dikes under various flow conditions.

Subject headings: Numerical models; Local scour; Spur dike; Turbulence; Sediment transport; Hydraulics; Three-dimensional flow; Numerical simulation.

Introduction

Spur dikes are generally used to protect riverbanks from erosion or to maintain in-stream hydraulic structures, such as bridges. A single spur dike only change the local flow field. Spur dikes in series are often more effective to stabilize the eroding banks and to re-align the channel. Pools formed due to the local scour around spur dikes can enhance aquatic habitat in unstable streams (Shields et al. 1995; Kuhnle et al. 2008). Better understanding of the interactions between the three-dimensional flow field and the bed geometry around the spur dikes will benefit the river engineering applications of spur dikes.

Over the last few decades, most studies have focused on local scour around river hydraulic structures by physical modeling of bridge piers, spur dikes, and abutments. Since spur dikes and abutments are similar in many aspects, the studies on these hydraulic structures are comparable. The investigations on this type of obstruction have been studied extensively (Garde et al. 1961; Laursen 1963; Gill 1972; Kwan and Melville 1994; Lim 1997; Rahman et al. 1998; Kuhnle et al. 2008). Those studies reveal that the local scour pattern depends on the complex flow field around bridge piers, channel bed materials, and pier characteristics (Nagata et al. 2005). Similar to the flow field around a vertical circular pier, flow field around dikes is characterized by several

vortex systems of different sizes, which are developed due to the presence of the dike and are considered as the basic mechanism for scour initiation and development (Posey 1949; Shen et al. 1969; Dargahi 1987; Raudkivi 1990; Ahmed and Rajaratnam 1998, 2000). Though a substantial amount of experimental research on flow field around a single or a series of dike like structures has been completed (Melville 1992; Uijttewaal et al. 2001; Uijttewaal 2005, Weitbrecht et al. 2003; Stevens et al. 1991) flow hydrodynamics, especially turbulence properties, is yet to be fully comprehended.

Most previous studies have examined the impacts on flow field due to groynes orienting at 90° , 45° , 135° and 150° to the flow (Chrisohoides et al. 2003; Biron et al. 2005; Nagata et al. 2005; Haltigin et al. 2007). The local scour initiates as the shear stress exceeds the critical shear stress of sediment transport (Kuhnle et al. 2008). The three-dimensional flow field around a series of spur dikes is complex because of the interactions between flow and sediment transport as the scouring develops. Accurate prediction of scour depends on accurately resolving the flow turbulence structure and sediment transport (Mendoza and Cabrales 1993).

Better methods for predicting three-dimensional flow field and local scour have been developed through the application of three-dimensional hydrodynamic models (Richardson and Panchang 1998). Olsen and Melaan (1993) used a steady state Navier-Stokes solver coupled with a sediment transport algorithm to simulate the growth of a scour hole around a circular pier and concluded that "three-dimensional numerical models may be able to calculate the scour around an obstacle in a general complex geometry." Since the early work of Olsen and Melaan (1993), several numerical models have been developed and used to calculate the three-dimensional flow field around different river hydraulic structures (Jia and Wang 1993, 1996; Mayerle et al. 1995;

Ouillon and Dartus 1997; Richardson and Panchang 1998; Olsen and Melaaen 1993; Olsen and Kjellesvig 1998; Roulund et al. 1998; Haltigin et al. 2007; Smith and Foster 2005; Salaheldin et al. 2004; Ferguson et al. 2003; Bradbrook et al. 2001; Zhang et al. 2005; Nagata et al. 2005). With the advancements in computing technology, Computational Fluid Dynamics (CFD) analysis has emerged as a powerful hydraulics design tool (Griffith et al. 2007). The recent developments in computer software have advanced the use of CFD models to analyze flow field around the spur dikes. This study selected commercial CFD software, FLOW-3D, which has been approved as a robust three dimensional hydrodynamic model for studying the complex flow field and the scour initiation process around bridge piers of various sizes, shapes, and dimensions.

Several turbulence closure models have been used in simulating three dimensional flow fields around spur dikes and bridge piers. Mendoza-Cabrales (1993) used the $k-\varepsilon$ turbulence closure model to solve three-dimensional flow around circular piers and computed the associated bed shear stress. Melville (1975) found a large discrepancy between the experimental data and his numerical model results showing inadequacy of the $k-\varepsilon$ turbulence model for vertical three-dimensional flow. Smith and Foster (2005) compared the results of the large eddy simulation (LES) and the standard $k-\varepsilon$ turbulence model for three-dimensional flow around a cylinder over a scoured bed and confirmed the accuracy of the $k-\varepsilon$ model. The RNG $k-\varepsilon$ model of Yakhot and Orszag (1986) is an extension of $k-\varepsilon$ model (Rodi 1980) that requires less reliance on empirical constants and provides better solutions in areas affected by high shear flow (Sicilian et al. 1987). Yakhot and Orszag (1986) improved the RNG $k-\varepsilon$ model by systematically

removing the smallest scales of turbulence and calculating their effect on the remaining flow scales. Haltigin et al. (2007), Bradbook et al. (2001), and Richardson and Panchang (1998) showed that the renormalization-group (RNG $k - \varepsilon$) model performs well for simulating flows of extensive separations and recirculation.

The goal of this research is to examine the accuracy of various turbulence models for simulating the three-dimensional flow field around the spur dikes on a flat and scoured bed surface. The simulation results are evaluated with the laboratory data obtained at the University of Arizona. This paper summarizes the experiments, the model equations, turbulence closure, the computational domain, and the simulation results. The simulated results of mean flow velocities in three directions and turbulent kinetic energy are compared with the experimental measurements.

Experimental Procedure

The experiments were conducted in a recirculating flume 12.2 m long, 0.6 m wide, and 1.2 m deep located at the courtyard of Civil Engineering and Engineering Mechanics, University of Arizona. The channel sides were of painted metal with a 3m long smooth glass observation section on the right wall of the flume. Three spur dikes of 30 cm length, 4-mm thickness and 40 cm height were protruded from the left-wall of the channel facing upstream at an angle of 150° with a distance of 30 cm in between. The first angled dike was located at 1.8 m downstream of the flume inlet. The origin of the Cartesian coordinate was set at the intersection of the bed surface before scouring occurs, at the flume right wall, and 0.63 m upstream of the tip of the first spur dike [Fig. 1(a)]. A broad-crested weir of 10 cm height was placed at 10.6 m downstream of the inlet. A valve was used to maintain the required mean water depth of 20 cm at the weir with

the height of water above weir as 10 cm. The weir equation is $Q = KLH^{1.5}$, where L is the crest length, H is the height of water flowing over the weir, and K is some constant, was used. For this study, $K = 6678$ (for units of m^3/hr). The total discharge at weir was $0.035m^3/s$. A 16MHz SonTek micro-ADV was used to measure instantaneous velocity field. The acoustic sensor consists of one transmitter and three receivers. The receivers are aligned to intersect with the transmit beam at a small sampling volume located about 5cm away from the probe in order to reduce the interference with the flow. The control volume of SonTek ADV is a cylinder of diameter 4.0 mm and height of 5.6 mm. The micro-ADV was attached to a point gauge fixed on an instrument cart that was mounted on horizontal steel rails and moved on wheels. The u , v and w velocity components were defined in the longitudinal, transverse and vertical direction of the flume. The ADV was moved manually in all three directions to measure flow velocities at any location in the cross sections. Flow velocity data at each point were collected at 25 Hz for 4-5 minutes duration for 5000 instantaneous velocities.

Experiments were carried on for both flat fixed bed surface and mobile bed surface with 10 cm thick of a well-sorted sand and gravel mixture. The median grain diameter of sediment is 0.85 mm. The duration of the experimental run was 24 hours to allow the local scour reach an asymptotic state. After the scoured bed reached the equilibrium state, bed sediment was immobilized with a thin layer of cement from 0.50 m downstream of the channel inlet to the weir section for measuring flow field. The study reach was divided into 41 cross sections. Flow velocities were measured at 304 locations on the x-y plane as shown in Fig. 1 (b). The turbulent flow field around the dikes was measured in a grid; starting at 5 mm from the bed, 10 cm from the left wall and extending to 10 cm from the right wall [Fig 1(b)]. The measurement grid was

arranged such that the nodes were denser around the dikes and becoming sparser away from the dikes. At each location, velocity measurements were made at ten vertical positions: $z = 0.5, 1.5, 2.5, 3.5, 4.5, 5.5, 6.5, 7.5, 8.5$ and 9.5 cm, which results in a total set of 3,040 point-velocity measurements. All velocity records were processed using the public domain software WinADV to obtain the signal-to-noise ratio (SNR) values of each point velocity record. The signal-to-noise ratio (SNR) is a measure of the relative quality of the acoustic signal received by the ADV whose value should be at least higher than 15 when measuring turbulence (SonTek 2001). Measurements were filtered using WinADV to reject points with a SNR less than 20. In the present study, 80% or more of the data was above this cutoff value. The approach bed-shear velocity was calculated from the measured velocity profile at 63 cm upstream from the tip of the first spur dike and in the center of the channel. The shear velocity, $u_* = 1.30$ cm/s, and zero velocity level, z_0 , were determined by fitting logarithmic velocity profile and assuming the von Karman constant as 0.41 for the erodible bed run. The mean velocity of approaching flow was 29.10 cm/s.

Model

The CFD model selected for this study is the commercially available software 'FLOW-3D' (Flow Science 2009), which simultaneously solves the three dimensional, transient Navier-Stokes equations on a structured grid. Flow3D involves very little approximation with the exception of turbulent closure parameterizations to model internal stresses (Rodi 1980). A detailed description of FLOW-3D can be found in FLOW-3D User's Manual V9.4 (Flow Science 2009). The program is based on the fundamental laws of mass, momentum and energy conservation and applicable to almost any type of flow process. This model is capable of fluid-

boundary tracking by resolving fluid-fluid and fluid-air interfaces with rectangular non-boundary fitted coordinates. This model has been used for various hydraulic and coastal engineering applications, such as flow and scour around a bridge pier (Richardson and Panchang 1998), flow over a sharp-crested weir, and the near shore transformation of waves (Bradford 2000; Chopakatla 2003). The model also has a number of other features including the ability to construct non-uniform grids, automatic time-step selection, graphical post processing, etc. It utilizes a finite difference solution scheme and is able to calculate solutions using various implicit and explicit solver options. FLOW-3D uses a simple grid of rectangular elements. Therefore, it has the advantages of easy mesh generation, regularity for improved numerical accuracy, and minimal memory storage requirement. Geometry is defined within the grid by computing the fractional face areas and fractional volumes of each element that are blocked by obstacles. The use of a multiple and nested meshes, and the re-run capability available in FLOW-3D software, are other options that make the numerical model suitable for hydraulic structure modeling.

The governing equation is the Navier-Stokes equation for incompressible flows as follows:

$$\frac{\partial}{\partial x_i}(u_i A_i) = 0 \quad (1)$$

$$\frac{\partial u_i}{\partial t} + \frac{1}{V_f} \left(u_j A_j \frac{\partial u_i}{\partial x_j} \right) = -\frac{1}{\rho} \frac{\partial P}{\partial x_i} + G_i + f_i \quad (2)$$

where u_i =mean velocity; P =pressure; A_i =fractional open area open to flow in the i direction; V_f =fractional volume open to flow; f_i represents the viscous accelerations; G_i represents the body accelerations.

For a variable dynamic viscosity μ , the viscous accelerations f_i are

$$\rho V_f f_i = \tau_{w,i} - \left\{ \frac{\partial}{\partial x_j} (A_j \tau_{ij}) \right\} \quad (3a)$$

$$\tau_{ij} = S_{ij} = -\mu_{tot} \left(\frac{\partial u_i}{\partial x_j} + \frac{\partial u_j}{\partial x_i} \right), \quad \tau_{ii} = S_{ii} = -2\mu_{tot} \left(\frac{\partial u_i}{\partial x_i} \right) \quad (3b)$$

where S_{ij} =strain rate tensor; $\tau_{w,i}$ =wall shear stress; ρ =density of water; μ_{tot} =total dynamic viscosity, which includes the effects of turbulence $\mu_{tot} = \mu + \mu_T$; μ =dynamic viscosity; and μ_T =eddy viscosity.

For non-transport closure schemes (e.g., LES models), the wall shear stress, $\tau_{w,i}$ is computed as:

$$\tau_{w,i} = \frac{(\mu + \rho a u k_s) u}{d} \quad (4)$$

where u =parallel component of the velocity computed adjacent to the wall; d =normal distance of the computed velocity from the wall; a =a constant equal to 0.246; and k_s = roughness .

The wall boundary conditions are evaluated differently depending on the turbulence closure scheme. In two equation closure schemes (e.g., RNG $k-\varepsilon$ model, standard $k-\varepsilon$ model), boundary conditions for turbulent kinetic energy and energy dissipation rate are computed using the logarithmic law of the wall formulation and calculated as:

$$k = \frac{u_*^2}{\sqrt{C_\mu}}, \quad \varepsilon = \frac{u_*^3}{\kappa d} \quad (5)$$

where u_* is the local shear velocity determined from the log-law:

$$u = u_* \left[\frac{1}{\kappa} \ln \left(\frac{\rho u_* d}{\mu} \right) + 5.0 \right] \quad (6)$$

where κ =von Karman constant.

Smagorinsky Large Eddy Simulation (LES) model uses the non-transport closure scheme.

The characteristic length scale, L , and the LES kinematic eddy viscosity, ν_T are defined as:

$$L = (\delta x \delta y \delta z)^{1/3} \quad (7)$$

$$\nu_T = (cL)^2 \sqrt{e_{ij} e_{ij}} \quad (8)$$

where c = a constant equal to 0.1- 0.2; e_{ij} denotes the strain rate tensor components given as:

$$e_{ij} = \frac{1}{2} \left(\frac{\partial u_i}{\partial x_j} + \frac{\partial u_j}{\partial x_i} \right) \quad (9)$$

The volume of fluid (VOF) method (Hirt and Nichols 1981) is employed in FLOW-3D for tracking fluid-air or fluid-fluid interfaces. The VOF method of tracking has the ability to ignore the air surrounding the flowing water and records the volume of fluid in each rectangular cell. This method also allows the numerical model to create a sharp interface between the water and air without using the fine meshes required by other CFD software. The interfaces with solid boundaries are simulated with the fractional area-volume obstacle representation (FAVOR) method (Hirt and Sicilian 1985) for modeling solid obstacles. It allows the program to use fully structured grids that are very easy to generate throughout the entire flow domain. Other CFD programs may require the use of deformed grid to model flow over and around structures. Additionally, it accounts for cells that are not wholly wet or dry by determining their fractional influence on the flow. Because of those advantages, relative good representations of flow of complex geometries can be obtained from comparatively coarse meshes. In this study, the three angled dikes were resolved nicely by this method. Most of the terms in the equations are evaluated using the current time-level values of the local variables in an explicit fashion, though a number of implicit options are available.

FLOW-3D supports several turbulent closures using a number of advanced and widely accepted numerical schemes (Launder and Spalding 1972; Rodi 1980; Abbot and Basco 1989; Shaw 1992). These include Prandtl's mixing length, one equation turbulent energy (k), the two-equation($k-\varepsilon$), Renormalization-Group (RNG), and Large Eddy Simulation (LES) closure schemes. For flow field around dikes, an advanced turbulence closure model is required. The kinematic turbulent viscosity is related to the turbulent kinetic energy, k , and the turbulent dissipation, ε , via the Kolomogorov- Prandtl expression (Flow Science 2009)

$$\nu_T = C_\mu \frac{k^2}{\varepsilon} \quad (10)$$

The closure transport equations for turbulent kinetic energy, k , and turbulent dissipation rate, ε , are given by

$$\frac{\partial k}{\partial t} + u_i \frac{\partial k}{\partial x_i} = \frac{\partial}{\partial x_i} \left(\frac{\nu_t}{\sigma_k} \frac{\partial k}{\partial x_i} \right) - \nu_t \left(\frac{\partial u_i}{\partial x_j} + \frac{\partial u_j}{\partial x_i} \right) \frac{\partial u_i}{\partial x_j} - \varepsilon \quad (11)$$

and

$$\frac{\partial \varepsilon}{\partial t} + u_i \frac{\partial \varepsilon}{\partial x_i} = \frac{\partial}{\partial x_i} \left(\frac{\nu_t}{\sigma_\varepsilon} \frac{\partial \varepsilon}{\partial x_i} \right) - C_{1\varepsilon} \frac{\varepsilon}{k} \left[\nu_t \left(\frac{\partial u_i}{\partial x_j} + \frac{\partial u_j}{\partial x_i} \right) \frac{\partial u_i}{\partial x_j} \right] - C_{2\varepsilon} \frac{\varepsilon^2}{k} \quad (12)$$

The empirical constants for the standard $k-\varepsilon$ model are:

$$C_\mu = 0.09, C_{1\varepsilon} = 1.44, C_{2\varepsilon} = 1.92, \sigma_k = 1.0, \text{ and } \sigma_\varepsilon = 1.30, C_{1\varepsilon} = 1.44, C_{2\varepsilon} = 1.92, \sigma_k = 1.0$$

and $\sigma_\varepsilon = 1.30$. The original turbulence model (Yakhot and Orszag 1986) using renormalization group (RNG) theory, results in a model similar to the standard $k-\varepsilon$ model, but with different values for the constants. An extra production term for ε was added in a modification by Yakhot et al. (1992). However, equation constants that are found empirically in the standard $k-\varepsilon$ model are derived explicitly in the RNG model. These differences result in greater dissipation of

turbulence in areas of strong strain, and therefore lead to reduction in eddy viscosity that improves velocity predictions. The empirical constants for RNG $k - \varepsilon$ model are:

$$C_{\mu} = 0.085, C_{1\varepsilon} = 1.42, \sigma_k = 0.7194, \sigma_{\varepsilon} = 0.7194$$

where $C_{2\varepsilon}$ is computed from the turbulent kinetic energy (k) and turbulent production

$$\left(\nu_t \left(\frac{\partial u_i}{\partial x_j} + \frac{\partial u_j}{\partial x_i} \right) \frac{\partial u_i}{\partial x_j} \right) \text{ terms.}$$

To initialize the model, volume flow rate, mean approach velocity of 0.29 m/s, and flow depth of 0.25 m in z-direction were entered at the inlet of the channel. The boundaries bordering the dikes were assumed to have a no-slip rough surface. The roughness values for the flume and the bed for these simulations was 0.00085 m. The inflow boundary was assumed to have a known uniform velocity. An outflow boundary with no re-entry of the fluid condition was used at the downstream boundary. Wall boundary was applied to the bed and sidewalls, which were defined as no-slip conditions. Boundary condition at the water surface was specified Pressure boundary with the fluid fraction is equal to zero.

A non-uniform computational mesh was constructed within a rectangular coordinate system (Fig. 2). A relatively fine mesh was used around the dikes but coarser ones away from the dike to minimize the computational cost and to efficiently improve the resolution in the vicinity of the spur dikes. The spur dikes were created as the solid objects and inserted into the domain at the appropriate locations as in the experimental setup. The smallest horizontal grid size is 3 mm, which provided adequate discretization of the spur dike geometry. The mesh spacing near the base was dense in both the vertical direction. As a result, 40 vertical layers were used in the

vicinity of spur dikes. The modeling grid with 197,000 nodes was found to be sufficient to reproduce the flow field accurately.

All the simulations were run for a long period until the flow field reached the steady state. FLOW-3D uses explicit time stepping and adjusts the time step continuously during the computation. After the turbulence flow field reached steady state, the changes of the volume of fluid, mean kinetic energy, and average turbulent kinetic energy was less than 2% resulting the steady state solutions. Results from each simulation were used to compare with the experimental measurements. In all calculations, default values of the various turbulence model coefficients were used. Simulations were performed for the initial flat bed and scoured bed cases. In the present investigation, a comparative study of three different turbulence models, RNG $k-\varepsilon$, standard $k-\varepsilon$ and LES models was made to analyze flow field around the spur dikes and the computed results are compared with the experimental data.

Results and Discussions

Simulated results of mean flow and turbulence for the plane and scoured bed cases were compared with the experimental measurements to evaluate the accuracy of different turbulence closure models in reproducing the three-dimensional flow field around a series of spur dikes. Yaeger (2009) carried out the laboratory experiment on the fixed plane bed for a constant flow depth of 20 cm using the ADV. Yaeger (2009) measured the near bed turbulence and the velocity field using the experimental setup and procedure similar to this study for the scoured bed surface. The bathymetry of the scoured bed surface was directly imported into the model as the model input. Three turbulence closure schemes: standard $k-\varepsilon$ model, the Renormalized $k-\varepsilon$ model and the LES model, were used. In order to compare simulated velocities with the measurements

using the ADV, the model output was sampled at the grid cells of the measurements.

Fig. 5 shows the computed velocity vectors in the lateral sections: C-C, D-D and H-H. It is seen that flow is fully three dimensional in the vicinity of the spur dikes and downward flow develops along the upstream wall of the first dike. Vortical flow is seen to form in front of the spur dikes near the bottom [Fig. 5(a) and 5(b)]. A strong transverse flow towards the left sidewall at $y = 30\text{-}50$ cm in section C-C can be seen in Fig 5 (a), which is caused by the lateral flow contraction. Further downstream of the 1st dike at section D-D Fig 5 (b), and H-H Fig 5 (c), a clockwise secondary flow circulation (looking downstream) is formed, a typical feature of the flow near dikes.

Fig. 6, 7, 8 and 9 shows a comparison of the vertical distributions of the longitudinal velocity (u), transverse velocity (v), vertical velocity (w) and Turbulent Kinetic Energy (TKE) between the observed and computed results at nine sections from A-A to I-I for the scoured bed. At the approaching flow section A-A, the vertical distributions of the longitudinal velocity, u , obtained using standard $k-\varepsilon$, RNG $k-\varepsilon$, and the LES models fall in a narrow band and agrees with the experimental data (Fig. 6). At section BB, the predicted values of u near the bottom using the standard $k-\varepsilon$ and RNG $k-\varepsilon$ models are higher than the results using the LES model. The LES model underestimates the longitudinal velocity throughout the entire profile. The disagreement is especially pronounced near the bottom and decreases towards the free surface. At section C-C at the tip of the first dike, results from the RNG $k-\varepsilon$ model show the closest match with the experimental measurements. Further, as the vortical flow fully develops from section D-D to F-F, the results from LES model best match the experimental measurements, whereas the results of u , using the standard $k-\varepsilon$ and RNG $k-\varepsilon$ model, deviate from the

experimental values. As flow approaches to the weak region from section G-G to I-I, the result from the RNG $k-\varepsilon$ model best matches the measurements while the results of LES model becomes less accurate.

At the approaching flow section A-A, the vertical distributions of the transverse velocity, v , obtained using the RNG $k-\varepsilon$ model fall in a narrow band and agrees with the experimental data while the standard $k-\varepsilon$ and the LES models over-predicted the experimental data (Fig.7). At section B-B, the predicted values of v near the bottom using the standard $k-\varepsilon$ and RNG $k-\varepsilon$ models predict the results better than using the LES model. The LES model underestimates the transverse velocity throughout the entire profile up to the middle of the channel and overestimates the other half. The disagreement is distinct near the bottom and reduces towards the free surface. At section C-C at the tip of the first dike, results from the RNG $k-\varepsilon$ model shows the closest match with the experimental measurements. Further downstream from Section D-D to F-F, none of the models best matches the experimental measurements. The results of v using the standard $k-\varepsilon$, RNG $k-\varepsilon$ and LES model deviate from the experimental values. As flow approaches to the weak region from section G-G to I-I, the results from the RNG $k-\varepsilon$ model best match the measurements at the bottom layers and the gap widens towards the free surface. The results of LES model also become less accurate

At the approaching flow section A-A, the vertical distributions of the vertical velocity, w obtained using the standard $k-\varepsilon$, RNG $k-\varepsilon$, and the LES models over-predict the measured data at the bottom layers and agree well with the experimental data towards the surface layers (Fig. 8). At section B-B, the predicted values of w using the standard $k-\varepsilon$ and the RNG $k-\varepsilon$

models are smaller than the results using the LES model. The LES model overestimates the vertical velocity throughout the entire profile. The remarkable disagreement is at the free surface and decreases towards the bottom. At section C-C, the RNG $k-\varepsilon$ model shows better results than the other two models and shows the closest match with the experimental measurements. Further downstream of the vortical flow sections from D-D to F-F, the results from LES model best match the experimental measurements. At the wake region from section G-G to I-I, the results from the RNG $k-\varepsilon$ model best match the measurements at the free surface but deviate towards the bottom. The LES model mostly under-predicts the experimental data in this region.

At the approaching flow section A-A, the vertical distributions of the Turbulent Kinetic Energy, TKE, obtained using the standard $k-\varepsilon$ and RNG $k-\varepsilon$ models over-predict the experimental data at the bottom and agree well towards the free surface (Fig 9). At section B-B, the predicted values from both models fall in a narrow band and agree with the experimental data. At section C-C at the tip of the first dike, results from the RNG $k-\varepsilon$ model show the closest match with the experimental measurements, but the pronounced disagreement is seen at the middle layers with the model not being able to follow the data trend correctly. Further downstream as the vortical flow fully develops from Section D-D to F-F, none of the models predicts the experimental data correctly. The results from the standard $k-\varepsilon$ and RNG $k-\varepsilon$ model deviate from the experimental data. As flow approaches to the wake region from section G-G to I-I, the predicted values of TKE using the standard $k-\varepsilon$ model are greater than the results using the RNG $k-\varepsilon$ model. However, The RNG $k-\varepsilon$ model also overestimates the TKE throughout the entire profile. The disagreement is evident near the bottom and decreases

towards the free surface. These results indicated that the RNG $k-\varepsilon$ model is most suitable in the regions of flow contraction and turbulence wake and is not as accurate as the LES model in highly turbulent flow region with strong turbulence concurrent structures.

To compare the simulated results from FLOW-3D using different turbulence closure models, statistical parameters are calculated for the errors between the simulated and measured data in Table 1 and Table 2. Four statistical measures of model predictions are adapted in this study. The first one is R-squared correlation that measures the model's accuracy in predicting the velocities in three dimensions. Similar tests in the recent literature on CFD applications to open channels (Ferguson et al. 2003; Bradbrook et al. 2001; Biron et al. 2007) have reported R^2 , the squared correlation between simulated and measured values of a flow property. In applications to smooth-walled flumes, R^2 values up to 0.95 for u and 0.75 for w have been achieved (Bradbrook et al. 1998), but results for natural rivers showed worse agreement between modeling results and measurements: R^2 values of 0.50–0.89 for the horizontal velocity component and 0.01–0.50 for the vertical component (Hodkinson and Ferguson 1998; Lane et al. 1999; Nicholas and Smith 1999; Bradbrook et al. 2000a). The model's accuracy in predicting the velocity magnitudes is evaluated using the mean absolute error (MAE), mean square error (MSE), and root mean square error (RMSE). The MAE, MSE and RMSE are defined as:

$$MAE = \frac{1}{n} \sum_{i=1}^n |O_i - P_i|; MSE = \frac{1}{n} \sum_{i=1}^n (O_i - P_i)^2; RMSE = \sqrt{\frac{1}{n} \sum_{i=1}^n (O_i - P_i)^2} \quad (13)$$

where n = number of velocity data points within each individual longitudinal velocity profile; O_i and P_i = the observed and predicted values, respectively. The R^2 , MAE, MSE, and RMSE are

calculated for the horizontal mean velocity, u , the transverse velocity, v , the mean vertical velocity, w , and the Turbulent Kinetic Energy, TKE.

The correlation coefficients show an overall good agreement for the longitudinal and transverse velocity, with average R^2 values for the flat and scoured bed case being 0.870 and 0.714, respectively. However, much weaker agreements are found for the vertical component (w) and turbulent kinetic energy (TKE), with R^2 ranging between 0.187-0.464 and 0.384 - 0.434 for w and TKE, respectively. Because of the smaller range of velocities in the vertical component, lower velocity correlations have been seen in most three dimensional CFD studies (e.g., Bradbrook et al. 2001; Ferguson et al. 2003; Haltigin et al. 2007). In addition, the lower correlation is also due to differences in the position of the center of the simulation cells compared to the ADV sampling volume. Table 1 and Table 2 show the statistical parameters between the predicted and observed mean velocity and turbulent kinetic energy for all three turbulence models used in this study. Table 1 summarizes the results of 304 nodal points measured near the bed whereas Table 2 includes the results of 3040 points in the scoured bed experiment. Better agreements (as measured by R^2 ; Table 1 and Table 2) than in most of these previous studies (Lane et al. 1999; Nicholas and Smith 1999; Bradbrook et al. 2000a) are obtained, which gives some confidence in the use of the CFD models to identify and describe the flow structures.

Comparison of the results from the RNG $k-\varepsilon$ model with the standard $k-\varepsilon$ model and LES model shows the importance of selecting an appropriate turbulence models in simulating turbulent flow field around the spur dikes. The improvement in modeling results using the RNG $k-\varepsilon$ model is most evident in the transverse velocities for which the correlation between the

predicted and measured values in scoured bed is only 0.495 using the standard $k-\varepsilon$ model, 0.359 using the LES model, and 0.891 using the RNG $k-\varepsilon$ model (Table 2). Similarly, the correlation is 0.651 using the LES model, 0.846 using the $k-\varepsilon$ model, and 0.888 using the RNG $k-\varepsilon$ model in the plane bed case (Table 1). In addition, the correlation between simulated and measured vertical velocity is also higher using the RNG $k-\varepsilon$ model compared to the standard $k-\varepsilon$ model and LES model. The correlation between simulated and measured turbulent kinetic energy for plane bed and scoured bed case using RNG $k-\varepsilon$ is 0.658 and 0.620 respectively, which is higher than the standard $k-\varepsilon$ model. The simulated turbulent kinetic energies with the standard $k-\varepsilon$ model are generally higher than those using RNG $k-\varepsilon$ model, and an inspection of the values shows this is especially true within the recirculation zone. The study implies that the simulated turbulent kinetic energy with the RNG $k-\varepsilon$ model are generally lesser than those observed [Fig. 10(d) and 11(d)] and there is a prominent difference in the recirculation zone. The predictions using the RNG $k-\varepsilon$ model agree better than other turbulence models for the existing experimental results of flow field around a series of dikes on the plane bed and scoured bed. Using the RNG $k-\varepsilon$ turbulence model, the general agreements between model predictions and measured velocity components give sufficient confidence to use the numerical model to investigate the turbulence flow field and scour formation around dikes. Therefore, the Renormalization Group (RNG) model (Yakhot and Smith 1992), a widely used turbulence closure model for incompressible flow, is adopted for the comparative study of the simulated and experimental results for the plane and scoured bed experiments.

Fig.10 and Fig.11 show plots of measured versus predicted values for the simulation using

the RNG $k-\varepsilon$ turbulence model. The point velocities from the model match the measured data with very little systematic error in Fig. 10 and 11, although some discrepancies in the recirculation zone are apparent. In the main channel and near the upstream side of the spur dike, the predicted velocities are very close to those measured. For the simulation with the RNG $k-\varepsilon$ turbulence model, the equations of the regression lines for the longitudinal velocity and transverse velocities are very close to the line of perfect agreement. Although the correlation for the vertical velocity is lower, it is still very reasonable. The lower correlation for the vertical velocity attributes to ADV measurement errors as it approaches to the bed surface. The correlation for turbulent kinetic energy is much lower, and the highest values are under-predicted by about 50%. Given the success of the model in predicting the mean velocities, the performance of the RNG $k-\varepsilon$ turbulence model appears to be preferable to the standard $k-\varepsilon$ and the LES turbulence model. However, none of the turbulence closure models is accurate in predicting the measurements of turbulent kinetic energy (Lane et al. 1999). The inaccuracies in TKE prediction are caused by the limitations of turbulence closure models and the errors of ADV measurements especially near the bed surface. This result further confirm that the existing turbulence closure models are suitable for predicting mean flow field and limited in predicting turbulence properties (e.g. TKE). Direct simulation of turbulence flow field without any turbulence closure models perhaps will provide better results of turbulence flow field.

Conclusions

This study employed FLOW-3D model to simulate the three-dimensional turbulent flow field around a series of three spur dikes in a flat fixed and a scoured bed. This study examined one

equation mixing length model, Prandtl's mixing length model, one equation turbulent energy (k) model, standard two-equation ($k - \varepsilon$) model, RNG turbulence model, and large eddy simulation. Prandtl's mixing length model and one equation turbulent energy (k) model were not used for the detailed analysis due to their inability to simulate the flow field near the dikes effectively.

Experimental data on a flat and a scoured bed were used to verify the results from the numerical model. Although the simulated mean flow field is close to the experimental data, the simulated turbulence properties from different turbulent model deviate considerably. The MSE for the mean longitudinal velocity ranged from 0.001-0.005 for the RNG $k - \varepsilon$ model, 0.010 - 0.011 for the standard $k - \varepsilon$ model and 0.011-0.013 for the LES model. The correlation (R) for mean horizontal velocity ranged from 0.796 to 0.976 for the RNG $k - \varepsilon$ model, 0.545 - 0.790 for the standard $k - \varepsilon$ model, and 0.531-0.602 for the LES model. The model predicted quite good estimations of the longitudinal mean velocity regardless of turbulence closure schemes. However, the predictions of vertical velocity showed more variability using different closure schemes. The overall agreement between the simulated and measured velocities is good, with the exception of a systematic discrepancy in areas where the transverse and vertical velocity components are negative. This occurs primarily downstream of the spur dike in the recirculation zone.

Although the standard $k - \varepsilon$ model and LES model are considered superior in different studies of three-dimensional flow field, these models performed poorly compared to the RNG $k - \varepsilon$ model in estimating the flow velocity and turbulent kinetic energy around a series of spur dikes. The LES model largely underestimated the velocity field near the bed, while the results

using the standard $k-\varepsilon$ model showed over 50% discrepancy from the measured TKE. The RNG $k-\varepsilon$ model is found to give good results for estimating the longitudinal and transverse velocity field whereas the results are only satisfactory for the vertical velocity field and the turbulent kinetic energy. The results show that the differences between the simulated and experimental values are smaller at the measurement positions further downstream from the dikes (such as 1mm) as flow becomes steady uniform. Since the simulated results of mean flow field qualitatively agree with the experimental data, this study recommends the use of RNG $k-\varepsilon$ model for simulating the mean flow field around the dikes for fixed flat and scoured bed. Since none of the turbulence closure model was able to predict accurately the turbulence properties (e.g. TKE) near the dikes, improvements in FLOW3D is needed for better predicting turbulence flow properties by using direct numerical simulation technique.

Notations

The following symbols are used in this paper:

x = horizontal longitudinal direction

y = horizontal transverse direction

z = vertical direction

h = depth of water at the weir (m)

H = height of water flowing over the weir (m)

D = distance between two dikes at the base (cm)

Q = volumetric discharge ($\text{m}^3 \cdot \text{s}^{-1}$)

K = weir constant for discharge units $\text{m}^3 \cdot \text{hr}^{-1}$

L = weir crest length (cm)

l = dike length (cm)

V_x = velocity in horizontal direction ($\text{m} \cdot \text{s}^{-1}$)

u, v, w = mean flow velocities ($\text{m} \cdot \text{s}^{-1}$)

u_* = shear velocity ($\text{m} \cdot \text{s}^{-1}$).

ρ = density of water ($\text{kg} \cdot \text{m}^{-3}$)

References

- Abbot, M., and Basco, D. (1989). *Computational fluid dynamics: An introduction for Engineers*.
- Ahmed, F., and Rajaratnam, N. (1998). "Flow around bridge piers." *J. Hydraul. Eng.*, 124(3), 288 – 300.
- Ahmed, F., and Rajaratnam, N. (2000). "Observations of flow around bridge abutment." *J. Eng. Mech.*, 126(1), 51 – 59.
- Biron, P. M., Haltigin, T.W., Hardy, R. J., and Lapointe, M. F. (2007). "Assessing different methods of generating a three- dimensional numerical model mesh for a complex stream bed topography." *Int. J. Comput. Fluid Dyn.*, 21(1), 37–47.
- Biron, P. M., Robson, C., LaPointe, M. F., and Gaskin, S. J. (2005). "Three-dimensional flow dynamics around deflectors." *River Research and Applications*, 21, 961–975.
- Bradbrook, K. F., Biron, P. M., Lane, S. N., Richards, K. S., and Roy, A. G. (1998). "Investigation of controls on secondary circulation in a simple confluence geometry using a three-dimensional numerical model." *Hydrol. Processes*, 12, 1371-1396.

Bradbrook, K. F., Lane, S. N., and Richards, K. S. (2000a). "Numerical simulation of three-dimensional, time-averaged flow structure at river channel confluences." *Water Resour. Res.*, 36, 2731-2746.

Bradbrook, K. F., Lane, S. N., Richards, K. S., Biron, P. M., and Roy, A. G. (2001). "Role of bed discordance at asymmetrical river confluences." *J. Hydraul. Eng.*, 127(5), 351-368.

Bradford, S. F. (2000). "Numerical simulation of surf zone dynamics." *J. Waterw., Port, Coastal, Ocean Eng.*, 126(1), 1-13.

Chopakatla, S. C. (2003). "A CFD model for wave transformations and breaking in the surf zone." *MS Thesis*, Ohio State University, Columbus, Ohio.

Chrisohoides, A., F. Sotiropoulos, et al. (2003). "Coherent Structures in Flat-Bed Abutment Flow: Computational Fluid Dynamics Simulations and Experiments." *J. Hydraul. Eng.*, 129(3), 177-186.

Dargahi, B. (1987). "Flow field and local scouring around a pier." *Bulletin No. TRITA-VBI-137*, Hydraulic Laboratory, Royal Institute of Technology, Stockholm, Sweden.

Ferguson, R. I., Parsons, D. R., Lane, S. N., and Hardy, R. J. (2003). "Flow in meander bends with recirculation at the inner bank." *Water Resour. Res.*, 39(11), 1322-1334.

Flow Science, Inc. (2009). *FLOW-3D user's manual*, 9.4 edition, Flow Science, Inc., Santa Fe, N.M.

Garde, R. J., Subramanya, K., and Nambudripad, K. D. (1961). "Study of scour around spur-dikes." *J. Hydraul. Div.*, ASCE, 87(6), 23–37.

Gill, M. A. (1972). "Erosion of sand beds around spur dikes." *J. Hydraul. Div.*, ASCE, 98(9), 1587–1602.

Griffith, A. R., Rutherford, J. H., Alavi, A., Moore, D. D., and Groeneveld, J. (2007). "Stability review of the Wanapum spillway using CFD analysis." *Bulletin*, Canadian Dam Association., 16–26.

Haltigin, T. W., Biron, P. M., and Lapointe, M. F. (2007). "Predicting equilibrium scour-hole geometry near angled stream deflectors using a three-dimensional numerical flow model." *J. Hydraul. Eng.*, 133(8), 983–988.

Hirt, C. W., and Nichols, B. D. (1981). "Volume of fluid (VOF) method for the dynamics of free boundaries." *J. Comp. Phys.*, 39, 201-225.

Hirt, C. W, and Sicilian, J. M. (1985). "A porosity technique for the definition of obstacles in rectangular cell meshes." *Proc., 4th Int. Conf. Ship Hydrodynamics*, Washington, D.C.

Hodskinson, A., and Ferguson, R. I. (1998). "Numerical modeling of separated flow in river bends: Model testing and experimental investigation of geometric controls on the extent of flow separation at the concave bank." *Hydrol. Processes*, 12, 1323-1338.

Jia, Y., and Wang, S. S. Y. (1993). "3D numerical simulation of flow near a spur dike." *Adv. Hydrosci.*, 1, 2150-2156.

Jia, Y., and Wang, S. S. Y. (1996). "A modeling approach to predict local scour around spur dike-like structures." *Proc., 6th Federal Interagency Sedimentation Conf.*, Subcommittee on Sedimentation, Interagency Advisory Committee on Water Data. II, 90-97.

Kuhnle, R. A., Jia, Y., and Alonso, C.V. (2008). "Measured and simulated flow near a submerged spur dike." *J. Hydraul. Eng.*, 1348(7), 916-924.

Kwan, T. F., and Melville, B. W. (1994). "Local scour and flow measurements at bridge abutments." *J. Hydraul. Res.*, 32(5), 661-673.

Lane, S. N., Bradbook, K. F., Richards, K. S., Biron, P. A., and Roy, A. G. (1999). "The application of computational fluid dynamics to natural river channels: Three-dimensional versus two-dimensional approaches." *Geomorphology*, 29, 1-20.

Lauder, B. E., and Spaulding, D. B. (1972). *Mathematical models of turbulence*. Academic Press, New York, N.Y.

Laursen, E. M. (1963). "Analysis of relief bridge scour." *J. Hydraul. Div., Am. Soc. Civ. Eng.*, 89(3), 93–118.

Lim, S. Y. (1997). "Equilibrium clear water scour around an abutment." *J. Hydraul. Eng.*, 123(3), 237–243.

Mayerle, R., Toro, F. M., and Wang, S. S. Y. (1995). "Verification of a three-dimensional numerical model simulation of the flow in the vicinity of spur dikes." *J. Hydraul. Res.*, 33(2), 243–256.

Melville, B. W. (1975). "Local scour at bridge sites." *Rep. No. 117*, Dept. of Civil Engineering, School of Engineering, Univ. of Auckland, Auckland, New Zealand.

Melville, B. W. (1992). "Local scour at bridge abutments." *J. Hydraul. Eng.*, ASCE, 118(4), 615–631.

Mendoza-Cabrales, C. (1993). "Computation of flow past a cylinder mounted on a flat plate." *Proc., Hydraul. Eng.*, ASCE Reston, Va., 899-904.

Nagata, N., Hosoda, T., Nakato, T., and Muramoto, Y. (2005). "Three-dimensional numerical model for flow and bed deformation around river hydraulic structures." *J. Hydraul. Eng.*, 131(12), 1074-1087.

Nicholas, A. P., and Smith, G. H. S. (1999). "Numerical simulation of three-dimensional flow hydraulics in a braided channel." *Hydrol. Processes*, 13, 913-929.

Olsen, N. R. B., and Melaan, M. C. (1993). "Three dimensional calculation of scour around cylinders". *J. Hydraul. Eng.*, ASCE, 119(9), 1048-1054.

Olsen, N. R. B., and Kjellesvig, H. M. K. (1998). "Three-dimensional numerical flow modeling for estimation of maximum local scour depth." *J. Hydraul. Res.*, 36(4), 579–590.

Ouillon, S., and Dartus, D. (1997). "Three-dimensional computation of flow around groyne." *J. Hydraul. Eng.*, 123(11), 962–970.

Posey, C. J. (1949). "Why bridges fail in floods." *Civ. Eng. (N.Y.)*, 19, 42–90.

Rahman, M. M., Nagata, N., Muramoto, Y., and Murata, H. (1998). "Effect of side slope on flow and scouring around spur-dike-like structures." *Proc., 7th Int. Symp. on River Sedimentation*, Hong Kong, China, 165–171.

Raudkivi, A. J. (1990). *Loose boundary hydraulics*, 3rd Ed., Pergamon, New York.

Richardson, J. E., and Panchang, V. G. (1998). "Three-Dimensional Simulation of Scour-Inducing Flow at Bridge Piers." *J. Hydraul. Eng.*, 124(5), 530-540.

Rodi, W (1980). *Turbulence models and their application in hydraulics: A state of the art Review*. IAHR.

Roulund, A., Sumer, B. M., Fredsoe, J., and Michelsen, J. (1998). "3D mathematical modeling of scour around a circular pile in current." *Proc., 7th Int. Symp. on River Sedimentation*, Hong Kong, China, 131–137.

Salaheldin, T. M., Imran, J., and Chaudhry, H. (2004). "Numerical modeling of three-dimensional flow field around circular piers." *J. Hydraul. Eng.*, 130(2), 91-100.

Shaw, C. T. (1992). *Using computational fluid dynamics*. Prentice Hall, New York, N.Y.

Shen, H. W., Schneider, V. R., and Karaki, S. (1969). "Local scour around bridge piers." *J. Hydraul. Div., Am. Soc. Civ. Eng.*, 95(6), 1919–1940.

Shields, F. D., Jr., Cooper, C. M., and Knight, S. S. (1995). "Experiment in stream restoration." *J. Hydraul. Eng.*, 121(6), 494–502.

Sicilian, J. M., Hirt, C. W., and Harper, R. P. (1987). "FLOW-3D: Computational modeling power for scientists and engineers." *Rep. FSI-8700- 1*, Flow Science, Los Alamos, N.M.

Smith, H. D., and Foster, D. L. (2005). "Modeling of flow around a cylinder over a scoured bed." *Journal of Waterway, Port, Coastal, and Ocean Engineering*, 131(1), 14-24.

Stevens, M. A., Gasser, M. M., and Saad, M. B. A. M. (1991). "Wake vortex scour at bridge piers." *J. Hydraul. Eng.*, 117(7), 891–904.

Uijttewaal, W. S. J. (2005). "Effects of groyne layout on the flow in groyne fields: laboratory experiments." *J. Hydraul. Eng.*, 131(9), 782–791.

Uijttewaal, W. S. J., Lehmann, D., and van Mazijk, A. (2001). "Exchange processes between a river and its groyne fields: model experiments." *J. Hydraul. Eng.*, ASCE, 127(11), 928–7936.

Weitbrecht, V., Uijttewaal, W., and Jirka, G. H. (2003). "2D particle tracking to determine transport characteristics in rivers with dead zones." *Proc., Int. Symp. Shallow Flows*, Delft, The Netherlands, 103–110.

Yaeger, M.A. (2009). "Mean flow and turbulence around two series of experimental dikes." *MS Thesis*, Department of Hydrology and Water Resources, University of Arizona, Tucson, AZ, 100 pp.

Yakhot, V., and Orszag, S. A. (1986). “Renormalization group analysis of turbulence.” *J. Sci. Comp.*, 1(1), 3.

Yakhot, V., and Smith, L. M. (1992). “The renormalization group, the ϵ -expansion and derivation of turbulence.” *J. Sci. Comp.*, 7(1), 35-61.

Yakhot, V., Orszag, S. A., Thangam, S., Gatshi, T. B., and Speziale, C. G. (1992). “Development of a turbulence model for shear flow by a double expansion technique.” *Phys. Fluids A*, 4(7), 1510-1520.

Zhang, H., Nakagawa H., Ishigaki, T, and Muto, Y. (2005). “Prediction of 3D flow field and local scouring around spur dikes.” *Ann. J. Hydraul. Eng.*, 49, 1003–1008.

Table 1. Statistical comparison of the experimental and modeled results for the fixed flat bed case

RNG model					
Parameters	MAE	MSE	RMSE	R ²	R
Longitudinal velocity (u)	0.024	0.001	0.032	0.952	0.976
Transverse velocity (v)	0.032	0.0017	0.042	0.789	0.888
Vertical velocity (w)	0.004	0.00004	0.006	0.187	0.432
Turbulent kinetic energy (m ² /s ²)	0.00156	0.00001	0.002	0.434	0.658
<i>k-ε</i> model					
Parameters	MAE	MSE	RMSE	R ²	R
Longitudinal velocity (u)	0.084	0.0112	0.106	0.625	0.79
Transverse velocity (v)	0.046	0.0033	0.058	0.716	0.846
Vertical velocity (w)	0.0041	0.00004	0.007	0.012	0.11
Turbulent kinetic energy (m ² /s ²)	0.00297	0.00002	0.004	0.189	0.435
LES model					
Parameters	MAE	MSE	RMSE	R ²	R
Longitudinal velocity (u)	0.087	0.013	0.114	0.282	0.531
Transverse velocity (v)	0.085	0.009	0.094	0.425	0.651
Vertical velocity (w)	0.006	0.002	0.047	0.004	0.063

Table 2. Statistical comparison of the experimental and modeled results for scoured bed case RNG model

Parameters	MAE	MSE	RMSE	R ²	R
Longitudinal velocity (u)	0.051	0.005	0.068	0.634	0.796
Transverse velocity (v)	0.026	0.002	0.043	0.795	0.891
Vertical velocity (w)	0.027	0.001	0.036	0.464	0.681
Turbulent kinetic energy (m ² /s ²)	0.002	0.000	0.004	0.384	0.620

k-ε model

Parameters	MAE	MSE	RMSE	R ²	R
Longitudinal velocity (u)	0.073	0.010	0.098	0.298	0.545
Transverse velocity (v)	0.075	0.008	0.092	0.246	0.495
Vertical velocity (w)	0.037	0.003	0.051	0.220	0.469
Turbulent kinetic energy (m ² /s ²)	0.006	0.000	0.008	0.212	0.460

LES model

Parameters	MAE	MSE	RMSE	R ²	R
Longitudinal velocity (u)	0.083	0.011	0.105	0.362	0.602
Transverse velocity (v)	0.082	0.010	0.100	0.129	0.359
Vertical velocity (w)	0.034	0.002	0.047	0.144	0.379

Figures

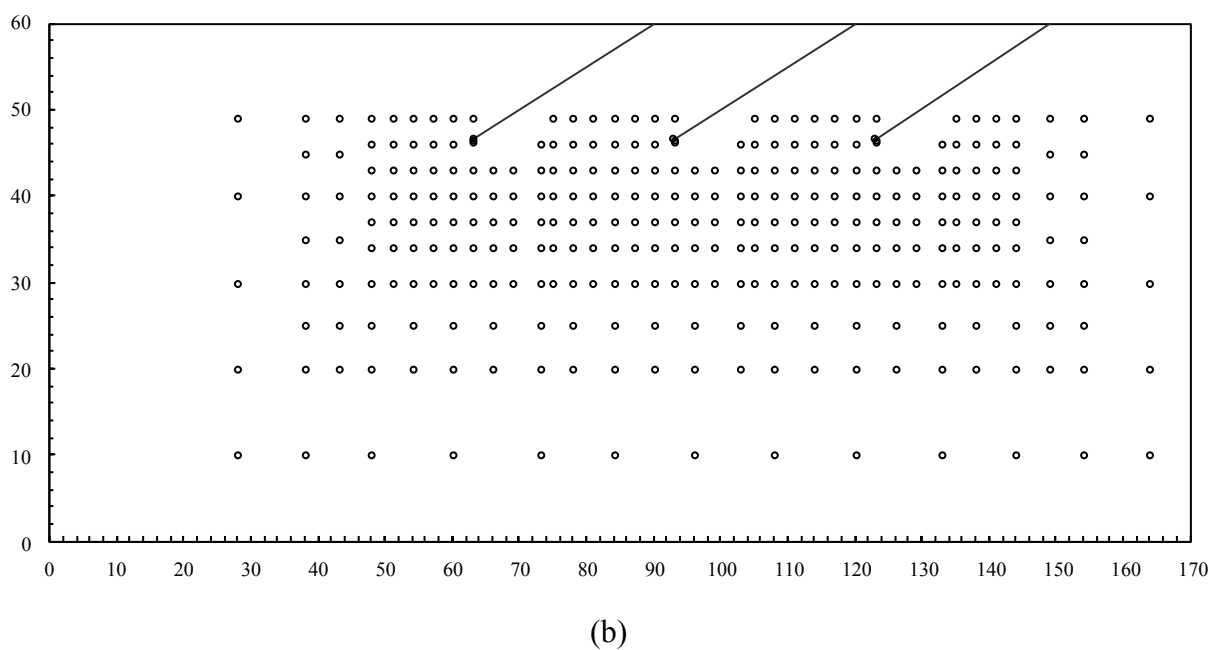
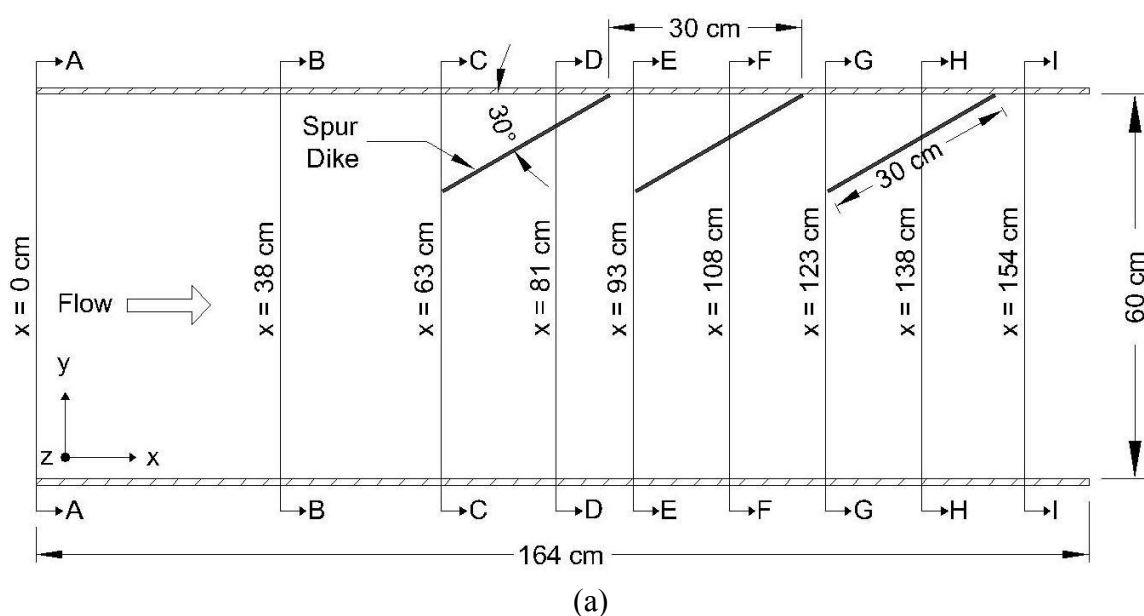


Fig.1. (a) Plan view of experimental setup (b) Diagram of the experimental section showing the relative position of spur dikes and the velocity profile measuring locations.

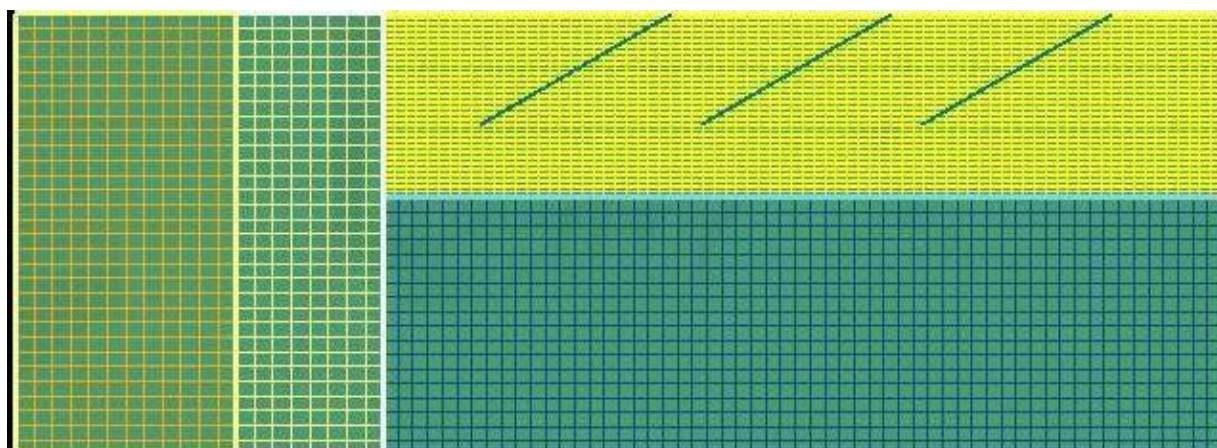


Fig.2. Computational mesh for a series of spur dikes in FLOW-3D



Fig.3. Picture of scoured bed surface at the equilibrium state

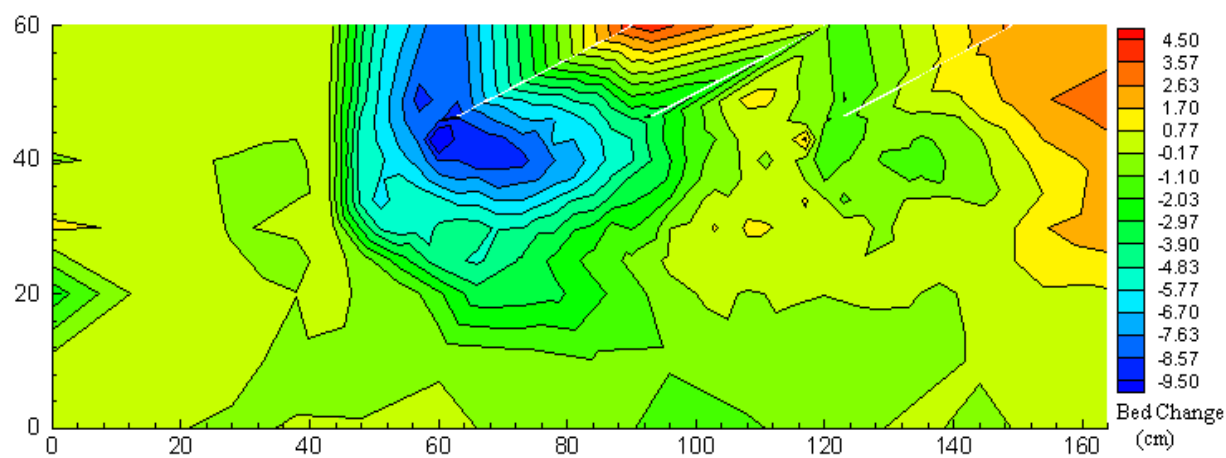


Fig.4. Bed bathymetry of the developed scour hole at $Q = 0.035 \text{ m}^3/\text{s}$

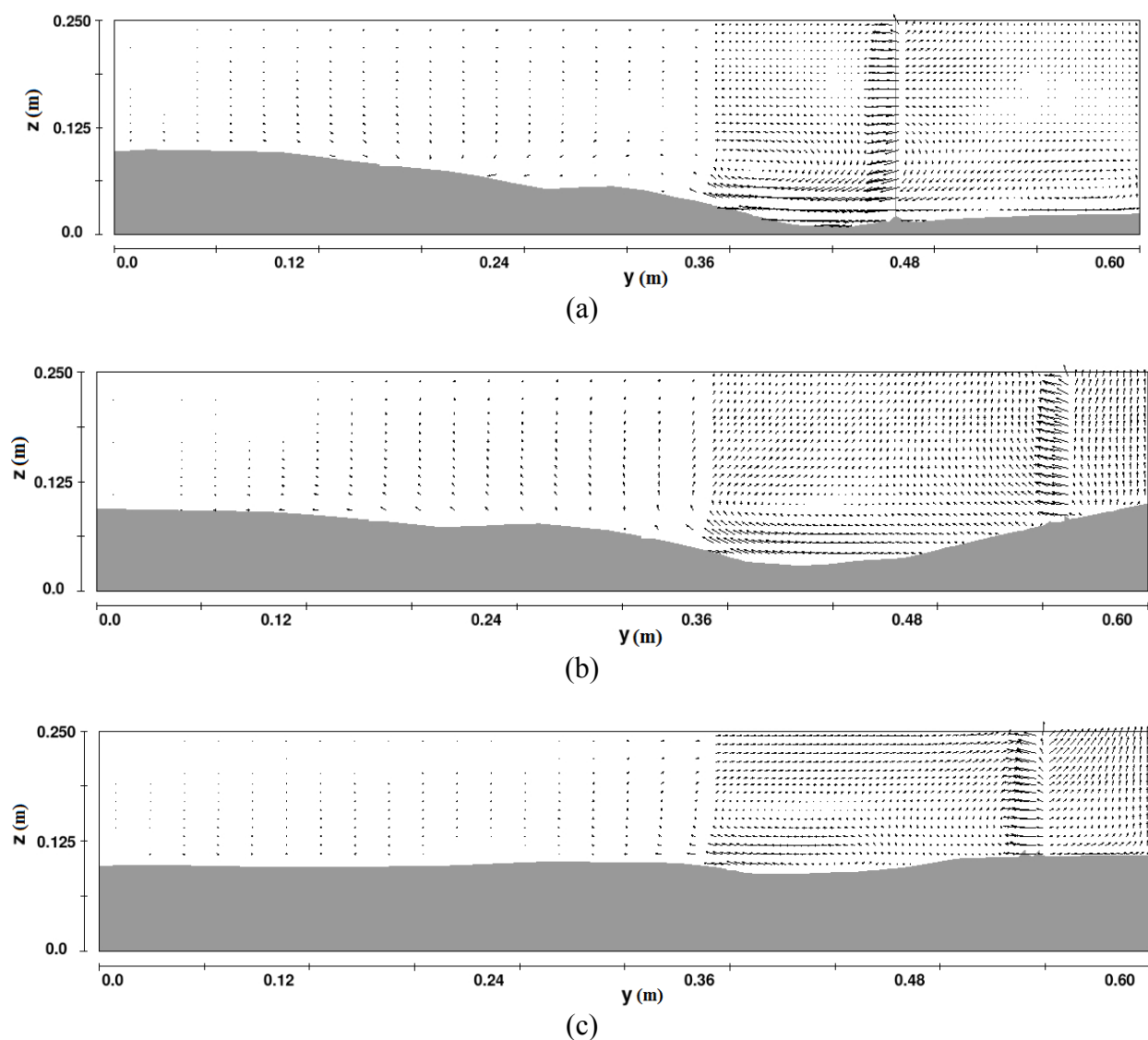
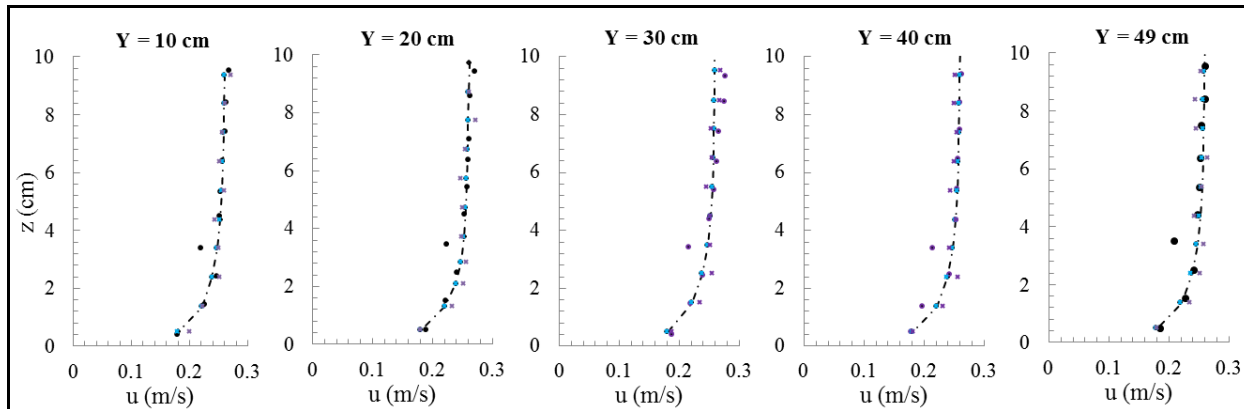


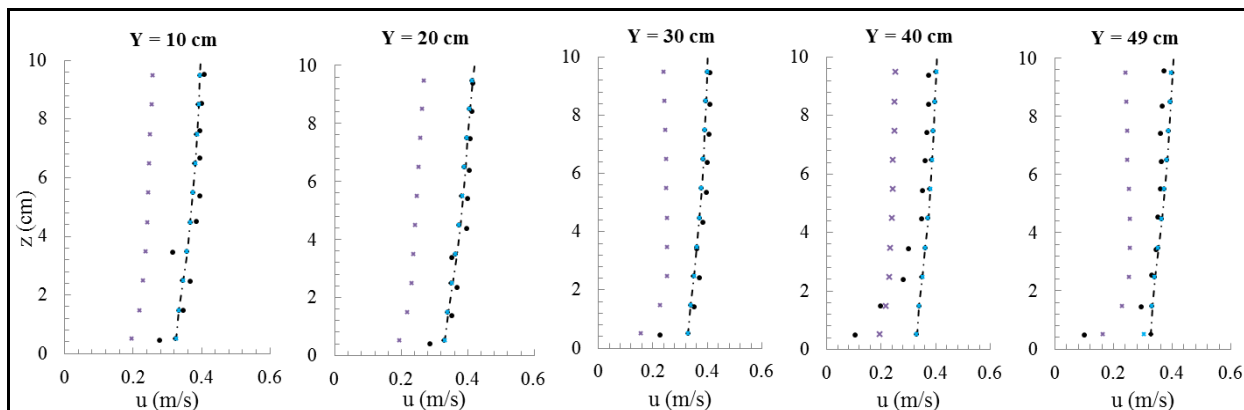
Fig.5. Computed velocity vectors in scoured bed for RNG k - ϵ turbulence closure scheme at different sections (a) C-C (b) D-D and (c) H-H

• Experiment * Standard K-ε ---◇--- RNG K-ε × LES

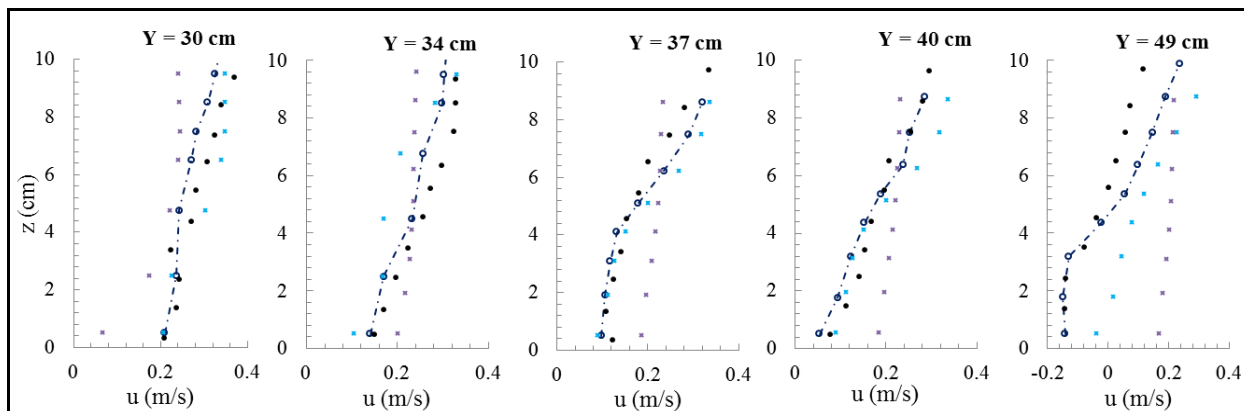
Section A-A



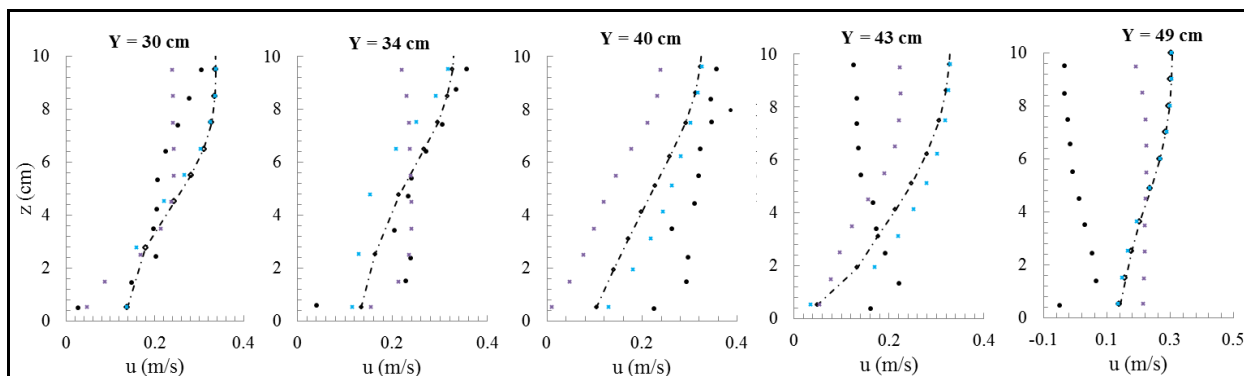
Section B-B



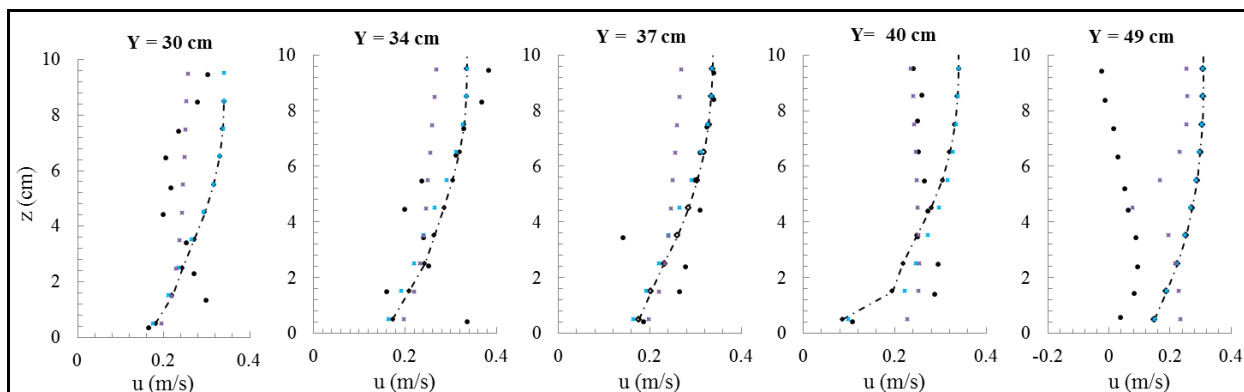
Section C-C



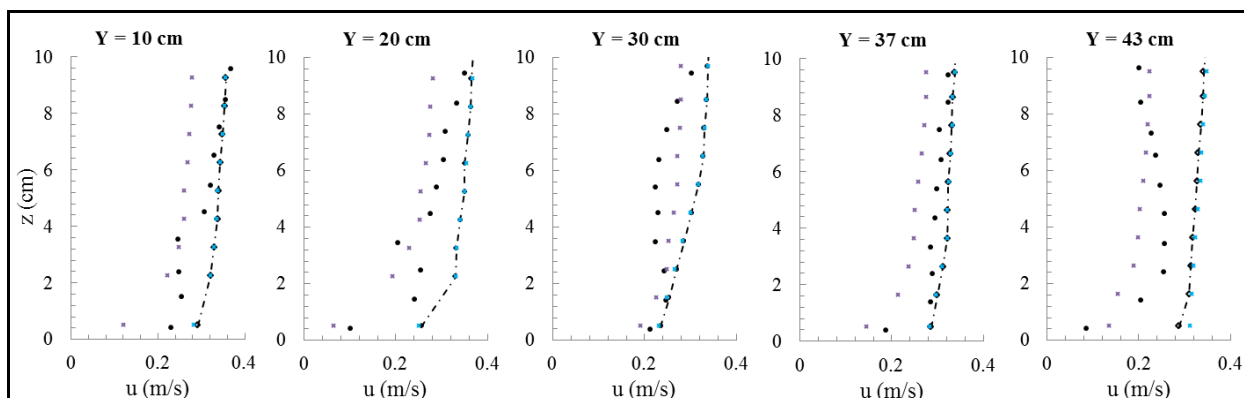
Section D-D



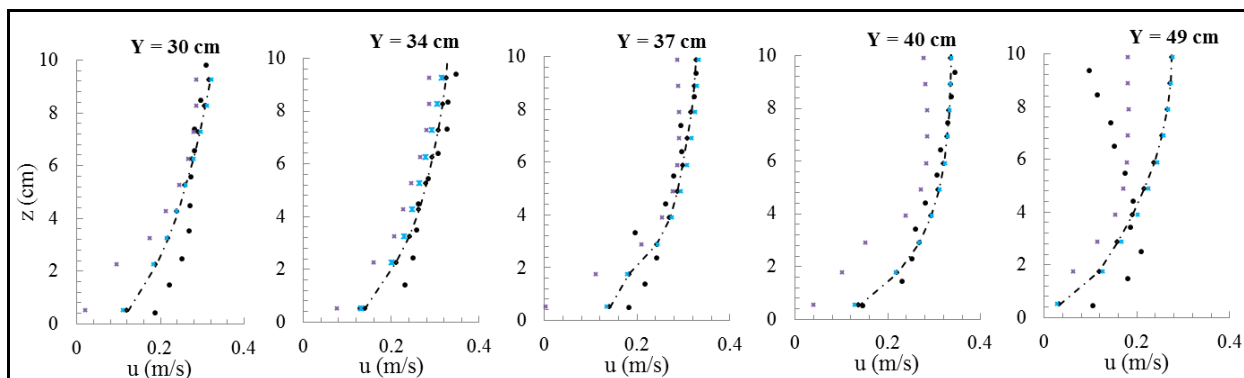
Section E-E



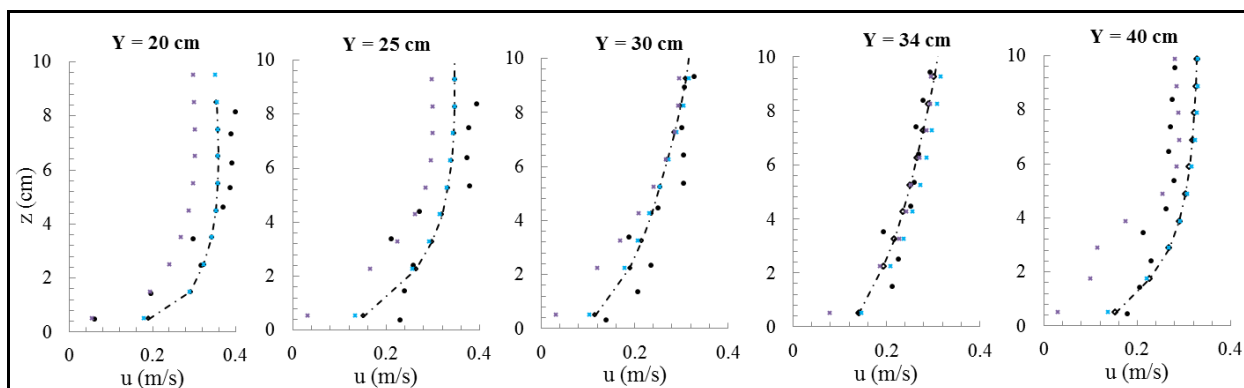
Section F-F



Section G-G



Section H-H



Section I-I

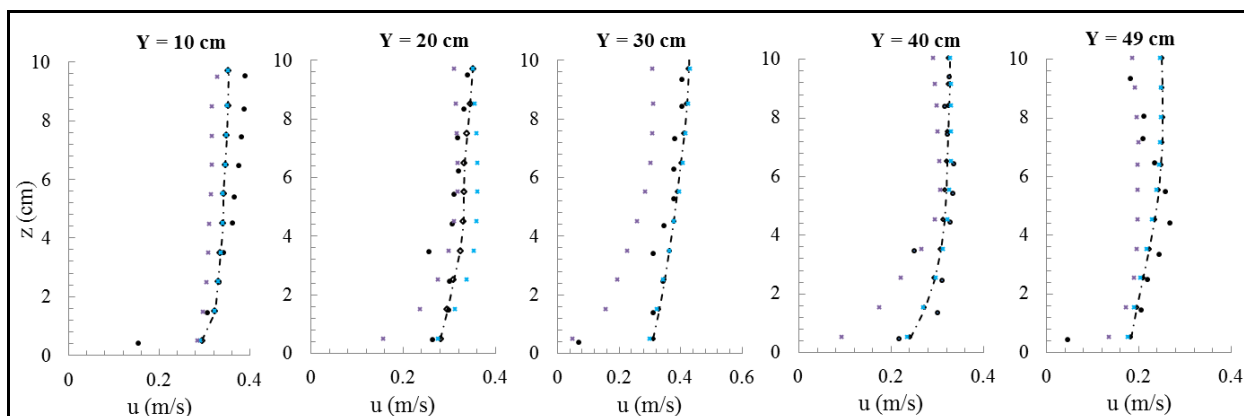
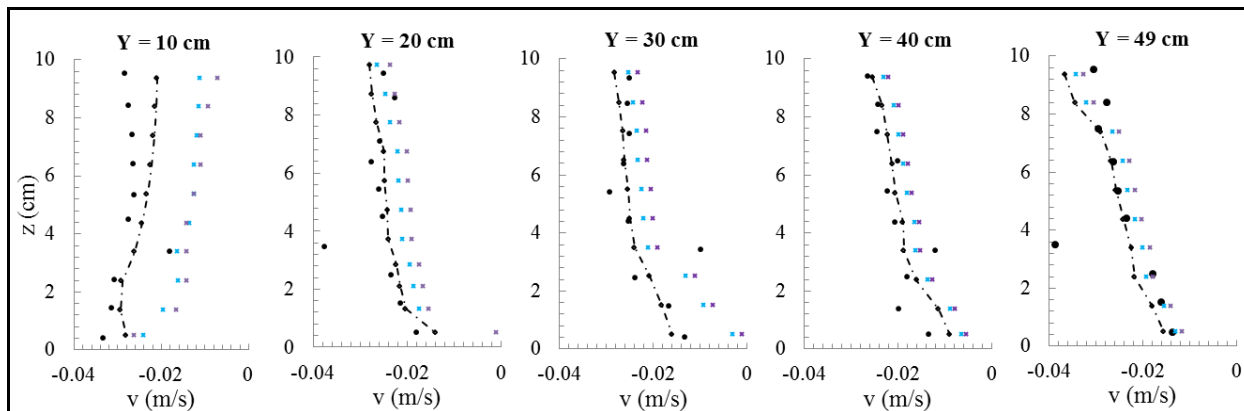


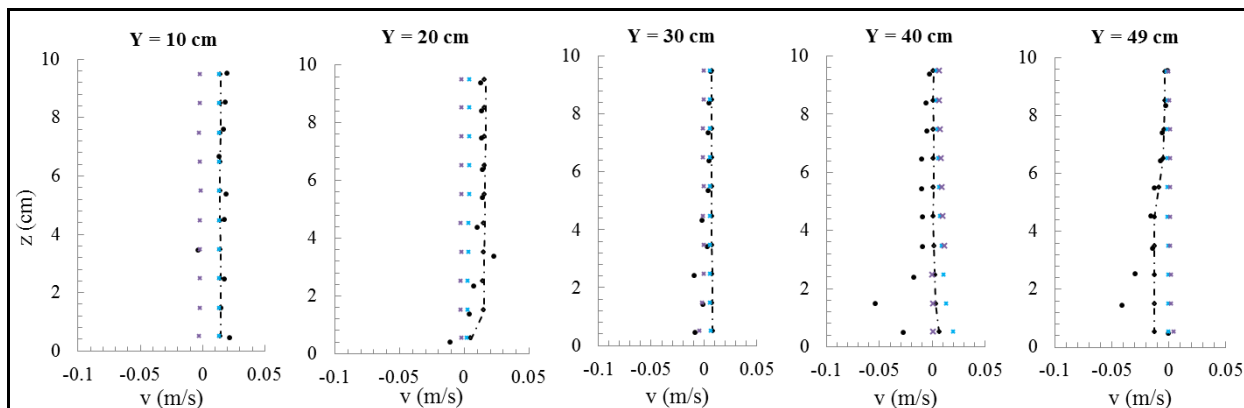
Fig.6. Comparisons of measured (closed and filled circles) and computed longitudinal velocity profiles in scoured bed case for standard $k-\epsilon$, RNG $k-\epsilon$, and LES turbulence closure schemes

• Experiment * Standard K-ε ---◇--- RNG K-ε × LES

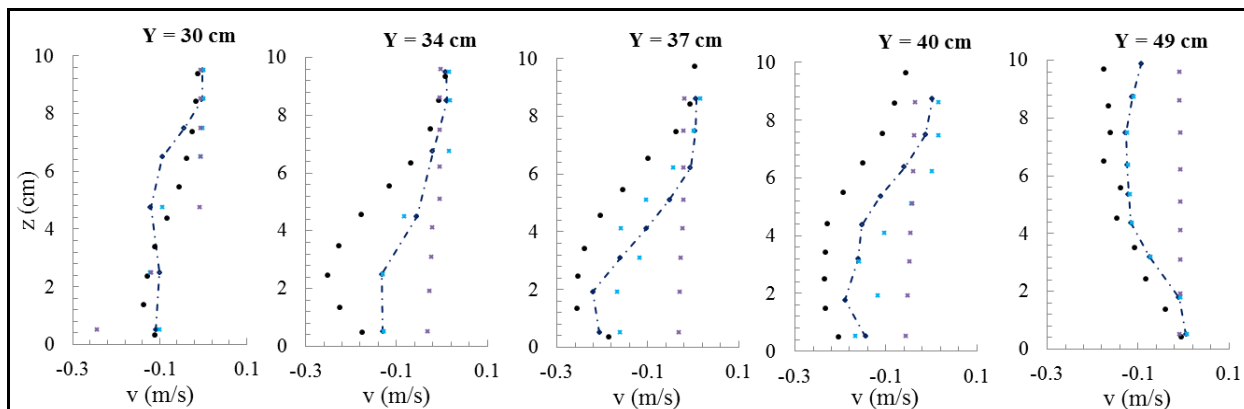
Section A-A



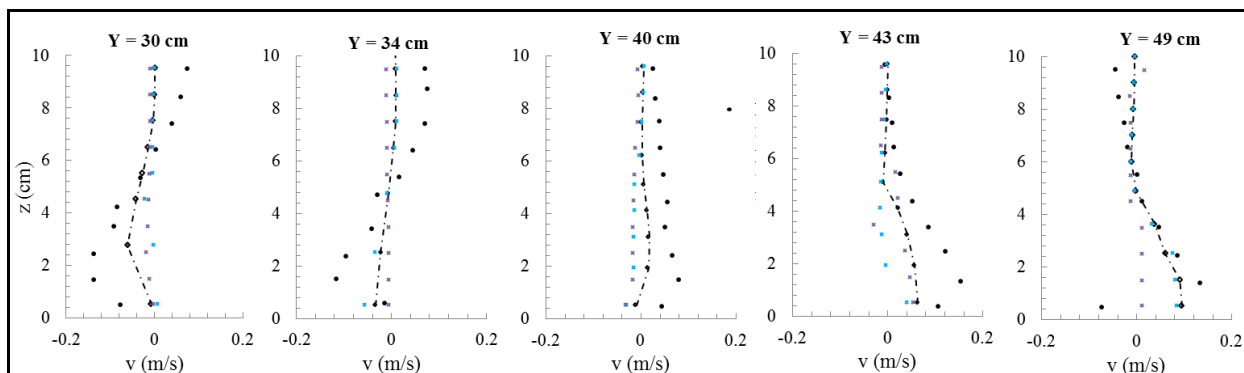
Section B-B



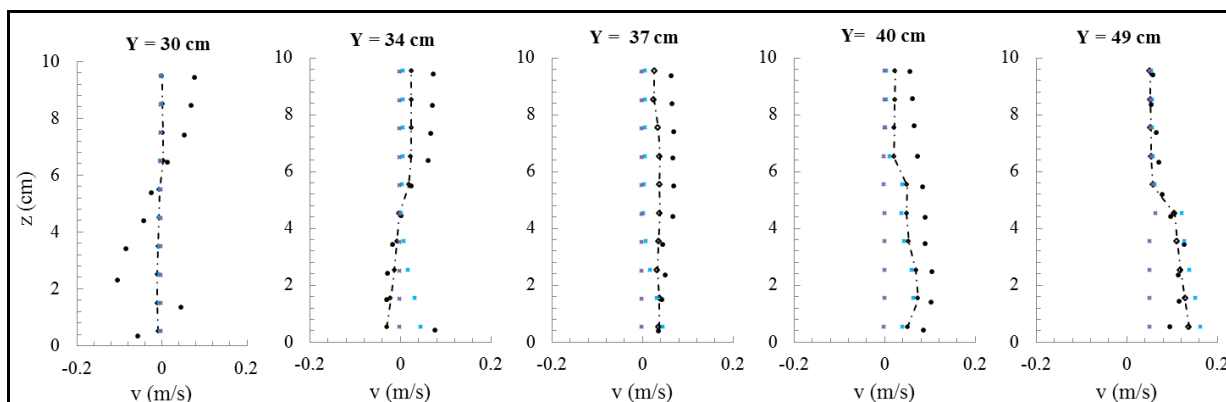
Section C-C



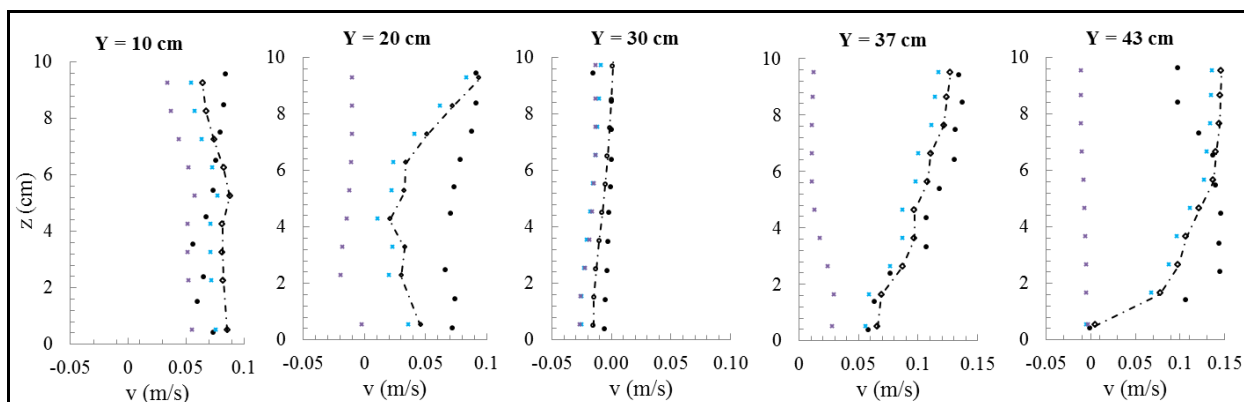
Section D-D



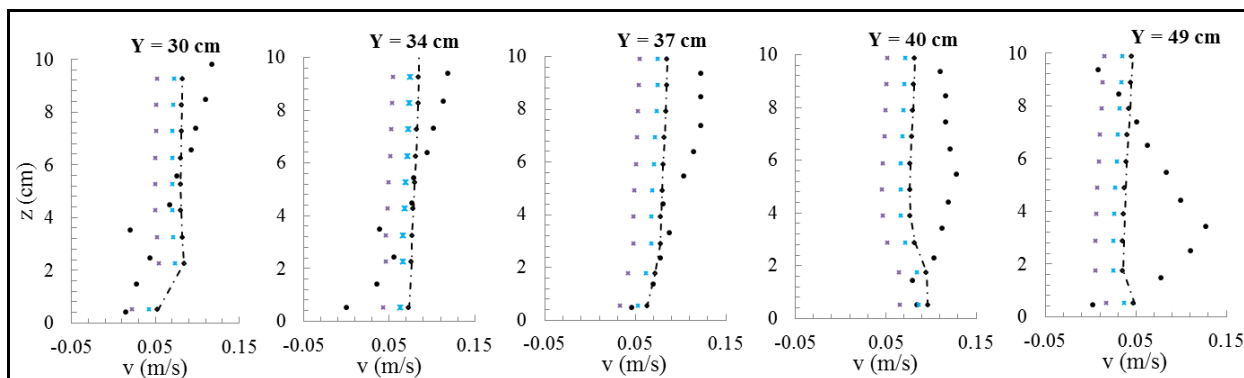
Section E-E



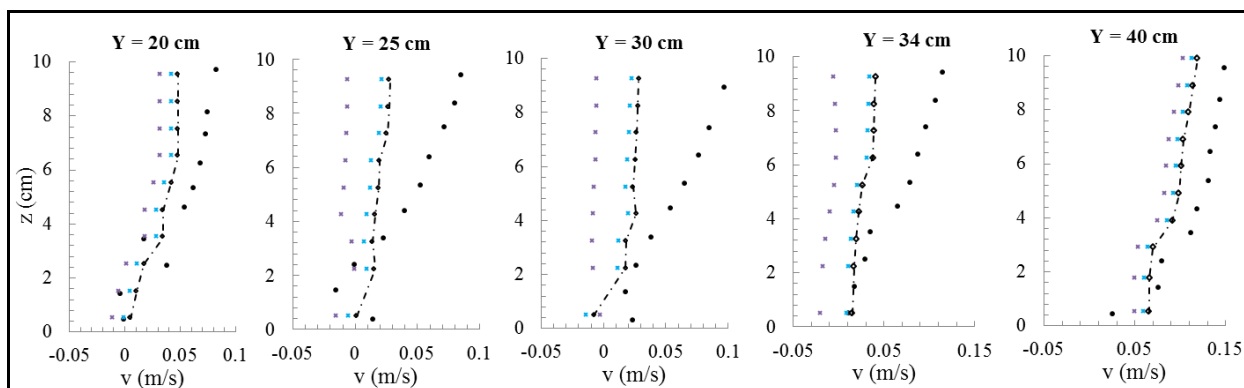
Section F-F



Section G-G



Section H-H



Section I-I

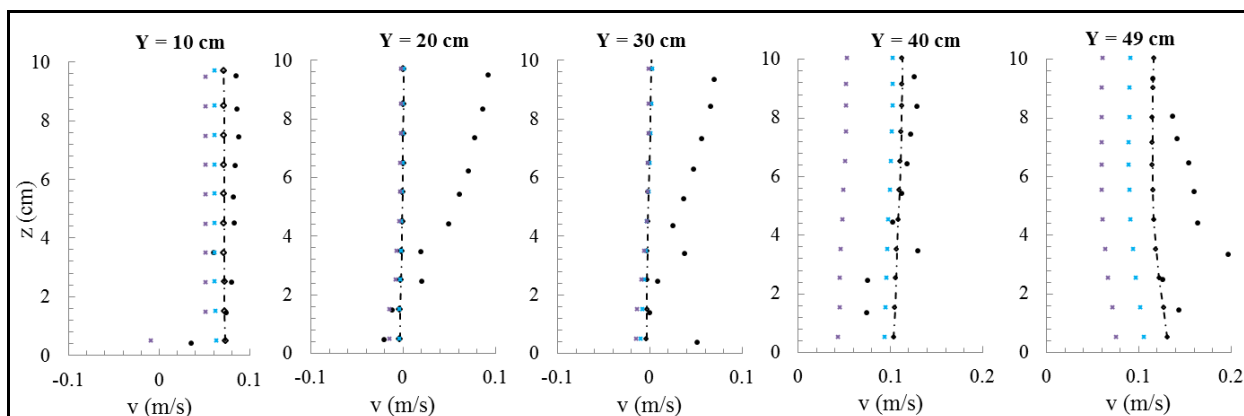
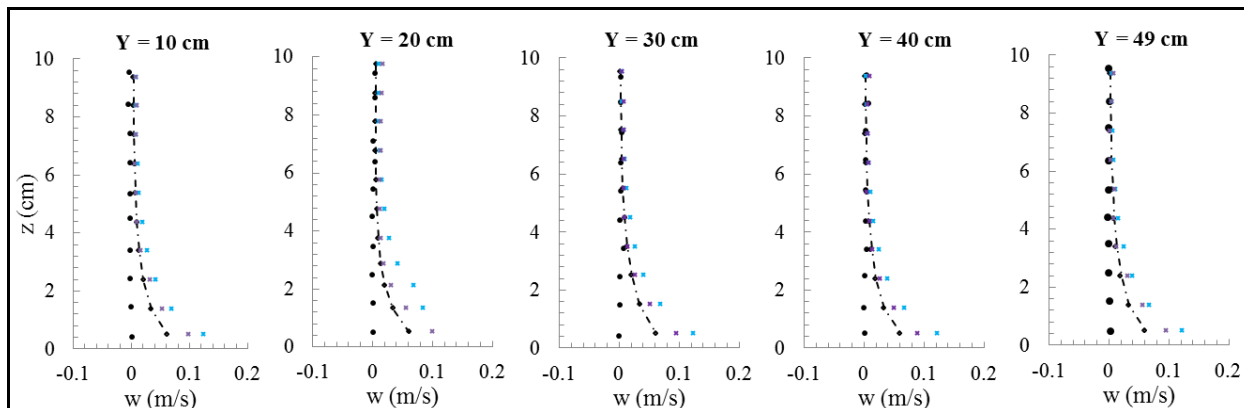


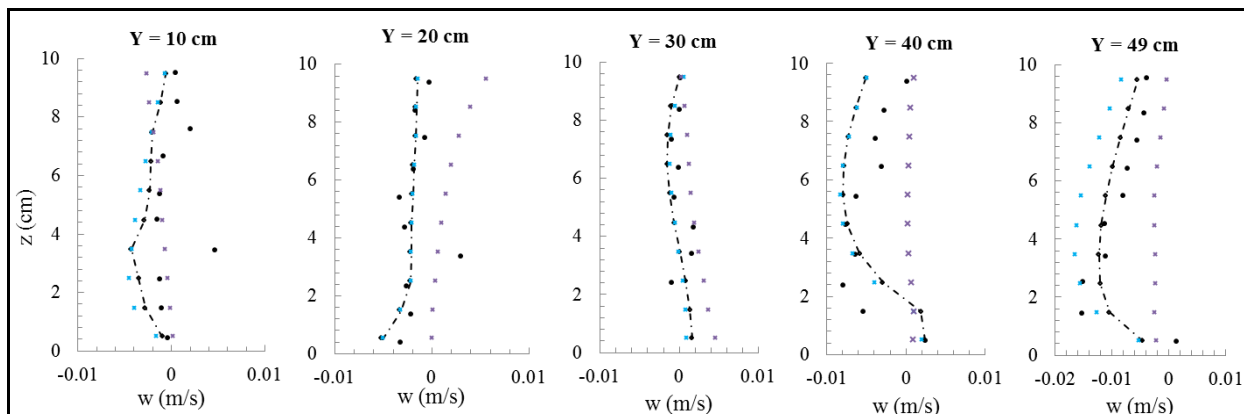
Fig.7. Comparisons of measured (closed and filled circles) and computed transverse velocity profiles in scoured bed case for standard $k-\varepsilon$, RNG $k-\varepsilon$, and LES turbulence closure schemes

• Experiment * Standard K-ε ---◇--- RNG K-ε × LES

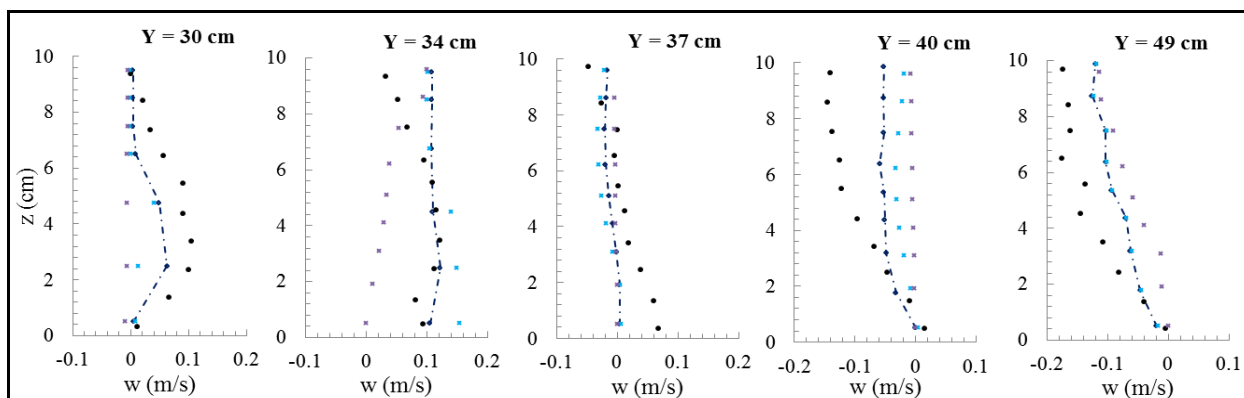
Section A-A



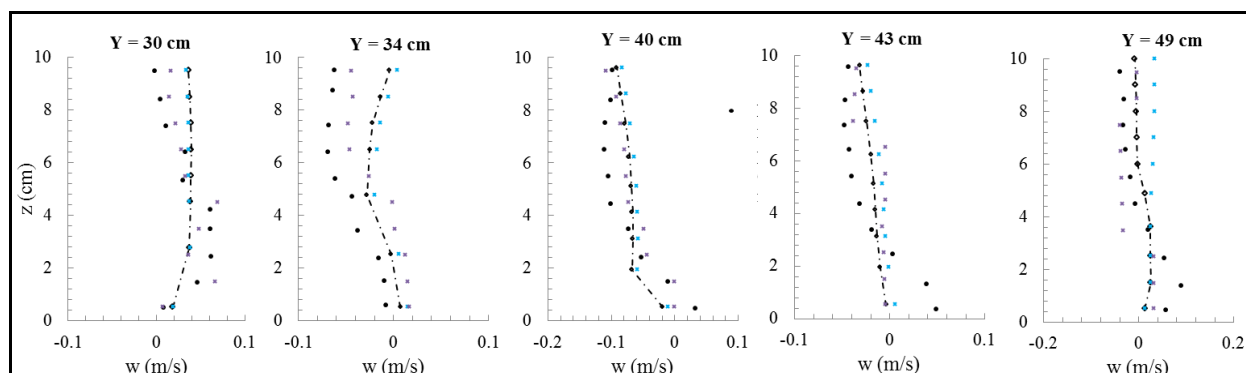
Section B-B



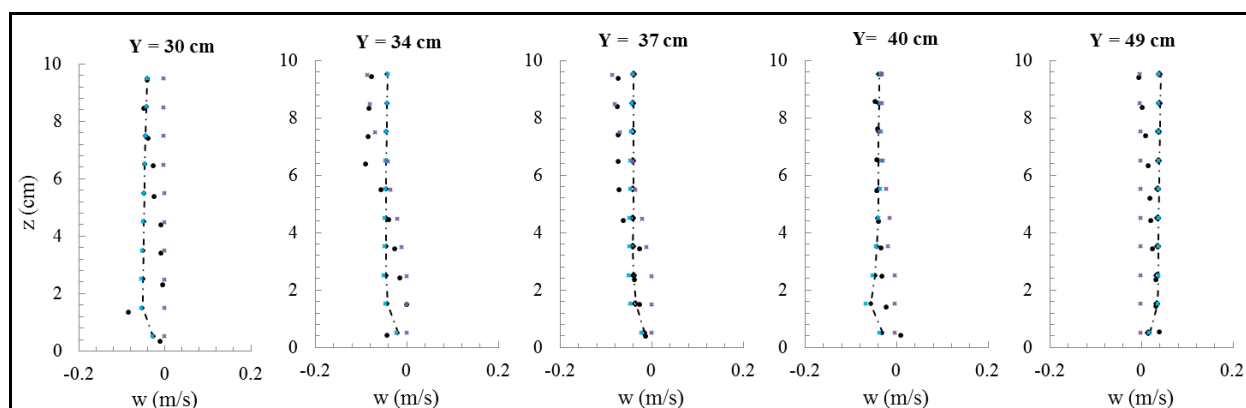
Section C-C



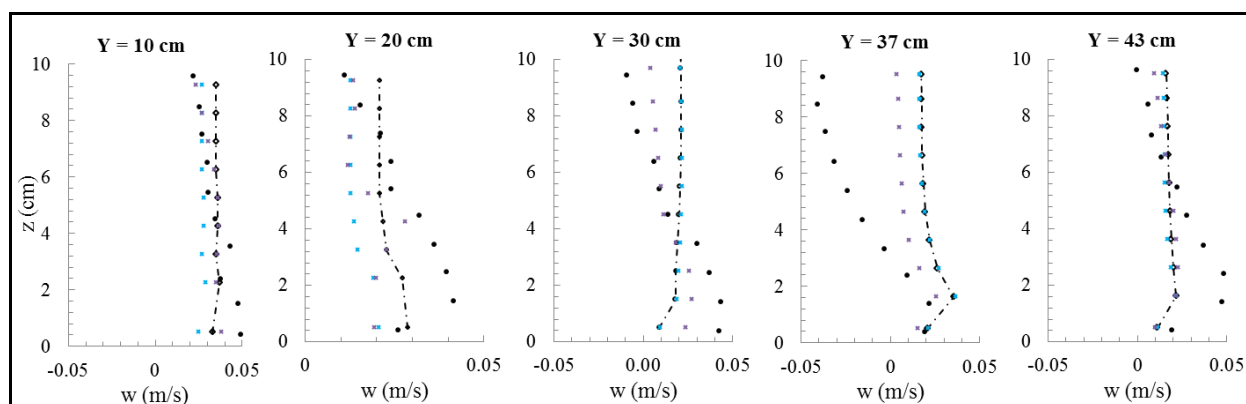
Section D-D



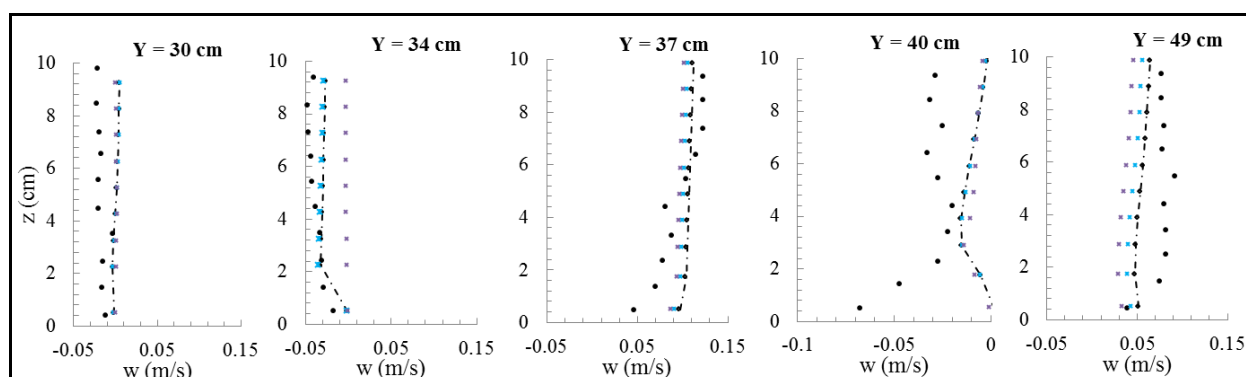
Section E-E



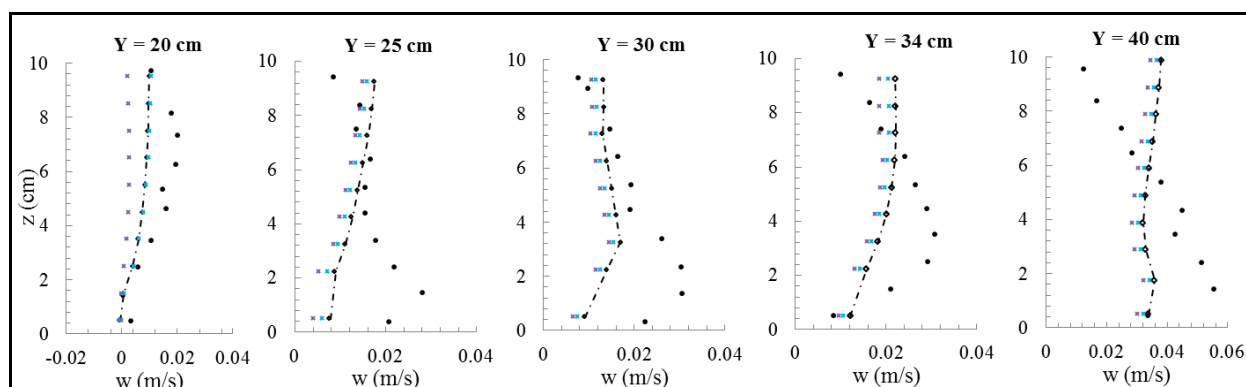
Section F-F



Section G-G



Section H-H



Section I-I

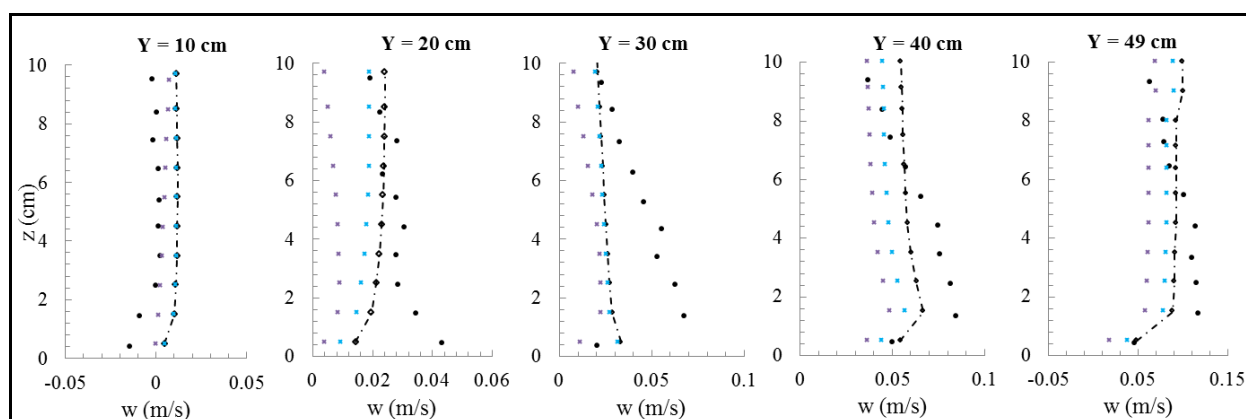
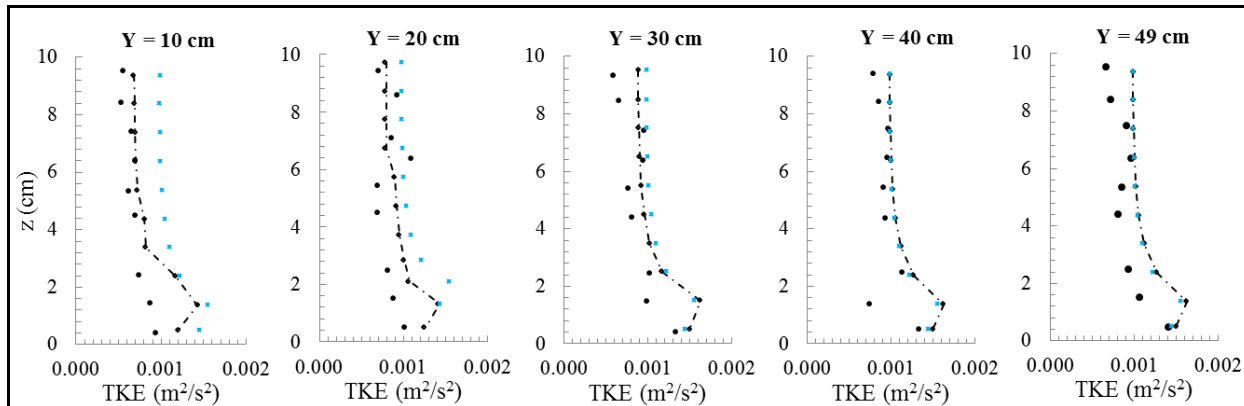


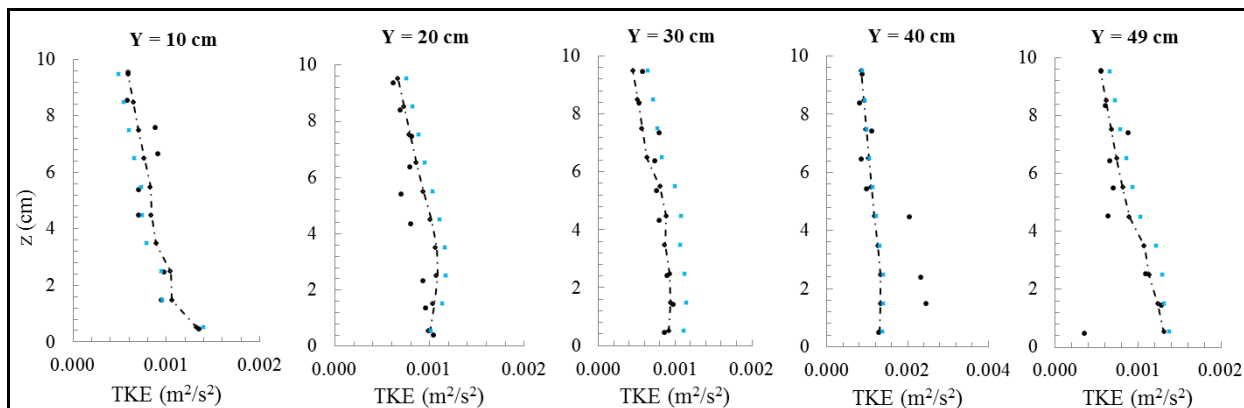
Fig.8. Comparisons of measured (closed and filled circles) and computed vertical velocity profiles in scoured bed case for standard $k-\epsilon$, RNG $k-\epsilon$, and LES turbulence closure schemes

• Experiment * Standard K-ε ---◇--- RNG K-ε × LES

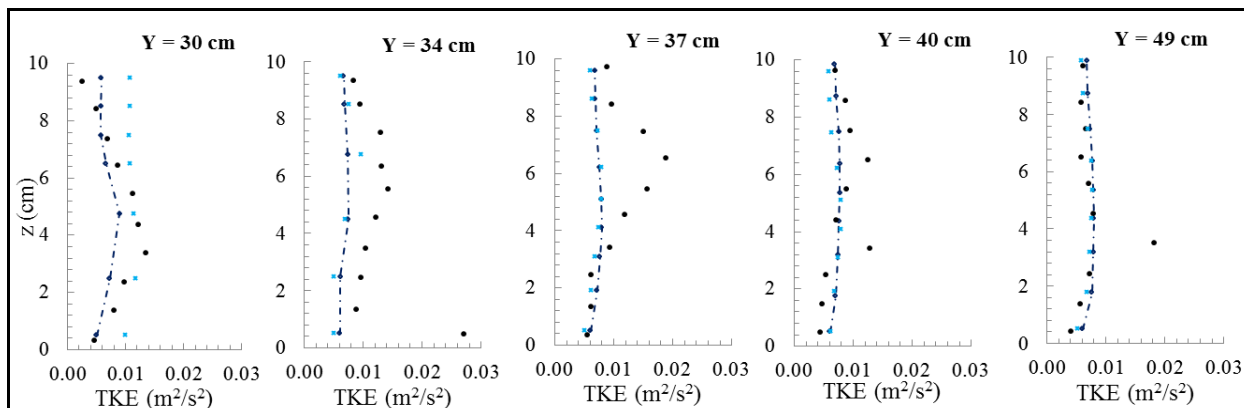
Section A-A



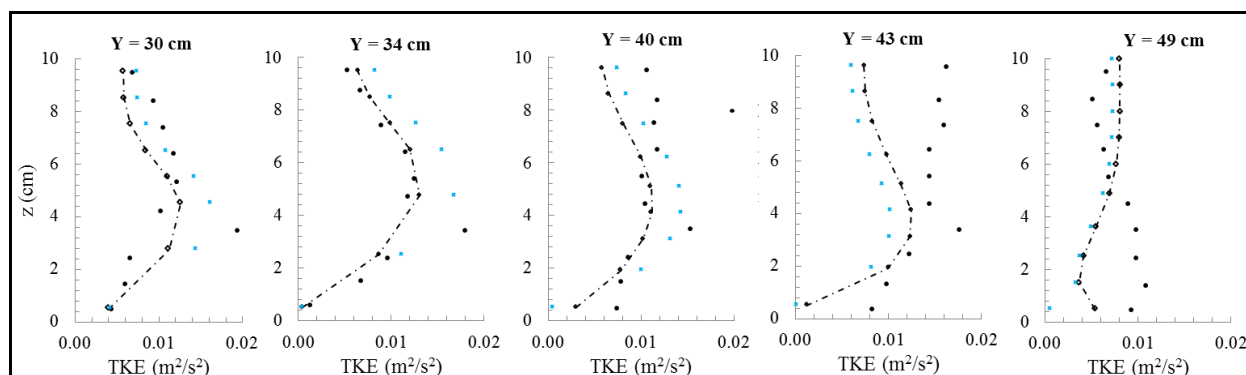
Section B-B



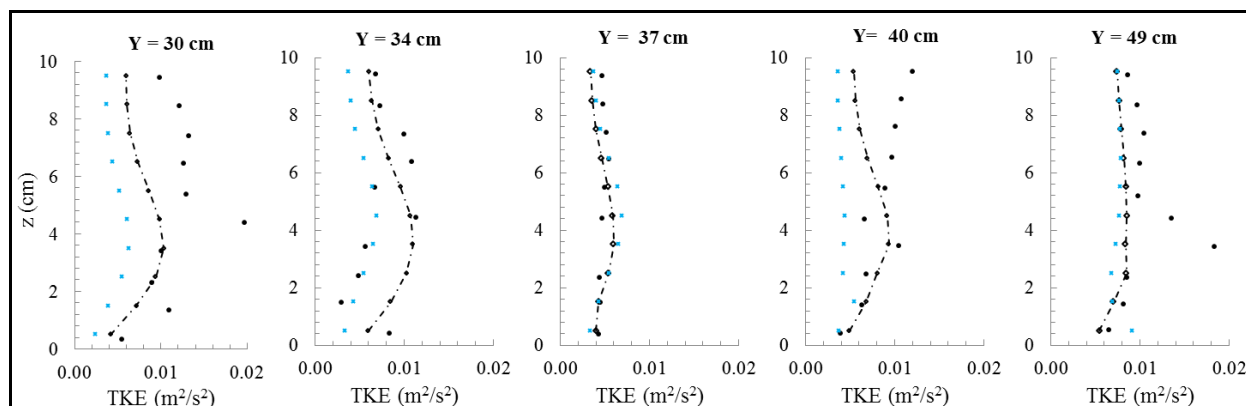
Section C-C



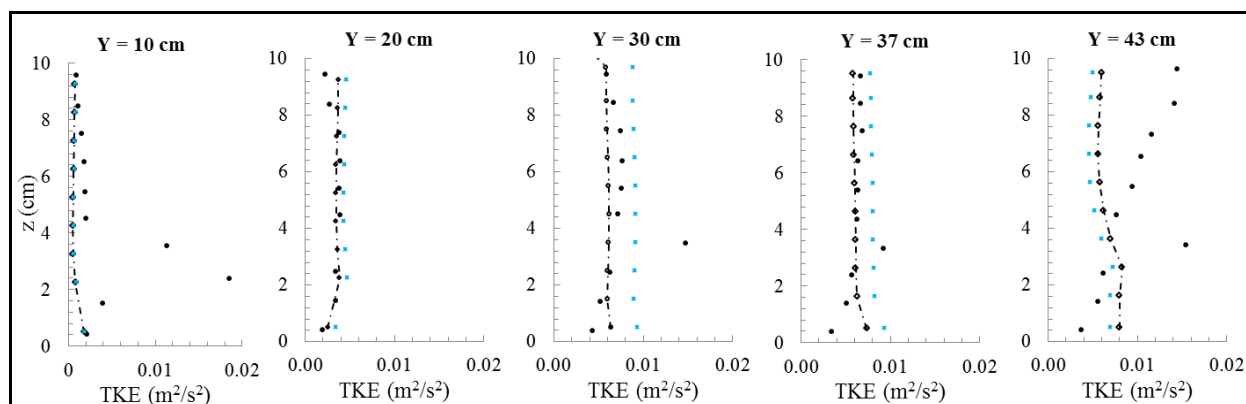
Section D-D



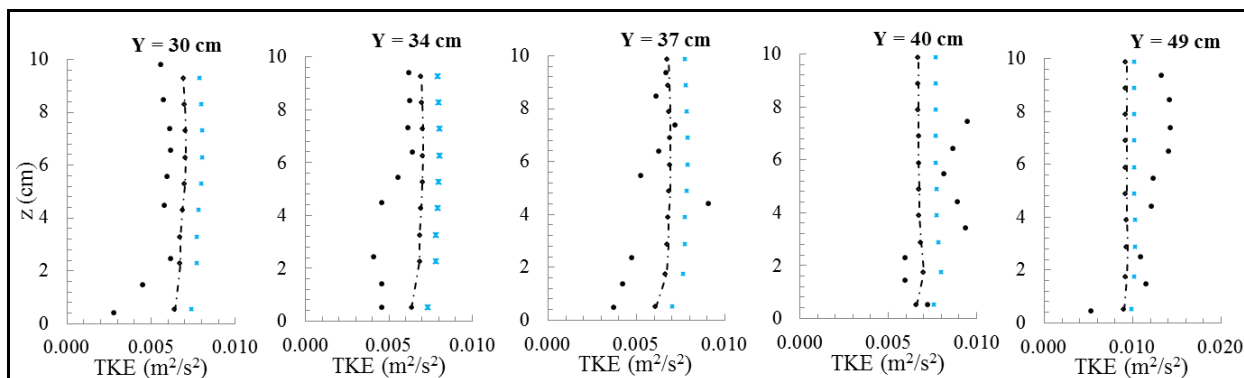
Section E-E



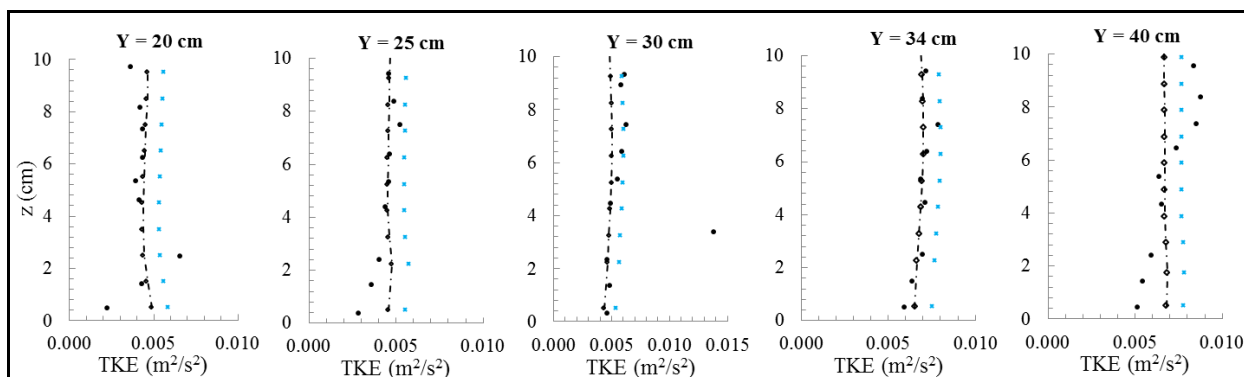
Section F-F



Section G-G



Section H-H



Section I-I

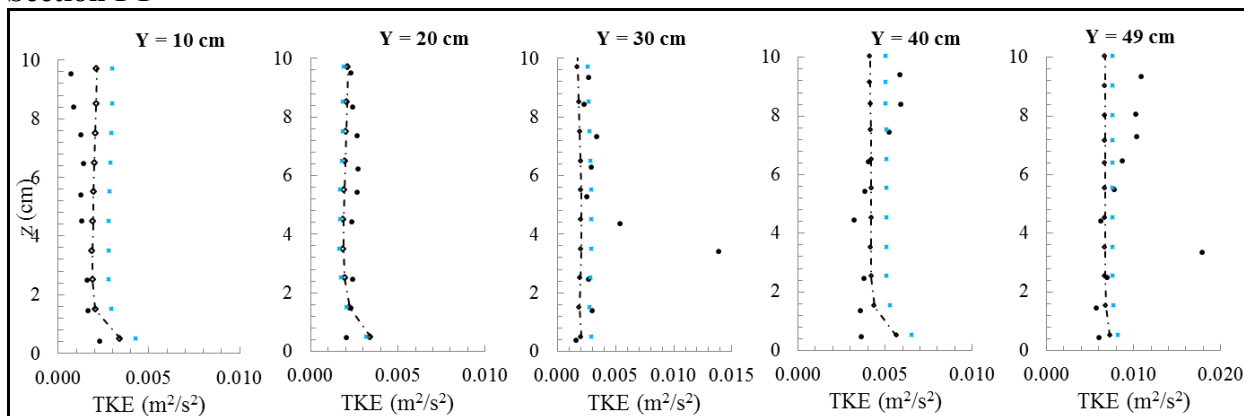
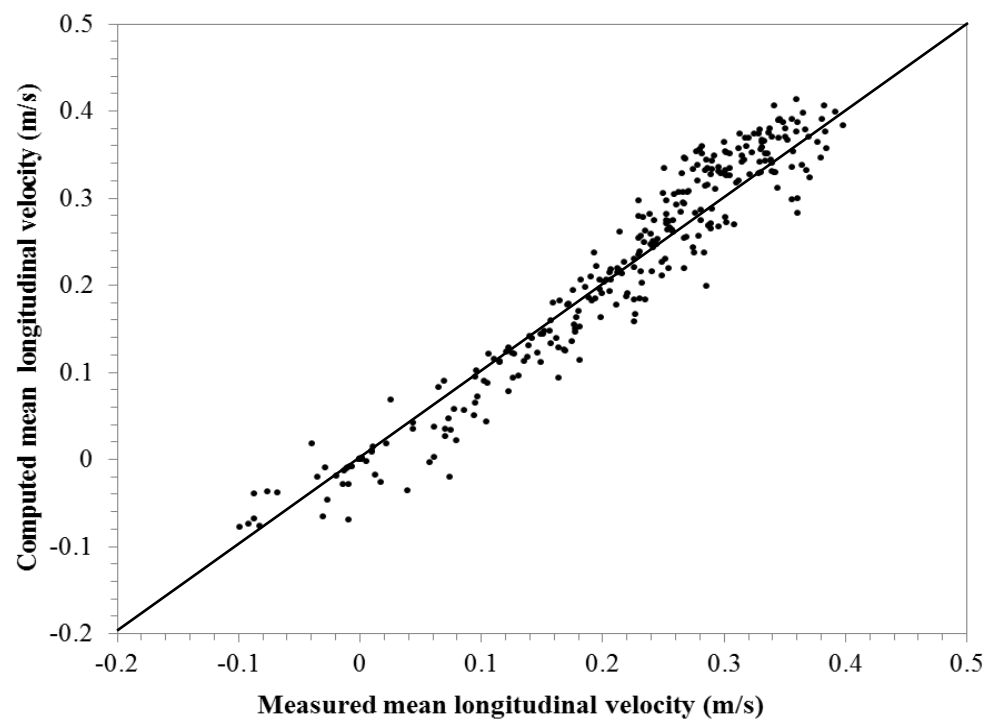
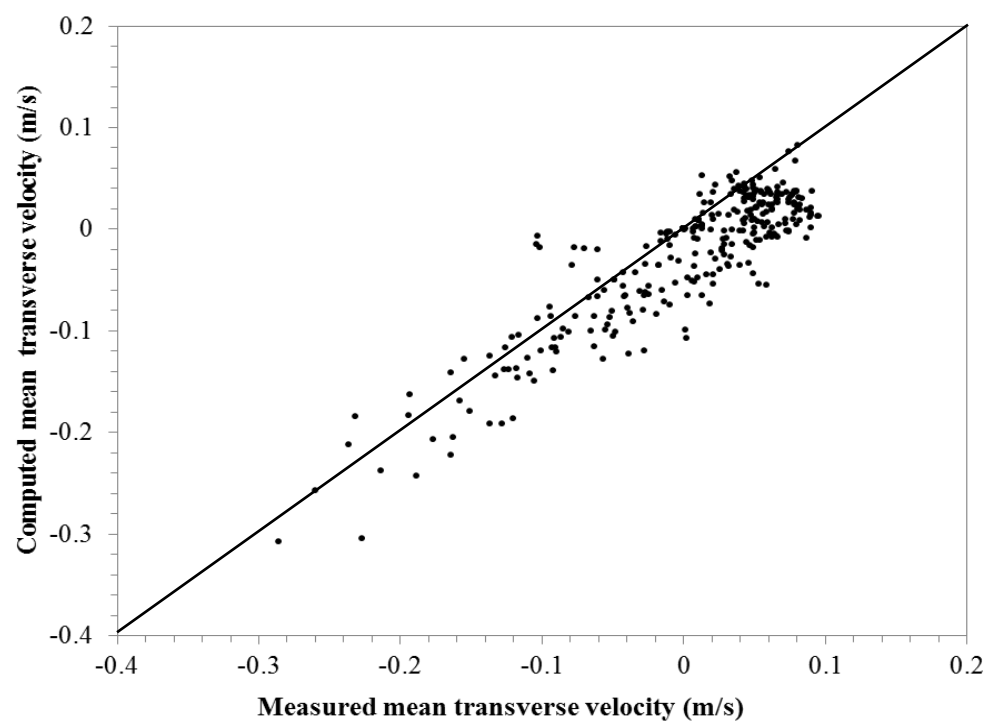


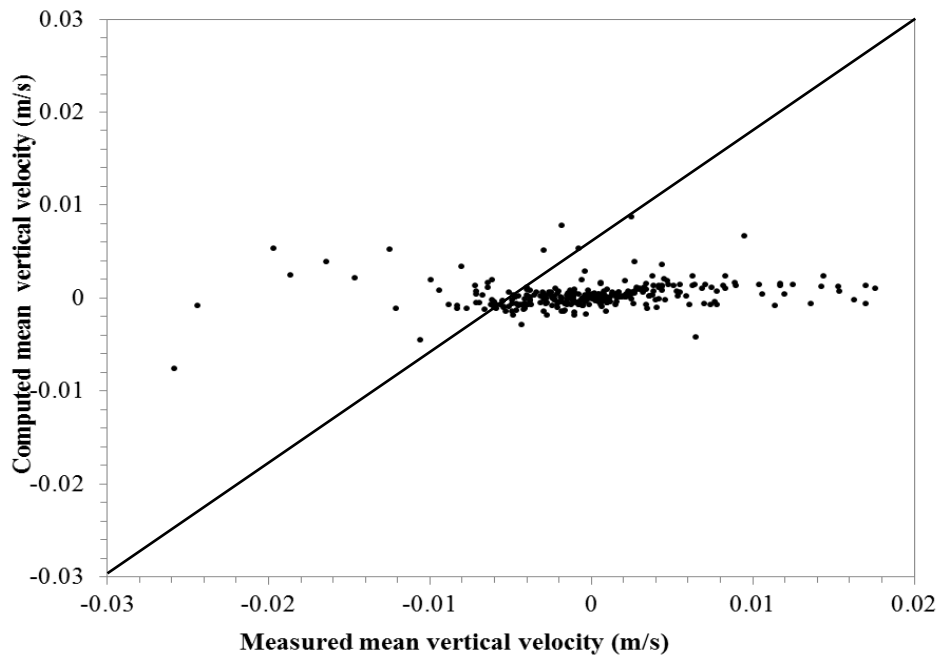
Fig.9. Comparisons of measured (closed and filled circles) and computed Turbulent Kinetic Energy (TKE) profiles in scoured bed case for standard $k-\varepsilon$, RNG $k-\varepsilon$, and LES turbulence closure schemes



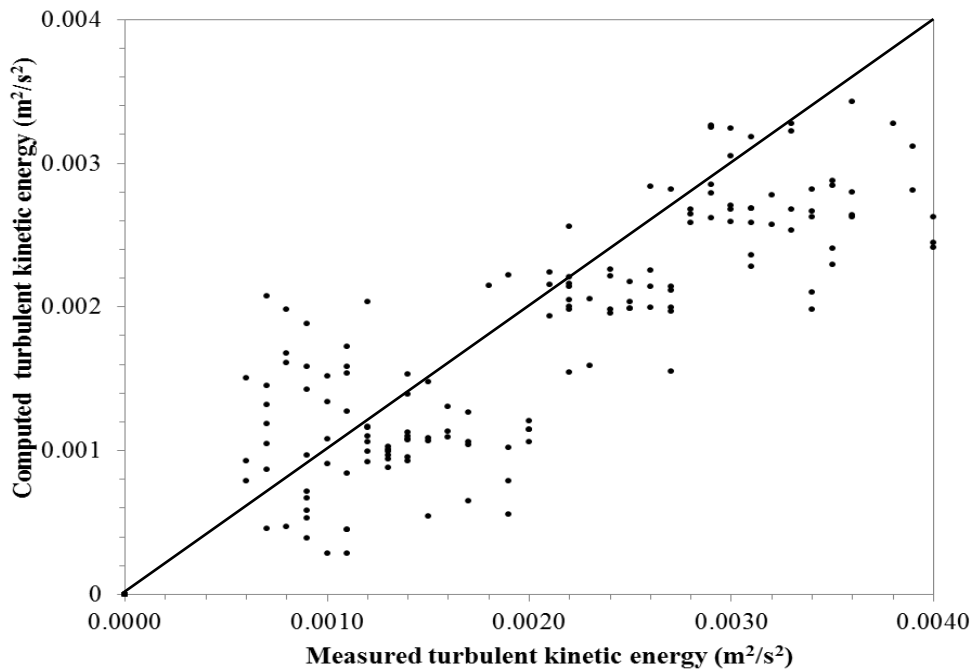
(a)



(b)

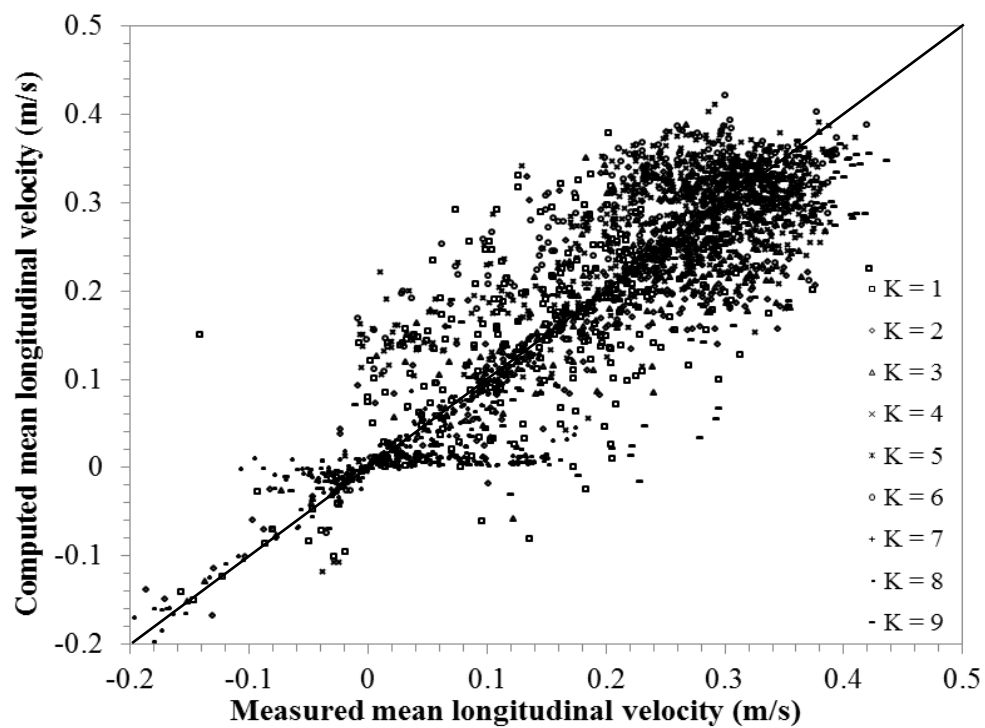


(c)

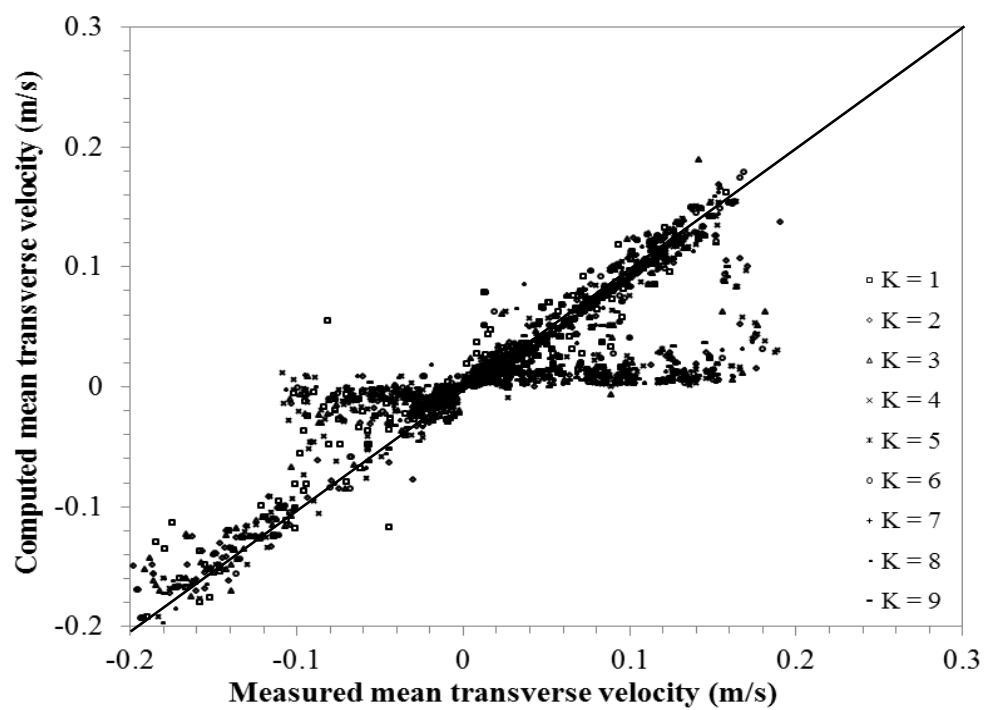


(d)

Fig.10. Comparison of simulated results from RNG $k-\epsilon$ model and measured values for fixed flat bed case: (a) longitudinal velocity; (b) cross-stream velocity; (c) vertical velocity; (d) turbulent kinetic energy



(a)



(b)

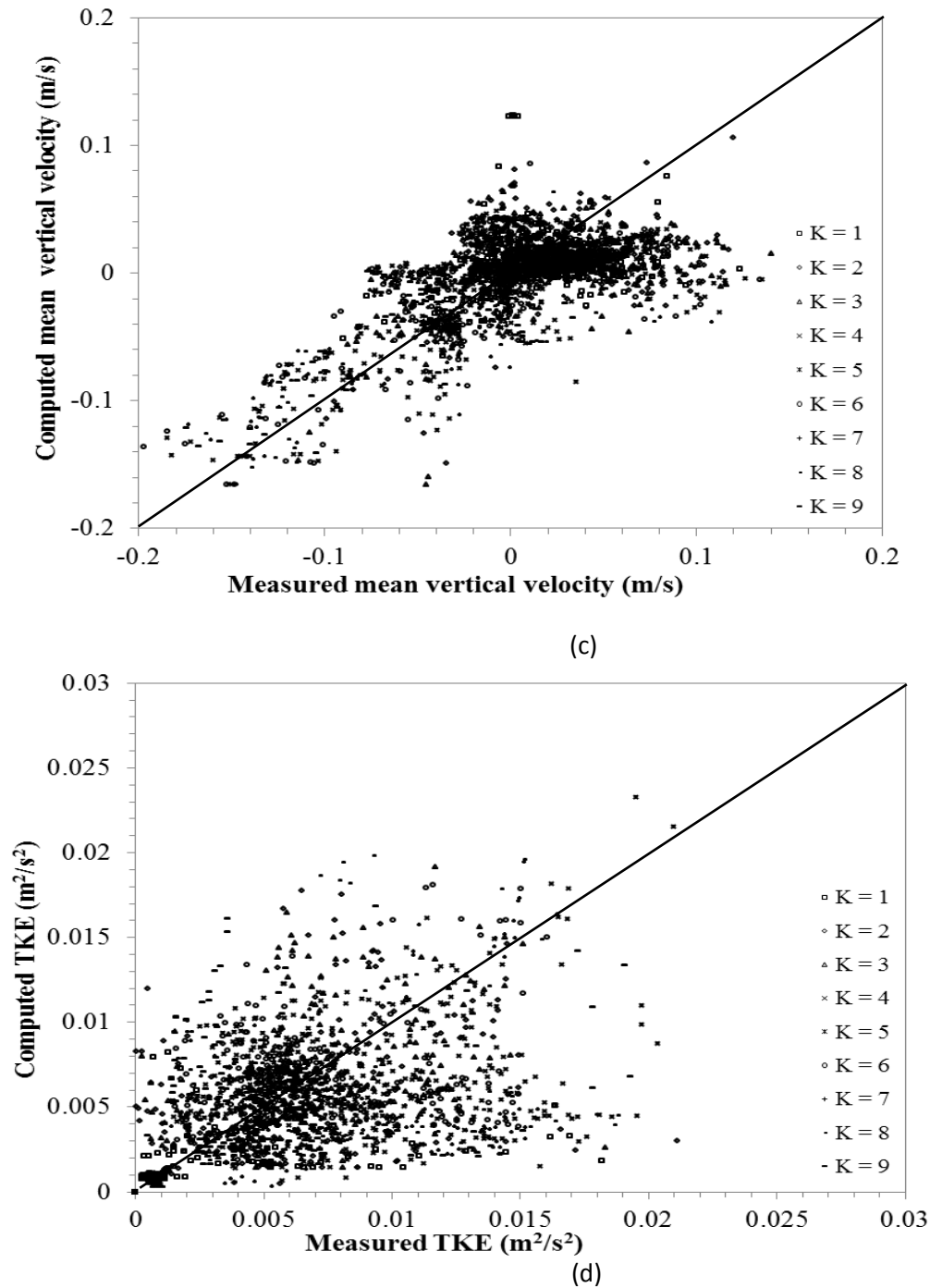


Fig.11. Comparison of simulated results from RNG $k-\epsilon$ model and measured values for scoured bed case: (a) longitudinal velocity; (b) cross-stream velocity; (c) vertical velocity; (d) turbulent kinetic energy. $K = 1, K = 2, \dots, K = 9$ indicate the distance of the velocities above the bed, $K = 1$ represents the level nearest the bed, and $K = 9$ represents the level nearest the water surface